DEVELOPMENT OF NON-DESTRUCTIVE TEST METHODS FOR ASSESSMENT OF IN-USE FIRE FIGHTER'S PROTECTIVE CLOTHING

A Thesis Submitted to the College of

Graduate Studies and Research

in Partial Fulfillment of the Requirements

for the Master of Science Degree

in the Department of Mechanical Engineering

in the College of Engineering at the

University of Saskatchewan

Saskatoon

By

Peter Thorpe

PERMISSION TO USE

In presenting this thesis in partial fulfilment of the requirements for a Postgraduate degree from the University of Saskatchewan, I agree that the Libraries of this University may make it freely available for inspection. I further agree that permission for copying of this thesis in any manner, in whole or in part, for scholarly purposes may be granted by the professor or professors who supervised my thesis work or, in their absence, by the Head of the Department or the Dean of the College in which my thesis work was done. It is understood that any copying or publication or use of this thesis or parts thereof for financial gain shall not be allowed without my written permission. It is also understood that due recognition shall be given to me and to the University of Saskatchewan in any scholarly use which may be made of any material in my thesis.

Requests for permission to copy or to make other use of material in this thesis in whole or part should be addressed to:

Head of the Department of Mechanical Engineering
University of Saskatchewan
Saskatoon, Saskatchewan , S7N 5A9

ABSTRACT

The very nature of the fire fighting environment makes thermal degradation of turnout gear inevitable. Standards that are currently in place to ensure that new gear performs adequately for the protection of the fire fighter do not provide a quantitative measure for assessing this gear once it is in service. When the performance of the gear is compromised due to degradation, it could put the fire fighter wearing the gear at unnecessary risk. A non-destructive test that indicates the end of the useable service of the garment would be a benefit to the fire service.

Full scale fire tests were conducted to suggest a range of heat fluxes that turnout gear specimens should be subjected to in order to simulate degradation caused by in-field use of the gear. A series of destructive tests were conducted on exposed specimens. A number of non-destructive tests were performed on the same specimens. The results of destructive and non-destructive tests were compared.

This research explored some options for non-destructive tests of turnout gear. Digital image analysis and colorimetry were both offered as possibilities for a diagnostic test of this gear. Correlations between destructive performance tests and the colour changes of the outer shell fabric could be used to develop non-destructive tests to evaluate every garment owned by a department. More work is required to improve these test methods, but the door has been opened to better testing for in-use gear, and ultimately to provide better protection for the fire fighters who use this clothing.

ACKNOWLEDGEMENTS

The supervision of Dr. David Torvi is gratefully acknowledged. Help from Dr. Spiro Yannacopoulos, Dr. Richard Burton, Dr. Jitendra Sharma is also appreciated. Financial support from the Mechanical Engineering Graduate Scholarship program is recognized.

Dr. Betty Crown of the Department of Human Ecology at the University of Alberta is recognized for her advice and assistance. Additional assistance from Helena Perkins and Lelia Lawson of the University of Alberta is also acknowledged. Support and advice from Dr. Doug Dale and Mark Ackerman of the Department of Mechanical Engineering is appreciated.

The expertise and equipment provided by Dr. Sammynaiken of the Saskatchewan Structural Sciences Centre is appreciated, as is the use of the equipment at the Department of Agricultural and Bioresource Engineering, supervised by Dr. Lope Tabil. Dr. Ajay Dalai of the Chemical Engineering Department also provided laboratory equipment and support.

Additional support from the Mechanical Engineering Department of the University of Saskatchewan is acknowledged. The faculty and staff have made it an enjoyable place to work and learn. Departmental assistants Dave Deutscher, Dave Crone and Hans Steinmetz all provided valuable support. The secretarial staff April Wettig, Sherri Haberman and Michelle Howe also contributed to the production of this thesis.

TABLE OF CONTENTS

LIST OF TABLES

LIST OF FIGURES

CHAPTER 1: INTRODUCTION

Fires are a major source of concern for modern civilization. When fires go out of control, people are injured and property is damaged. In the year 2000, Canada saw 53,720 fires reported, 327 deaths and 2490 injuries due to fire [1]. There was an estimated 1.2 billion dollars worth of property damage in the same year. In 2002 in the United States, 97 fire fighters were killed in the line of duty and more than 80,000 were injured [2]. One of the most important methods that have been established to reduce the damaging impact of fire is through fire fighting. In buildings and in cities in particular this is known as structural fire fighting. A fire fighting department consists of a team of individuals who are highly trained and are well equipped to face the various hostile environments that a fire can bring. The structural fire fighter is protected by numerous technologies; one of these technologies is known as turnout gear. Turnout gear is a blanket term for the pants and coat that a fire fighter wears to protect himself from the elements. These garments consist of materials designed to resist the impact of flame and heat, reduce the negative influence of water and other liquids, and minimize the effects of sharp surfaces while providing freedom of motion to perform a high degree of physical tasks.

Many different suppliers are involved in the production of turnout gear, from the manufacturers of the fibres, to the weavers of the fabrics and finally the manufacturers who sew the actual garments. The end result is a garment that has been refined over

years of research and service use. While much research has been conducted to create these garments, there has been less work to determine how the garments perform as they age. In the United States the National Fire Protection Association (NFPA) has developed a set of standards to which new gear must conform. NFPA 1971 Standard on Protective Ensemble for Structural Fire Fighting [3] provides a set of performance and construction standards that every new piece of turnout gear must meet. A problem exists however in that there is no quantitative standard for the continued use of this gear. The currently published standard, NFPA 1851 Standard on Selection, Care, and Maintenance of Structural Fire Fighting Protective Ensembles [4], gives a list of indicators of degradation to identify through examination, but falls short of providing quantitative measures of degradation. When the protective ensemble is purchased, it will typically come with a predicted life span, say 5 to 10 years. This prediction is problematic though because it does not account for the differences in the duties of the personnel wearing the garments. Roles are varied on the fire ground: the individual responsible for the first entry into a burning building will experience considerably more thermal exposure than the individual responsible for maintaining the water supply to the fire hoses. Similarly, different fire departments have different levels of fire incidence. A rural department will experience less direct fire fighting activity than will a busy urban department. These differences between fire departments also point to the inadequacy of the time based life expectancy.

Torvi and Hadjisophocleous [5] recognized this disparity and identified the need for improved standards for the retirement and maintenance of in-use turnout gear, and increased research into end of service life indications. The National Research Council

of Canada's Institute for Research in Construction [6] also identifies the need for guidelines for end of service life assessment and research that indicates the "key parameters that affect the durability of protective clothing". A further need to develop non-destructive test methods that allow for in-field testing for the assessment of the degradation of a fire fighter's apparel was also identified.

This research project was concerned with developing non-destructive tests to describe and quantify the level of degradation of in-use turnout gear. While there are a number of mechanisms by which these materials degrade (e.g. exposure to ultra-violet radiation, laundering, storage techniques) [5], the emphasis of this research is to examine the effects of high heat fluxes on turnout gear. The introductory chapter of this thesis will start with a discussion of the relevant background information: information about structural fire fighting, the specific design and performance challenges for structural fire fighting and how technology has been used to face these challenges. A discussion of the NFPA standards follows, describing in greater detail the minimum acceptable performance and construction levels required by the standards. A discussion of non-destructive testing requirements and goals is followed by a survey of what research has been conducted in the field of the durability of fire fighter's turnout gear. The background information concludes with a discussion of the measurement of colour and a suggestion for its use in assessing degradation of fire fighter's turnout gear.

1.1 Structural Fire Fighting Conditions

Structural fire fighting is defined by the Fire and Emergency Manufacturers and Services Association (FEMSA) as the "activities of rescue, fire suppression, and property conservation in buildings, enclosed structures, aircraft interiors, vehicles, vessels, or like properties that are involved in a fire or emergency situation [7]." Structural fire fighting is distinguished by the NFPA from wildland fire fighting, entry fire fighting and proximity fire fighting. Entry and proximity fire fighting are concerned with very high heat intensity fires, like those caused by the ignition of compressed gases, aviation fuel, etc [3]. Wildland fire fighting is "the activities of fire suppression and property conservation in vegetation that is not within structures but that is involved in a fire situation [3]." The technical clothing that is worn in each of these cases of fire fighting is slightly different due to the unique environmental situations faced in each. The environments that personnel encounter in the course of structural fire fighting can be dangerous; in the course of duty a fire fighter will be exposed to a wide variety of hazards. Some examples of fire ground hazards include: extreme heat, extreme cold, water exposure from sweat, fire hoses or sprinklers, sharp objects, gaseous attack, and attack from blood borne pathogens. The clothing that a fire fighter wears must provide some measure of protection from all of these hazards. The primary environmental condition that the turnout gear is designed to protect from is the extreme heat. High heat fluxes in the fire ground create a serious hazard to those working in it.

Much research has been done to quantify the level of heat intensity on the fire ground. In 1958, a town on the St. Lawrence River (Aultsville, ON) was slated for destruction to

facilitate construction of the St. Lawrence Seaway. This rare opportunity allowed researchers to destroy the town at their leisure while conducting controlled experiments [8]. Researchers at the National Research Council of Canada were able to instrument buildings and record heat flux levels and temperatures while the buildings burned to the ground. This research stands as the most comprehensive large scale fire study, and its results provide good information as to the exposure that a fire fighter would experience during the approach to a burning building.

While this study was large in scale and comprehensive in scope, it is now somewhat dated. Lawson [9] notes that the differences between the materials used in furniture and home construction in the 1950's and the materials used currently are very significant . The increased use of plastics and other synthetic polymers has led to an increase in the heat load in modern buildings. In a study Lawson completed for the National Institute of Standards and Technology, two different armchairs were burned and the heat release was measured. Design methods and construction materials (wood with some upholstery) typical of furniture produced before the 1950's were used in one of the chairs, while the second chair used more modern materials (more plastics and rubber foam). As the results of this test demonstrate (see Figure 1.1), modern materials give off much more energy when they burn than do their older counterparts. The result is that the energy released in house fires is much higher, and that fires burn more quickly now than ever before, so the data from the St. Lawrence burns may not provide a complete picture of the heat flux levels present in current structural fire fighting situations.

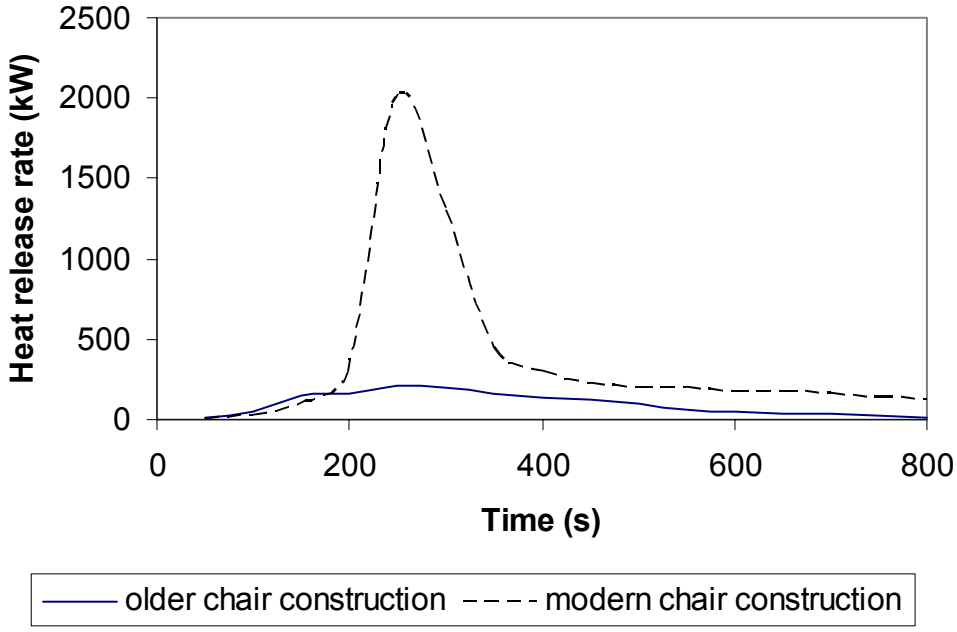

FIGURE 1.1: Heat release rates for different chair constructions [10]

Heat flux is a measurement of the intensity of heat; it is a common measurement for comparison in fire testing, so a brief discussion comparing heat flux values to intuitive phenomena is appropriate. Heat can be transferred in one of three modes: conduction, convection and radiation. In a fire all of these modes are in operation, but conduction is only a problem when in contact with hot objects and convection becomes significant only when the turnout gear is in direct flame contact. Radiation heat transfer is not so easy to avoid, a very hot fire will cause radiant heating on a fire fighter at a great distance. While conductive and convective exposures are less probable in the fire fighting situation, these exposures may cause significant degradation and danger if they do occur; as a result, NFPA 1971 and other standards provide tests to assess the ability of turnout gear to protect the fire fighter from these exposures. Table 1.1 gives a description of the effects of radiation heat transfer for a range of heat fluxes; this is

included to provide some intuitive sense of the heat intensity levels that will be discussed during the thesis.

TABLE 1.1: Effects of thermal radiation [10]

Radiant Heat Flux (kW/m^2)	**Observed effect**
0.67	Summer sunshine in UK
1	Maximum for indefinite skin exposure
6.4	Pain after 8 second skin exposure
10.4	Pain after 3 second skin exposure
12.5	Volatiles from wood may be ignited by pilot after prolonged exposure
16	Blistering of skin after 5 seconds
29	Wood ignites spontaneously after prolonged exposure
52	Fibreboard ignites spontaneously in 5 seconds

The results from the St. Lawrence burns were not directly related to fire fighting, but later, Veghte and others performed experiments to assess the risk to fire fighters based on the conditions that they were facing in duty. While there is some discrepancy between the researchers as to what conditions a fire fighter may reasonably encounter in the line of duty, a sliding scale is typically used to define categories of thermal exposure. Heath [11] condenses a number of these studies and defines routine, hazardous and critical conditions, but the most cited description of fire ground conditions is from Veghte's work. Veghte [12] summarized his findings in a chart (Figure 1.2) that defines the routine, ordinary and emergency conditions that a fire fighter would experience. The definitions of such general terms are useful only if the fire fighter has an intuitive understanding of what these conditions mean for him; as a retired fire fighter, Veghte has a good feel for the specific needs of the job. As shown

in Figure 1.2, conditions that a fire fighter would consider routine include temperatures up to 70°C and heat flux values up to 2 kW/m^2. The ordinary condition continues to temperatures of 200°C and heat fluxes of 20 kW/m^2 and emergency conditions are anything hotter than ordinary with a particularly intense heat flux. This research is important to the present study because it suggests the level of exposure a fire fighter would be exposed to in the course of typical fire ground activities, activities which might not carry the expectation of degradation to the protective ensemble.

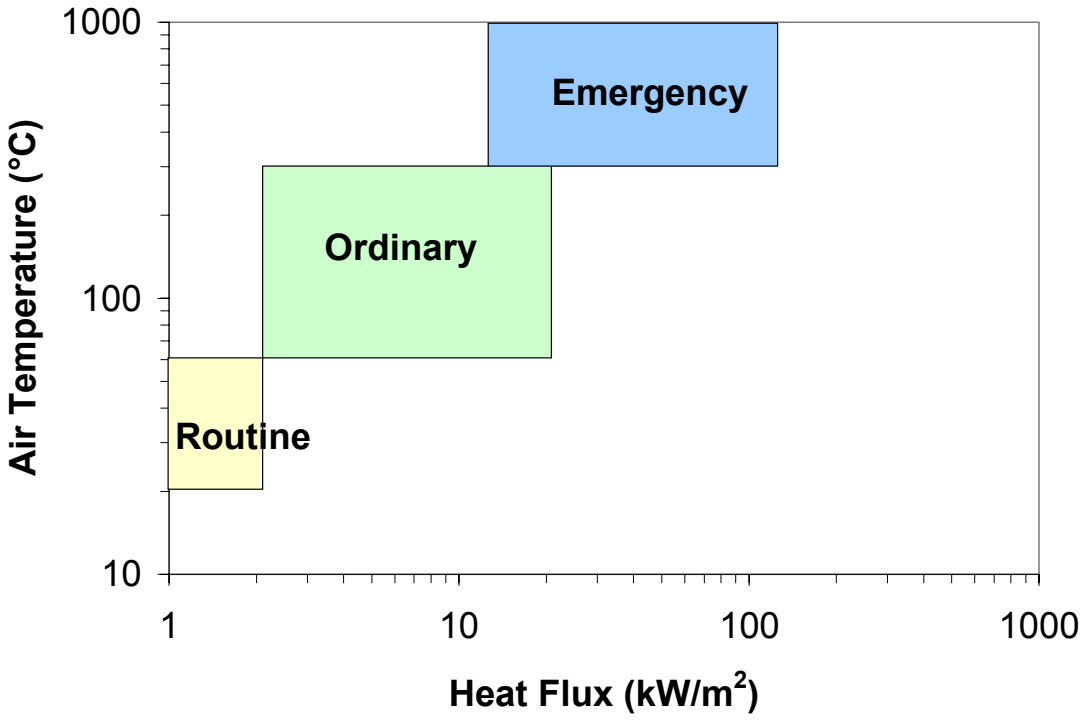

FIGURE 1.2: Classification of fire fighting conditions [12]

Randy Lawson [9] added to the knowledge of the fire ground situation in his research. He notes that often fire injuries occur outside the fire envelope, that is, the area of direct contact with flame. He concludes that better training for fire fighters and improvements in protective clothing should reduce burn injuries, and notes that fire

fighters must understand the performance limits of their clothing in order to make the best use of the technology.

It should follow that injuries should be reduced with increased protection, but in fact it has been shown that fireground injuries have not decreased as a result of improved technology. Lawson and other researchers have demonstrated that there are as many injuries to fire fighters today because they are more willing to go into increasingly hazardous environments, as a result of the improved protection afforded them by their gear [13],[14]. This finding reinforces the point that more thorough training about the limitations of the gear and the implications for fire fighting tactics is needed.

1.2 Materials Used in Turnout Gear

To provide a degree of protection from the conditions that fire fighters face during structural fire fighting, personal protective equipment is worn. The fire fighting ensemble consists of pants, coats, hoods and helmets, self-contained breathing apparatuses, gloves, boots and other additional equipment. The coat and pants together are known as the turnout or bunker gear; they form the largest element of the protection that the fire fighters wear.

A fire fighter's protective ensemble is typically constructed of three layers of fabric: the outer shell, the moisture barrier and the thermal liner. The outer shell is designed to provide maximal protection from heat and flame as well as cuts and abrasion. Outer

shells are usually made of polymeric weaves that incorporate high strength and excellent thermal resistance. The moisture barrier is designed to protect the fire fighter from external fluid exposures. As technology has improved, these moisture barriers are now designed to allow water vapour to be transpired from the body, reducing the chance of injury due to steam burns on the skin of the fire fighter. The thermal liner can be removable or permanent and is designed to provide an insulating layer to protect the fire fighter from heat or cold.

For this thesis work, samples of each of these layers were provided by Equinox Fire and Rescue, the Winnipeg based supplier of gear to the Saskatoon Fire and Protective Services. Figure 1.3 illustrates the location of the ensemble elements. The outer shell supplied by Equinox is made by Southern Mills (Southern Mills Inc., Union City, GA) and consists of a blend of 60% Kevlar® (poly para-aramid) and 40% Nomex® (poly meta-aramid), it is known by the commercial name Advance™. The outer shell materials used in the Saskatoon gear has been dyed brown, or khaki according to the manufacturer. This colour has been chosen to reduce the impact of soil on the aesthetics of the garment. The outer shell is woven in a rip stop pattern to increase strength.

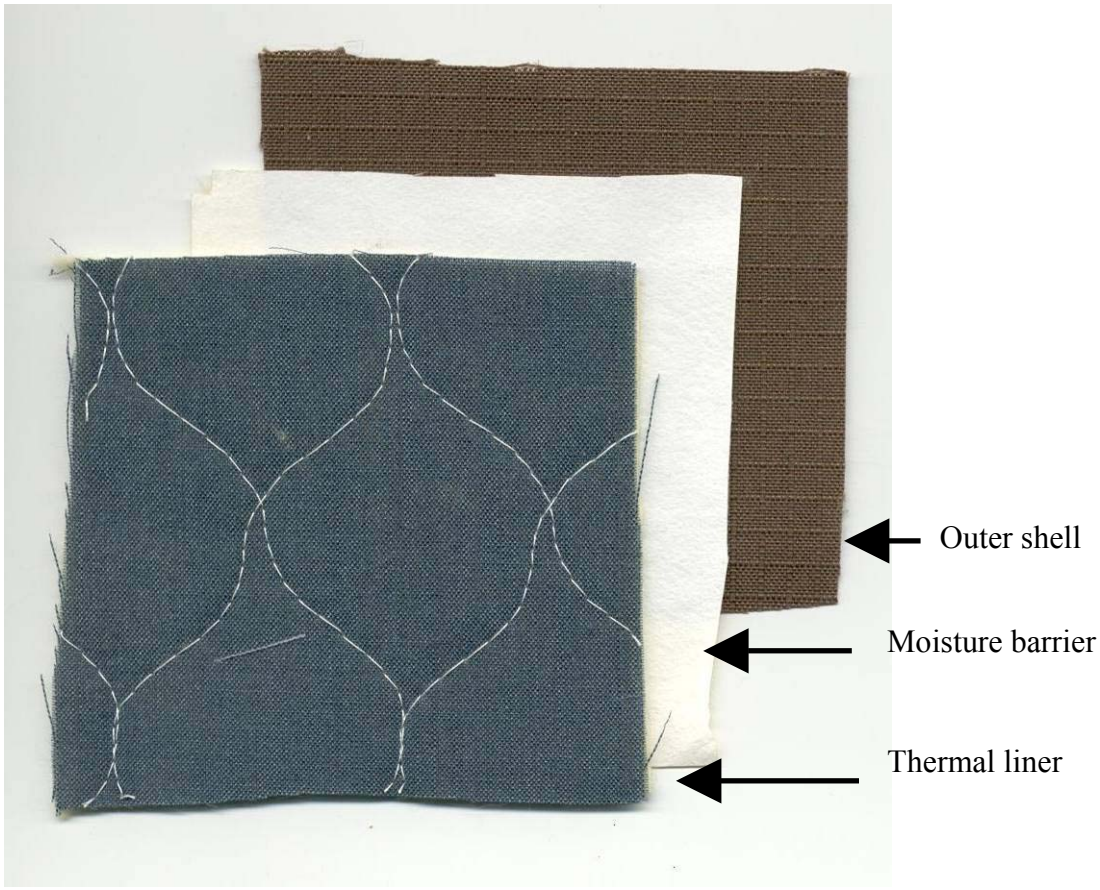

FIGURE 1.3: Ensemble layers for this research

Kevlar® and Nomex® are both aramids developed by Du Pont (Wilmington, DE) that provide an inherently flame resistant fibre with a high degree of strength. Both fibres are designed to exhibit good performance in high heat conditions. Due to differences in the chemical structure, Kevlar® has a higher degree of rigidity and strength than Nomex®, so the latter is typically used where more comfort is required [15]. Another beneficial property of these materials is that rather than melting or dripping or catching on fire, both of these fibres will char when exposed to very high temperatures.

This moisture barrier is a polytetrafluoroethylene (ptfe) based membrane layer, manufactured by W.L. Gore and Associates (Newark, DE). The moisture barrier fabric

is referred to by its commercial name, RT 7100. Polytetrafluoroethylene is commonly known as Teflon®, but when it is in its expanded form, a waterproof, breathable laminate is formed, one version of which is known commercially as Gore-Tex®. Expanded ptfe is used because it has pore sizes large enough to transmit water vapour but too small to transmit liquids [16]. This is beneficial to the fire fighter who would like to reduce body heat through perspiring but also needs protection from outside liquids.

The thermal liner consists of Nomex® face cloth and Kevlar® batting; it is manufactured by Southern Mills Inc. (Union City, GA) and is sold under the commercial name Aralite®. This liner is designed to provide thermal protection from both hot and cold. The batting is constructed of very fine fibres pressed into a sheet. The space between the fibres creates air pockets that provide the insulation; indeed the fibres act as "a large surface area medium to trap still air [17]." As a result, compression of the fibres results in reduction of the effectiveness of the fabric. The Nomex® face cloth is dyed blue while the batting is the natural yellow colour of Kevlar®.

1.3 Protective Clothing Standards

The National Fire Protection Association in the United States is a body that serves to improve fire safety in a number of ways, including improving the technology and knowledge base associated with fire protective services in the United States and in other countries. Part of its mandate is to provide standards for the gear that fire fighters wear.

To this end, a number of standards have been produced, two of which are particularly relevant to this research. NFPA 1971 Standard on Protective Ensemble for Structural Fire Fighting [3] describes the required construction for turnout gear, and a series of tests for evaluating various properties of the different elements of the turnout ensemble. The standard provides minimum performance requirements for each of these tests. NFPA 1971 includes information on the boots, the gloves, the helmet, the pants and the coats that comprise the total protective ensemble. Destructive tests are used throughout the standard to ensure that each ensemble provides the same level of protection to the fire fighter. Tests for new turnout gear evaluate a number of material properties, including: flame resistance, heat and thermal shrinkage resistance, conductive heat resistance, radiant heat resistance, thermal protective performance, thread melting, tear resistance, water absorption resistance, water penetration resistance, breaking strength.

NFPA 1851 Standard on Selection, Care, and Maintenance of Structural Fire Fighting Protective Ensembles [4] provides guidelines for the inspection of turnout gear to assess its level of degradation. A routine inspection after each use is suggested, with an emphasis on identifying soiling, rips, tears and cuts, and thermal damage such as charring, burn holes and melting. A more detailed "advanced inspection" is suggested every 12 months; this involves more detailed visual examination, now adding discoloration to the list of degradation indicators. This standard is not clear on when a garment should be retired, and what level of degradation will threaten the safety of the fire fighter, so this is a motivation for this research. Other standard issuing bodies like the Underwriters Laboratories of Canada and the Canadian General Standards Board offer suggestions for retiring gear [6]. Different guidelines are suggested by different

organizations, but these suggestions stop short of providing quantitative measures of degradation. One such guideline proposed by the Fire Industry Equipment Research Organization [18] is to retire turnout gear when the repair cost exceeds 50% of the replacement cost.

1.4 Degradation

There are many processes by which fire fighter's turnout gear can degrade. Slater [19] discusses degradation of textile materials in an extensive survey of literature on the subject. In the introduction to this survey, Slater defines degradation as:

> Changes in the molecular structure that bring about changes, usually adverse in nature, in any physical or chemical property of the fibres of which the textile material is made. These changes may include (but are not restricted to) a deterioration in physicomechanical properties such as strength, abrasion-resistance, tactile response, colour, and aesthetic characteristics.

He notes that physical abrasion, thermal exposure, ultraviolet light exposure, chemical exposures and other factors all contribute to textile degradation.

The need for careful examination is well documented. Visual degradation indicators include fading, brittleness, and others. Slater suggests that the level of degradation of a textile specimen may not be directly related to the visual indicators of degradation. He suggests that for textiles, the performance of the fabric may be compromised before the visual indicators are evident [20]. Figure 1.4 demonstrates this possibility: the performance axis could be any property of the fabric that affects its ability to protect a fire fighter; examples could be flammability, tensile strength or resistance to puncture.

This figure suggests the need for enhanced visual inspection or other non-visual methods of degradation inspection.

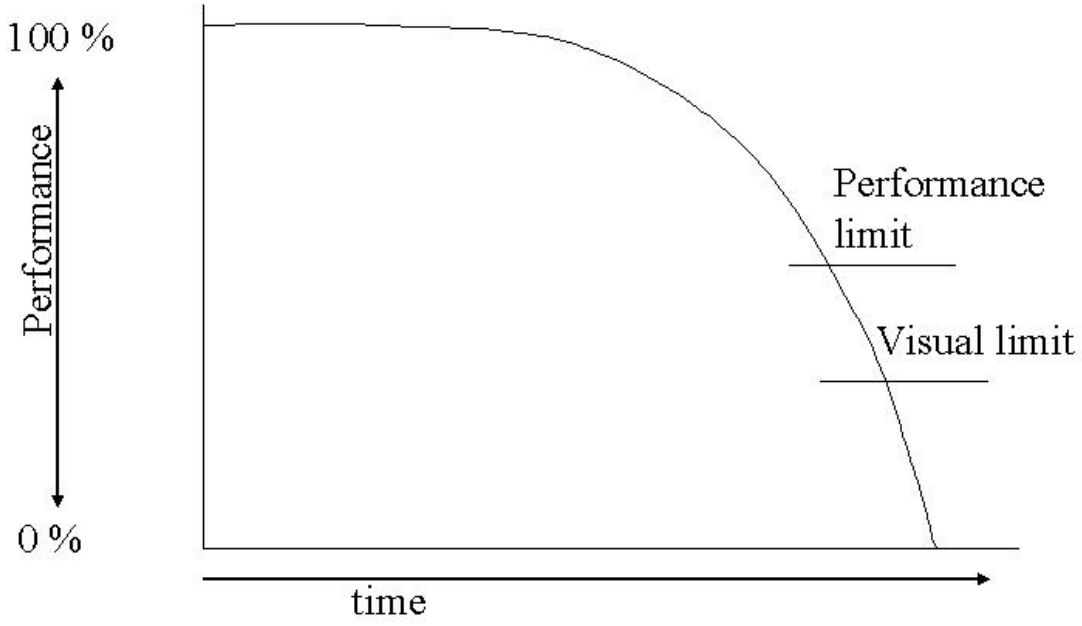

FIGURE 1.4: Potential performance loss before visual cues emerge (after Slater) [20]

Vogelpohl [21] at the University of Kentucky conducted the most important study into the performance of retired fire fighter turnout gear. She tested and studied 20 garments that had been used either in training facilities or in service departments. The garments were tested to determine how they would comply with the NFPA 1971 standard (1991 version) for new turnout gear. A number of the tests prescribed in the standard were used to identify the performance reduction as a result of degradation. Vogelpohl discovered that some of the garments met nearly all of the standards for acceptable use while others failed many of the tests. It was discovered that some indicators of performance such as the Thermal Protective Performance [22] test actually had improved over the life of the garment, attributed to an increase in thickness, perhaps as a result of wear and laundering.

This work was an important first step in understanding the results of degradation, but there are gaps left by the research. The garments tested by Vogelpohl were all retired, that is, there was enough visible degradation or hours of service on the garments to justify their retirement. However, the type of conditions that the garments had been exposed to and the durations were unknown at the point of retirement. A more complete picture would be provided by a detailed description of the service use of the garments, for example if the user of the garment would be diligent in recording the activities the garment had been used for. Work to this end has been initiated, and indeed included with the purchase of new gear are worksheets to attempt to track the progress of the turnout gear [18].

Torvi and Hadjisophocleous [5] note that non-destructive testing is desirable for the fire services because the budgets are often very restrictive. Large departments may have means to engage in destructive testing to sample a lot of similar garments that have the same exposure history, but as has been noted previously, exposures are varied in the field, so even a batch with the same service time may not be uniformly degraded. This suggests the need for non-destructive testing that can be performed on every garment, with some means of predicting its useful service life and suggesting an appropriate retirement schedule.

Berardinelli and Roder [23] examine the possibilities of field evaluation methods for assessing chemical protective clothing with the intention of providing information of in-use gear. They offer suggestions for receiving input on the gear from the wearers of the

garments but they stop short of demanding non-destructive test methods. Penetration testing is suggested in the examination of degradation of these chemical protective suits, which is noteworthy for fire fighter's turnout gear since the moisture barriers are designed to protect from chemical attack. Adapting some of the methods put forth in this paper to the goals of non-destructive testing may prove useful for this study.

1.5 Colour Analysis

The use of colour as a means of assessing degradation is not new; indeed the NFPA 1851 standard suggests that as a part of advanced inspection of turnout gear, garments should be examined for discoloration. Imaging technology has steadily advanced in the digital age such that with digital imaging hardware, there are a number of techniques available for testing. Digital image analysis is typically non-destructive because it involves shining light on a sample, measuring the reflected light coming off the same then using software to perform some analysis. Digital image analysis (DIA) is a term used to describe any digital technique that uses computer programs to measure and analyse digital image files. The use of DIA is well documented in the textile field; one such study was conducted by Cardamone et al [24]: the authors used black and white images to examine thickness, spacing and density of yarns in museum fabric specimens. The authors were able to develop a technique to verify the age and authenticity of historical fabrics. While the techniques seemed successful for this application, little work has been identified that uses digital image analysis techniques to assess degradation of fire fighter's clothing.

Taking a cue from the NFPA 1851 standard on the examination of in-use turnout gear, it was postulated that modern digital equipment could be used to perform enhanced visual inspection of used protective clothing ensembles. The fade of colour in the outer shell is one such process whose understanding might be improved with this approach.

Colour is measured using a number of different scales. The most common method for producing colour is the RGB system. This system employs three lights (red, green and blue, RGB) in different intensities and combinations to produce any colour required. The RGB system is the most common colour model used in the production of colour: it is used in televisions and computer monitors. The measurement of colour is infrequently done using this system however, because it is not an intuitive scale for the human eye [25]. The Commission Internationale de L'Eclairage (CIE) is an international body dedicated to the measurement and reproduction of colour. The CIE has produced what they claim to be a colour measurement scale that emulates human colour perception. For colour measurement, they have developed the CIE L*a*b* system, a Cartesian coordinate system with three axes, L, a and b (Figure 1.5).

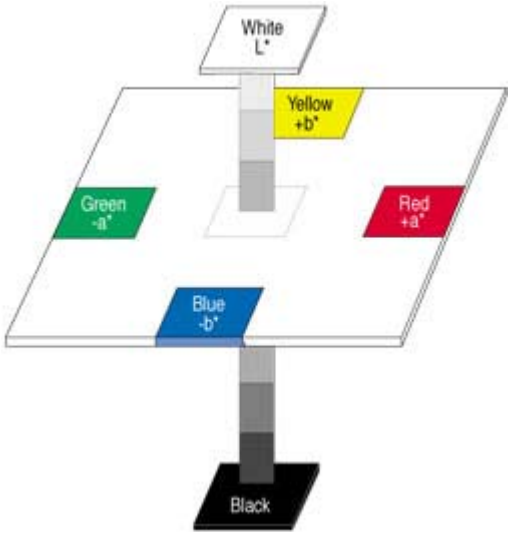

FIGURE 1.5: CIE Lab colour model [26] (reprinted with permission)

The lightness or intensity of the light is measured on the L axis, while the hue is measured on the a and b axes. The a axis progresses from pure green at a = -100 to pure red at a = 100. The b axis goes from pure blue at b = -100 to pure yellow at b = 100. To define the difference in colour, the CIE suggests using the Euclidean difference between points in the L*a*b* space [27]:

$$\Delta E = \left((L_2 - L_1)^2 + (a_2 - a_1)^2 + (b_2 - b_1)^2 \right)^{\frac{1}{2}} \qquad (1.1)$$

where subscripts 1 and 2 represent values for point 1 and 2 in L*a*b* colour space, and ΔE is the colour difference in that colour space.

1.6 Scope of Thesis Research

It was decided for this thesis work that an emphasis on non-destructive testing was appropriate. The crucial element of this research was to correlate the quantitative standard for new gear provided by NFPA 1971 with new non-destructive test results. To achieve this goal, three progressive steps were taken: the first step was to perform full scale fire testing to further specify what appropriate routine or ordinary conditions on the fire ground would be. Once this work was completed, a decision was made to simulate the conditions seen in these full scale tests with bench top scale exposures. A radiant panel performance test apparatus, specified in the ASTM Standard Test Method for Radiant Protective Performance of Flame Resistant Clothing Materials [28] was used to expose ensemble specimens to prescribed radiant heat fluxes of varying times. Once this laboratory exposure was completed, a number of non-destructive test methods were employed to assess the degradation and to compare with destructive tests that were performed after all other testing was complete. The final task was to correlate the results of the destructive testing with those of the non-destructive testing to assess the utility of the testing methods developed during this research.

This thesis will describe the results and discuss the implications of this research. Chapter 1 provides some background information regarding the problem of standardizing the retirement of used turnout gear; it introduces the particular environmental needs of fire fighting. The chapter also describes the fabrics used in the turnout gear studied for this research, fabric degradation and colour measurement and analysis. Chapter 2 describes the full scale fire testing that was conducted in Saskatoon

and Edmonton, and the artificial exposure of fabrics completed for this research. Chapter 3 discusses the destructive tests that were performed on these exposed fabrics. Chapter 4 details the non-destructive tests that were developed to assess the turnout gear. Chapter 5 correlates the results from the non-destructive and destructive testing to assess the viability of the non-destructive methods for the testing of in-use garments. Chapter 6 discusses the limitations and implications of this research.

CHAPTER 2: FULL SCALE FIRE TESTING AND LABORATORY EXPOSURES

In order to simulate the effects of actual fires in the laboratory, it is important to understand the conditions that a set of turnout gear may be exposed to in the field. The fire fighting environment is so chaotic and filled with variables that it is hard to model the behaviour of fires and fire fighters; as such empirical testing is necessary. Full scale fire tests are rarely conducted because they are very expensive to perform, but when they are they can provide a wealth of information about the fire ground. While some data describing the conditions faced by fire fighters is available (e.g. [9], [12], [29]), additional data was gathered for the purposes of this and other fire science research conducted at the University of Saskatchewan. In this chapter, two full scale fire tests are described along with laboratory tests used to simulate conditions to which turnout gear may be subjected.

2.1 Saskatoon Full Scale Fire Test

In one test, temperatures were measured during a controlled burn in a small training room. A live training exercise was conducted by Saskatoon Fire and Protective Services during Fire Prevention Week in October 2002. Thorpe and Torvi [30] summarize this test; additional detail is included in this discussion. For this exercise, a test room was instrumented with thermocouples and burned for the dual purpose of

training the fire-fighters and educating the public. A brick test room 2.8 m x 2.6 m x 2.3 m high was finished with gypsum board and filled with furniture (Figure 2.1). The test room had one single pane window 1 m^2 in area, and a door 0.8 m wide x 2 m high. Three 24 gauge K-type thermocouples were placed in an unobtrusive location in the room: one at floor level, one at waist level and one at the ceiling. The thermocouples were connected to a data acquisition system to record the temperature as a function of time. The data acquisition device was an Agilent (Agilent, Palo Alto) 34970A 3-slot data acquisition (DAQ) device.

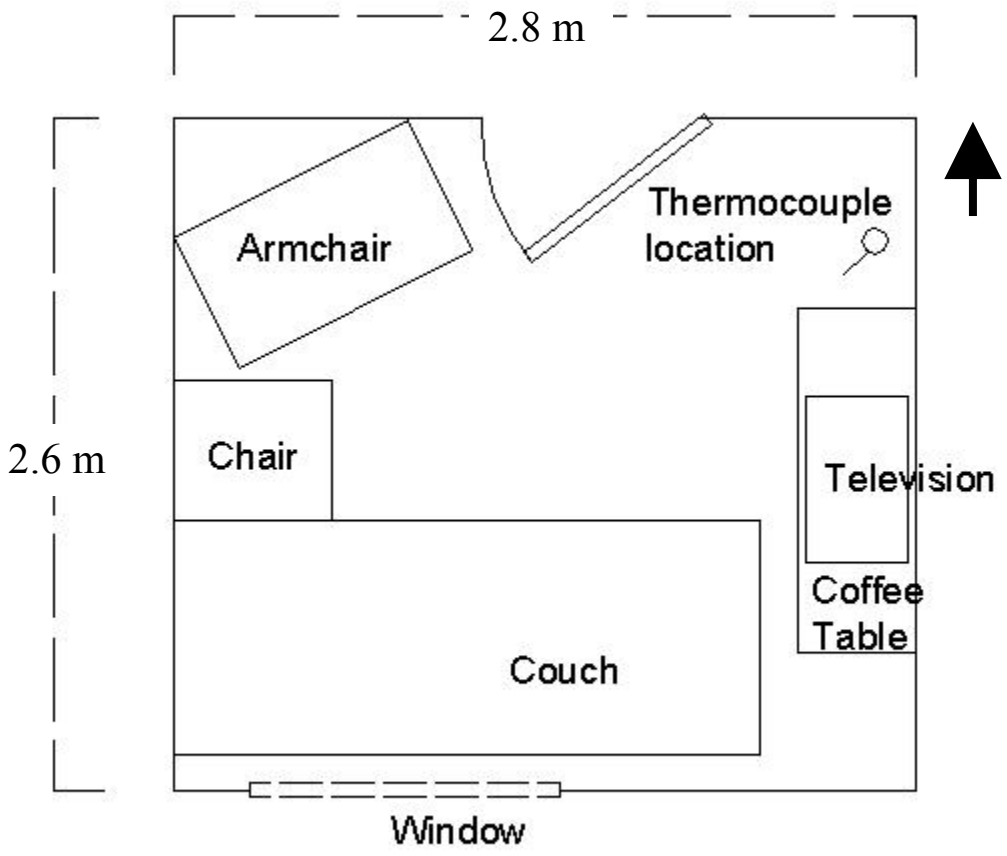

FIGURE 2.1: Test room for full scale fire test, arrow points north

The armchair was the initial source of heat as it was set on fire using matches with potato chips added as an accelerant; after ignition the door was closed. A video camera recorded the fire from outside the test room to provide external visual observations to compare with the measured thermocouple data. Once the fire was lit, a fire fighter used a chainsaw to cut a hole in the roof, providing more oxygen to the room. At approximately 65 seconds the window failed, adding cold air to the room, increasing the oxygen content of the fire but reducing the temperature of the room. During the development of the fire, fire fighting personnel were working in and around the test room: they had placed a manikin in the room to simulate a fallen comrade who needed rescue. The fire fighters breached the room cautiously, made a search for the manikin, conducted rescue operations, and then returned to the room with hoses to extinguish the blaze.

The data provided by the thermocouples in the room are given in Figure 2.2. The mid-range thermocouple data was very similar to the ceiling height data, so the former has been omitted from the figure for clarity. This is the temperature history for this fire; data of this kind along with information about the perceptions of the fire fighters during the fire serves to improve the general knowledge base about fire fighting and about the protective clothing worn for structural fire fighting. Temperature histories at the ceiling and floor of the room were plotted to observe the rise and fall of thermocouple temperatures during an actual fire. Peak temperatures measured during this test were approximately 850°C at the ceiling and at human chest height; and 700°C at the floor.

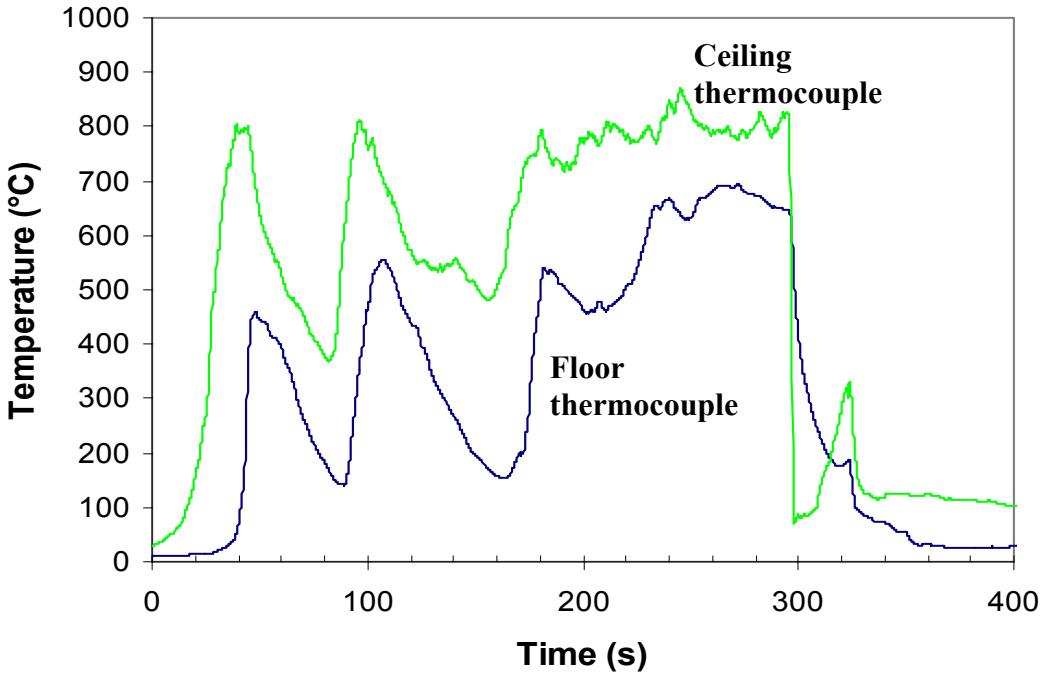

FIGURE 2.2: Thermocouple data for full scale fire test, Saskatoon, October 2002.

There are two major dips in the growth of the fire as demonstrated in Figure 2.2. Comparing this figure with the video of the fire, it was noted that the first dip, occurring around 65 seconds, corresponds with the time of the window breaking. The effect of the outside air coming in through the window opening was to cool the fire room. The second dip in the growth of the fire occurred at approximately 110 seconds, this dip corresponds with the fire room door opening as the fire fighters entered the room and removed the manikin. The door was closed again after the manikin was removed. Following these dips in the graph, the fire grew until the fire fighter's hose extinguished it at approximately 300 seconds. A fully developed fire happens when all of the elements in the room are involved in the fire; the point in time when this first occurs is known as flashover. The flashover point of a fire can be defined in a number of ways: one definition is the point in the fire history when there is no thermal gradient with height in a room, another definition calls for

a ceiling temperature of 600°C, while another is the point at which there is a heat flux of 20 kW/m^2 at the floor (hot enough for spontaneous ignition of paper on the floor); a final definition is the moment at which flames emerge from an opening [10]. It is noted that at no point in this test did the floor temperature reach the ceiling temperature, however visual observations revealed that flames did emerge from the window after approximately 2 minutes, and the ceiling temperature certainly reached 600°C so it can be suggested that flashover did occur.

2.2 Edmonton Full Scale Fire Tests

A second set of full scale fire tests was conducted in Edmonton, Alberta in July 2003 in collaboration with the University of Alberta Department of Mechanical Engineering and the City of Edmonton Fire Department, among others[1]. On a former military base in Edmonton, a block of residential houses were slated for relocation or demolition to allow for redevelopment of the area. One particular house was used for three controlled burns in which the local Edmonton fire department conducted training exercises. Each of these burns involved lighting a different room in the house, then extinguishing the flames. The house was then completely destroyed in a fourth and final burn. The house was instrumented with heat flux gauges and thermocouples. Figure 2.3 shows the general layout of the main floor of the house, a simple four room design. Figure 2.4 gives the layout of the living room, where the final burn was started, and the location of heat flux gauges (q'') and thermocouples (T/C). Further schematics of the house floor plan and other rooms are available in [31].

[1] This test involved collaboration between many different agencies, including the Royal Canadian Mounted Police Forensic Unit, Canadian Armed Forces and researchers from Simon Fraser University.

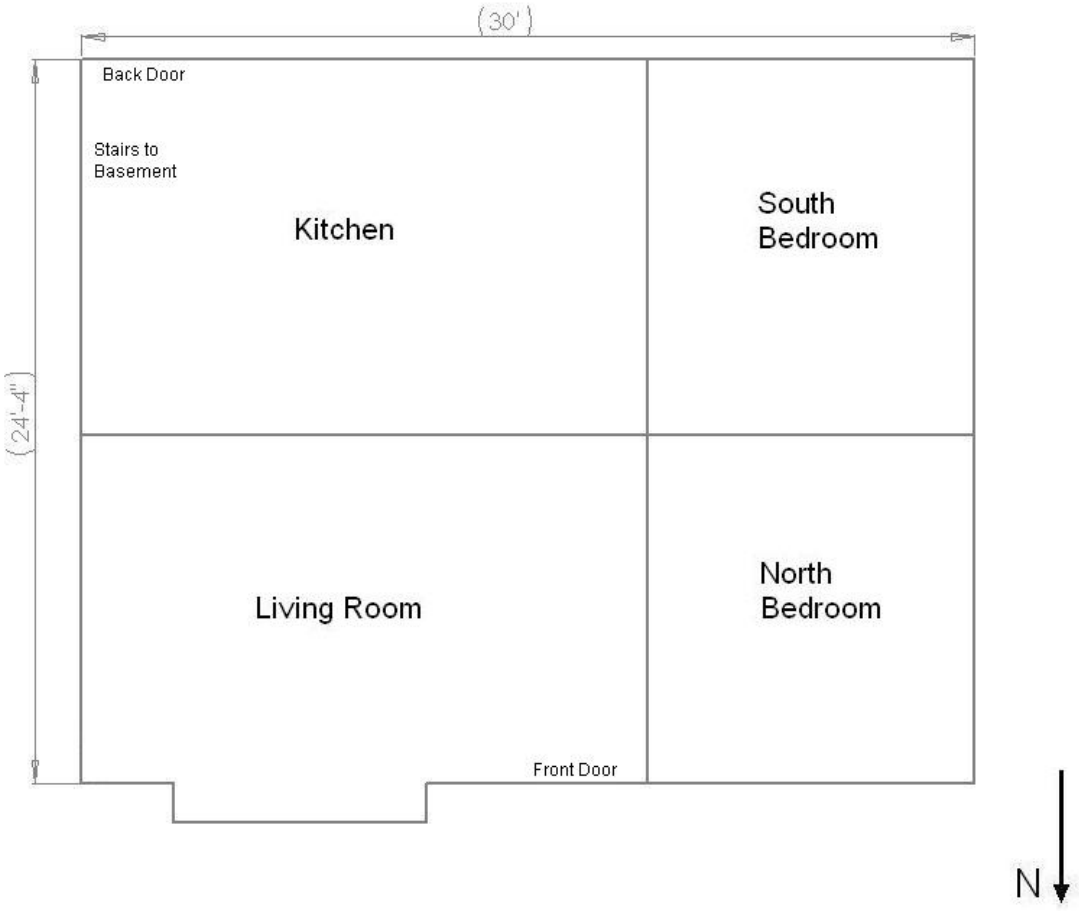

FIGURE 2.3: Edmonton full scale fire test bungalow main floor plan [31] (reprinted with permission)

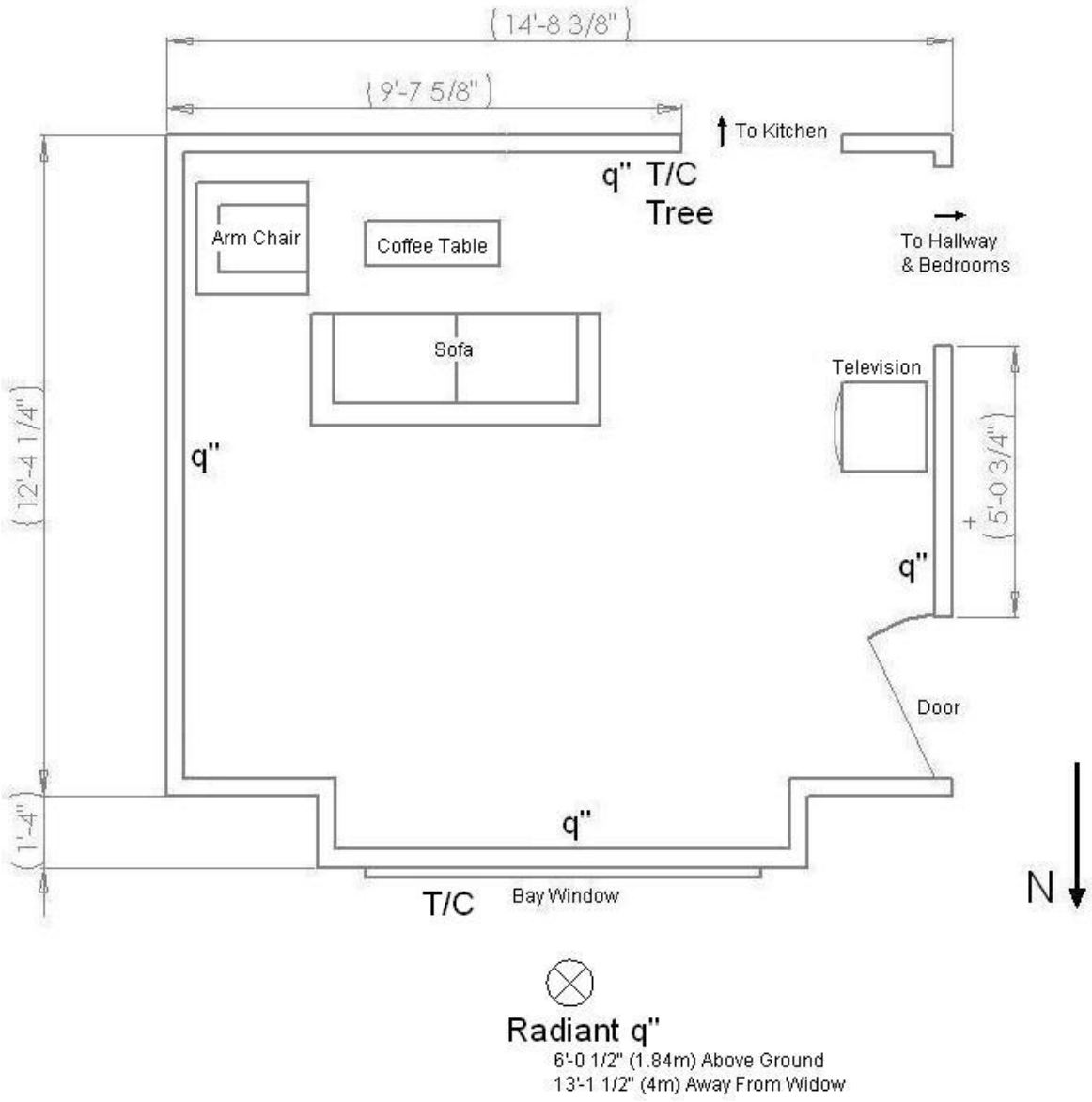

FIGURE 2.4: Living room, room of fire origin for final burn in Edmonton, 2003 [31] (reprinted with permission)

Described in detail by Threlfall, Torvi and Thorpe [32], and by Dale, Ackerman, Torvi, Threlfall and Thorpe [33], of note for this thesis is the examination of heat flux levels outside of the living room window of the house during the final burn. This location demonstrates heat fluxes outside the flame envelope but still within the range of potential degradation to protective equipment due to heat. Four gauges were used to

measure heat fluxes. Two of these gauges, a Gardon gauge and a Schmidt-Boelter gauge, were obtained commercially from Medtherm Corporation (Huntsville, AL). Two thin-film heat flux gauges, manufactured by the University of Alberta, were also used. A tripod was outfitted with the four heat flux sensors and placed 4 m from the base of the exterior wall and mounted 1.75 m above the ground in front of the bay window. This location for the heat flux gauges was considered appropriate as an example of a point from which fire fighters carry out typical operations, in conditions that would range from ordinary to emergency using Veghte's [12] criteria. Figure 2.5 tracks the temperature history at the measurement point outside of the house. The temperatures were measured using a thin-film heat flux gauge. The material used for this type of gauge is chosen because it has properties similar to human skin, so this temperature history may be similar to the temperatures that skin would experience when exposed to the same heat fluxes.

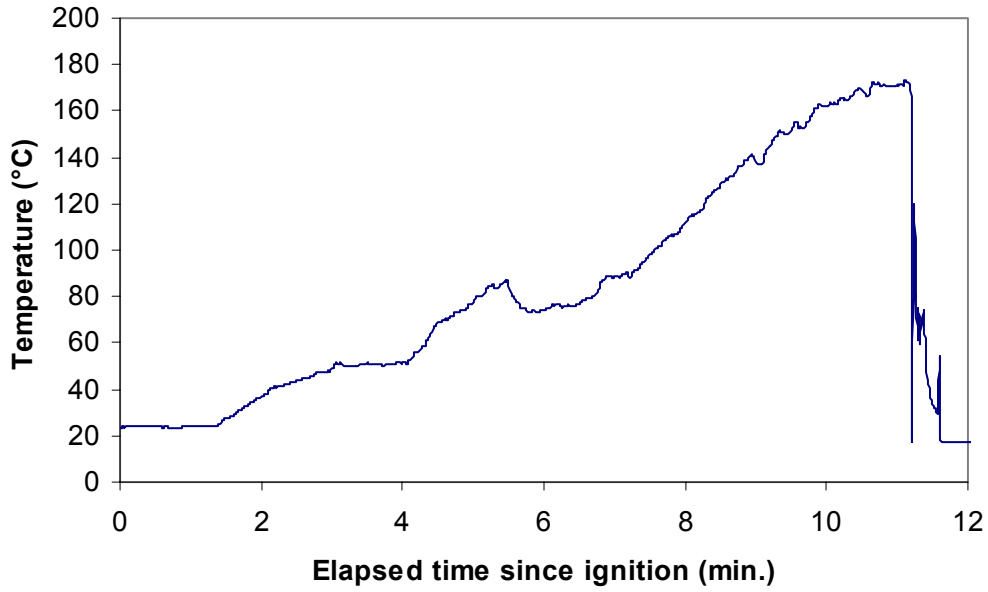

FIGURE 2.5: Temperature history of thin-film heat flux gauges outside house
After 11 minutes the test stand was removed to prevent damage to the equipment.

Figure 2.6 reports the heat fluxes during the final burn measured by a Gardon gauge on the measurement stand. The heat fluxes measured by the other three gauges were similar, so they are omitted for clarity.

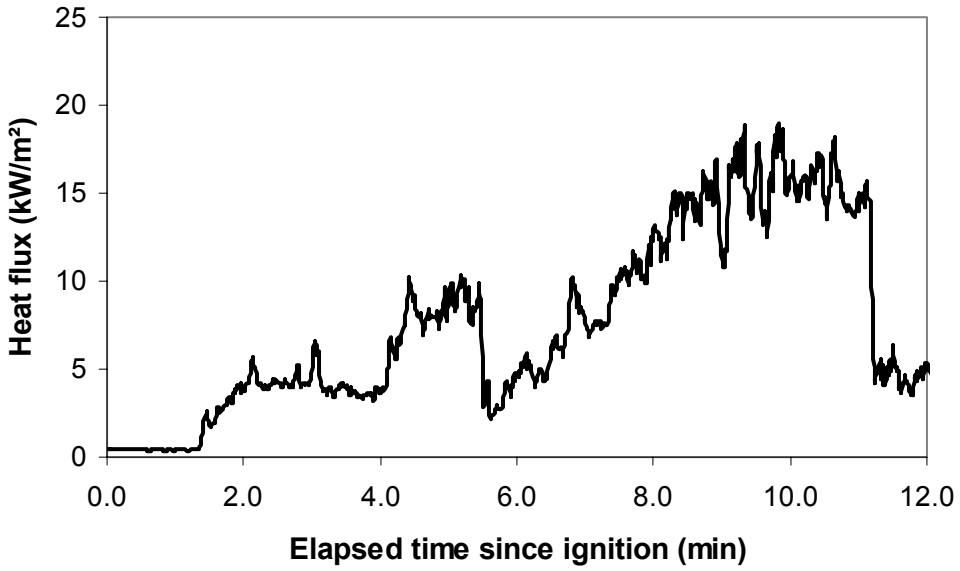

FIGURE 2.6: Heat flux data from Edmonton house burn

The heat flux escalates as the burning area of the exterior face of the house increases. This increases the area of the flames and hence the area that emits thermal radiation to the heat flux gauges on the tripod. The escalation of a fire depends on which pieces of the house have caught fire. Gypsum drywall acts as an insulator, so it provides some protection to the house; for this reason, it may be safely concluded that the structural elements of the house caught fire later than the furniture inside. The fire was lit from the inside under a chair and took some time to build up to the maximum intensity. During the initial stage of the fire, the heat flux outside the house fluctuated near 4.5 kW/m^2, then in the second stage the heat flux was approximately 9 kW/m^2. The heat flux drops at approximately 5.5 minutes. Examination of photographs of the test

suggests that the smoke became very thick and dark at this time. The smoke could serve to absorb the radiation from the inside of the house, reducing the radiation that reaches the heat flux sensors. Following these stages, the whole house caught fire so the heat flux grew steadily. The heat flux gauges were removed at approximately 11 minutes. Throughout the fire, fire fighting personnel were observed to assess their level of comfort with the hazards of the fire ground. It was noted that during the first two stages of this final burn, the fire fighters did indeed treat the exposure as routine and ordinary as their movements were casual and unhurried (see Figure 2.7). In the final stage, the response of the fire crew was one of increased diligence. Their movements became swift and deliberate as the exposure levels were turning towards an emergency condition (see Figure 2.8).

FIGURE 2.7: Fire fighters near heat flux gauge exhibiting casual response to exposure

FIGURE 2.8: Fire fighters approaching heat flux gauge with caution

Based on the results of these full scale fire tests radiant heat fluxes of 5, 10, 15, 20 and 30 kW/m^2 would be used in this research to simulate high heat flux exposures that turnout gear would experience in the field. This range of heat fluxes provided a mixture of Veghte's routine, ordinary and emergency exposure levels, but are lower than the

heat fluxes used in typical bench-top tests[2]. Selecting these exposures also allowed an examination of relatively long duration exposures to a range of heat flux levels.

2.3 Radiant Panel Exposures of Fabric Specimens

Fabric specimens were exposed to relatively low heat fluxes for a variety of times using a radiant panel apparatus at the University of Alberta's Textile Analysis Service. The apparatus is described in the ASTM Standard Test Method for Radiant Protective Performance of Flame Resistant Clothing Materials (ASTM F 1939) [28]. The standard uses this apparatus to test the resistance of protective clothing to a purely radiative heat flux. In the standard two different exposure situations are mandated: 84 kW/m^2 (2.0 cal/cm^{2}s) and 20 kW/m^2 (0.5 cal/cm^{2}s) for 40 seconds each. There is some concern whether the fabrics will perform differently in the two different situations; some fabrics may perform well in high heat flux but perform poorly in low heat flux with a long exposure. To investigate this possibility, the two exposure situations are mandated by ASTM F 1939.

The radiant panel performance tester (Figure 2.9) consists of a bank of five quartz tubes (Figure 2.10) that produce heat due to electrical resistance and a variable voltage supply that produces direct current voltage up to 5 Volts with a dial apparatus for voltage specification.

[2] The Thermal Protective Performance Test described in NFPA 1971 is a standard bench-top test that uses a heat flux of 84 kW/m^2 supplied by two flame burners and a bank of quartz tubes.

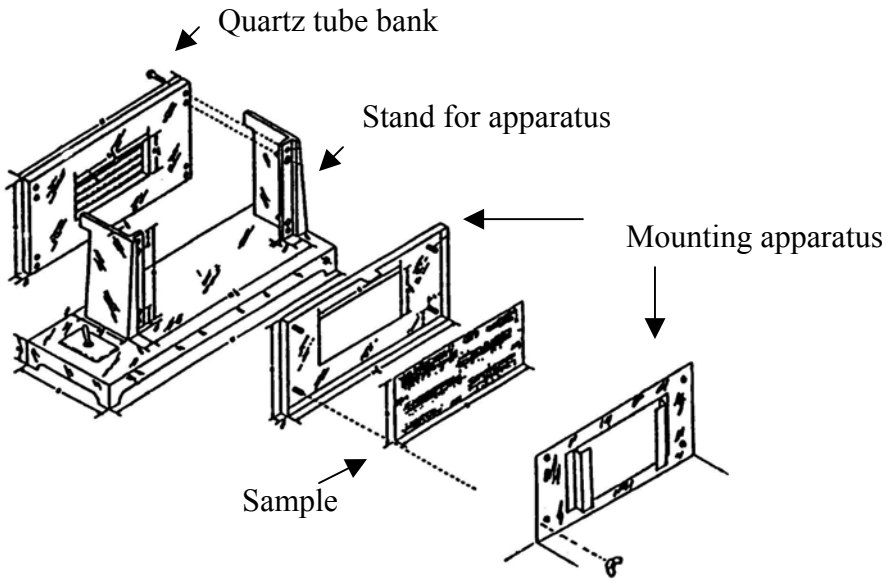

FIGURE 2.9: Radiant panel performance tester [28] (reprinted with permission)

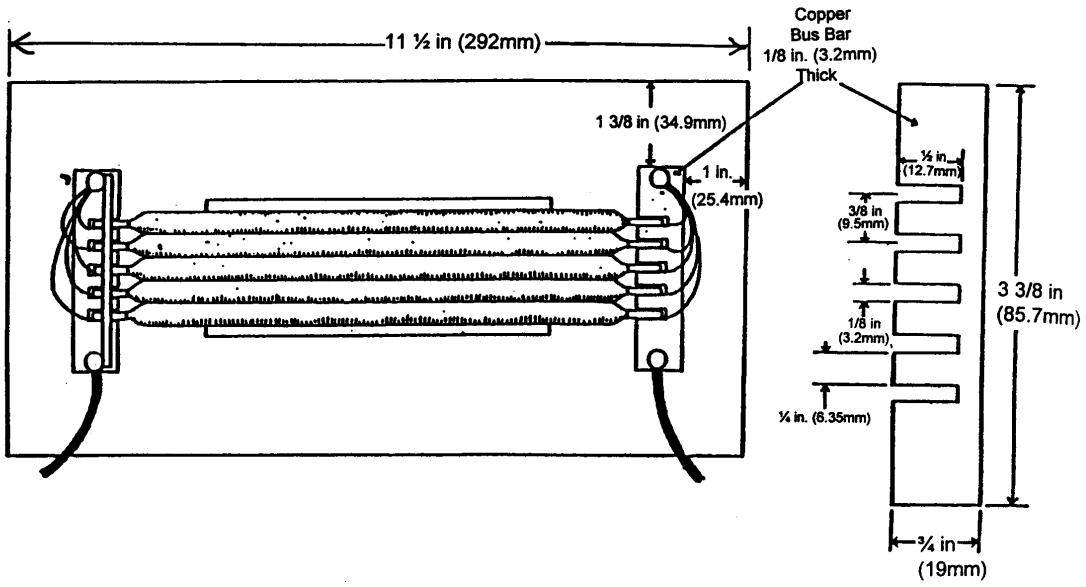

FIGURE 2.10: Detail of quartz tube bank [28] (reprinted with permission)

The digital voltmeter gives a precision of hundredths of a Volt, but fine tuning is fairly difficult. The apparatus is illustrated in the standard, but modifications have been made by University of Alberta researchers: the manually operated shutter has been water cooled by machining channels through it and adding a water pump to the total

apparatus. This was done to reduce the danger to the operator in manipulating the shutter and to reduce the heat flux to the fabric prior to the test.

The three layers that comprise the fabric ensemble were cut into rectangles 6 in. (15.2 cm) x 4 in. (10.2 cm) and selected at random to form ensembles. These ensembles were conditioned in a temperature and humidity controlled room for at least 8 hours[3], and then placed in the apparatus. A series of tests were run for each of the exposure levels that were selected. The heat exposures to which the ensemble samples were subjected are summarized in Table 2.1. Exposure times were chosen to provide a range of degradation. For the lowest exposure level, 5 kW/m^2, testing was conducted at 10 minute intervals and eventually stopped because the visible degradation was unchanged from 10 minutes to 60 minutes. For the highest exposure level, 30 kW/m^2, testing culminated at 120 seconds because the fabric was so charred and brittle that it could be deemed to be totally degraded.

TABLE 2.1: Heat flux levels and durations used to expose fabric specimens

Heat flux (kW/m^2)	**Exposure time (seconds)**							
5	600	1200	1800	2400	3000	3600		
10	120	240	480	600 [a]	720	900		
15	60	90	120	150	240	360	600	
20	30	45	60	75	90 [a]	105	120	180
30	30	45	60	120				

[a] Three ensemble specimens were exposed to this heat flux and duration.

The heat flux produced by the panel was calibrated by using the copper calorimeter specified in the ASTM standard and plotting temperature rise with time. The copper

[3] NFPA 1971 requires that all tests be conducted on specimens that have been conditioned at a temperature of 21°C, ±3°C,and a relative humidity of 65 %, ± 5 % for a minimum of 8 hours [3]

calorimeter consists of a disk made of electrical grade copper with diameter 40 mm, and 1.6 mm thickness. Four 30 gauge thermocouples are connected in series and peened to the back of the disk. The disk is mounted in insulation board and the front surface is painted with flat black spray paint. The thermocouples measure temperature and time using digital data acquisition. The slope of the temperature-time line is used to calculate heat flux, q'' (W/m^2), since the material properties of known thermal mass is known. Using the formula for a lumped capacitance,

$$q'' = \rho \cdot w \cdot c_p \cdot \frac{\Delta T}{\Delta t}, \qquad (2.1)$$

where ρ is the density of the copper (8954 kg/m^3), w is the thickness of the disk (0.016 m), c_p is the specific heat of the copper (385 J/kg·°C), T is temperature in Celsius and t is the time in seconds. The heat flux is calculated using the temperature rise measured over an interval of 10 seconds after the beginning of an exposure to the panel.

Using the heat flux measured by the copper calorimeter, heat flux levels were selected by varying the voltage control until the required heat flux was measured. Due to a limited supply of fabric, only one fabric specimen was used at each of the heat fluxes and durations listed in Table 2.1, with the two exceptions noted. Therefore, a statistical representation of each exposure time was not obtained. However, three specimens were exposed to two representative heat flux levels and durations to determine the repeatability of this testing.

Real time observations during the exposures were limited due to the apparatus obscuring the view of the ensemble, but the level of smoke production and odour was deemed to be one indication of degradation. The end condition of the samples varies

according to the level of heat to which the sample was exposed. The outer shell material was the closest to the heat source and as such suffered the most damage due to the radiant exposure. Outer shell samples start brown, then as they are exposed to more heat, begin to fade to yellow and then turn a darker brown and eventually black. Moisture barrier samples show a light browning on the backing fabric and embrittlement of the ptfe membrane. With more heat the membrane becomes very flaky and turns black. The thermal liner exhibited little degradation with the exposures used in this testing, but the more heavily exposed liners exhibited browning in the batting fabric and some fading and browning of the face cloth. The thermal liner also became harder and less flexible as it experienced more heat exposure.

Figures 2.11 through 2.13 show the examples of the effects of radiant heat flux exposures on the outer shell material. Shown is a progression for an exposure level of 10 kW/m^2; refer to Appendix A for images of all of the exposures. Note the fade to yellow and subsequent darkening of the fabric as this will become important in later chapters of the thesis.

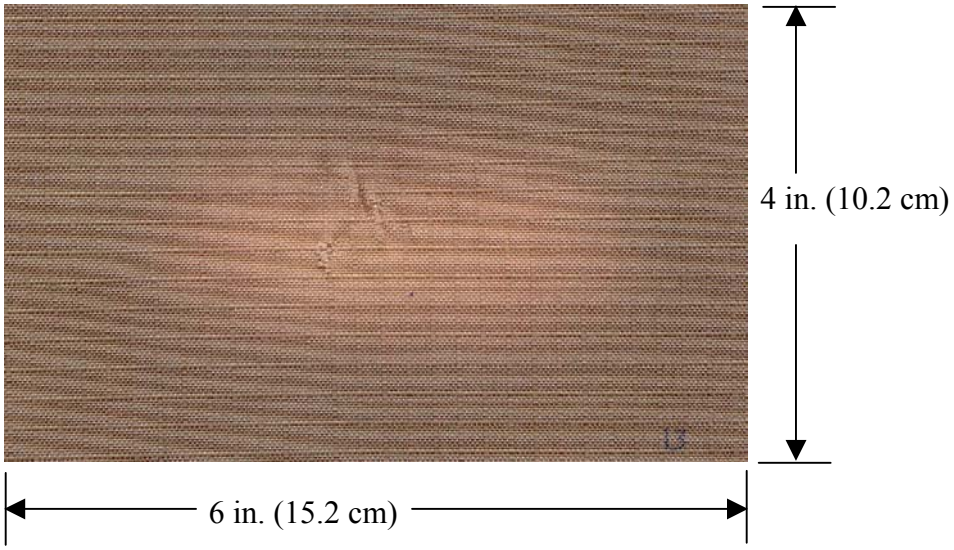

FIGURE 2.11: Outer shell fabric sample after 120 seconds of 10 kW/m^2 radiant heat flux exposure

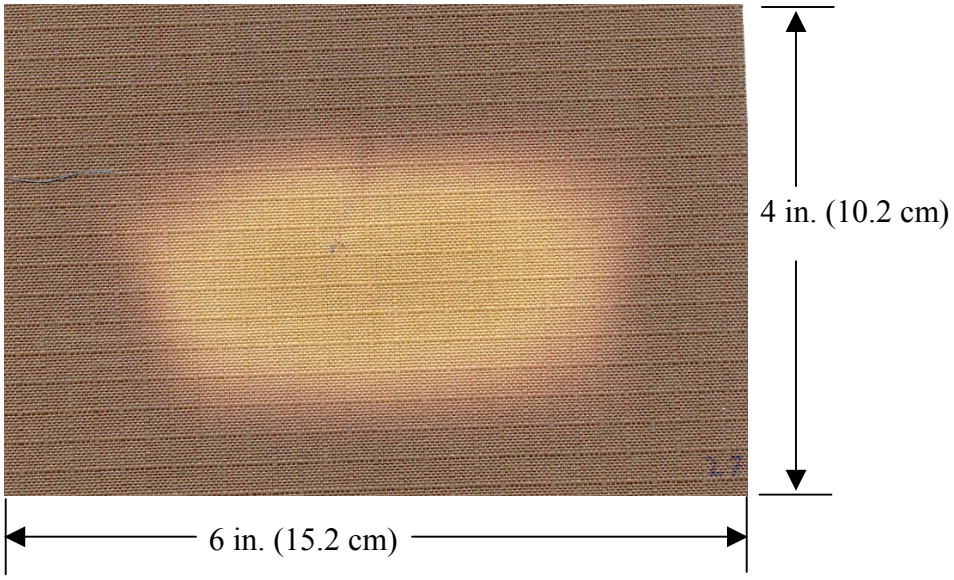

FIGURE 2.12: Outer shell fabric sample after 600 seconds of 10 kW/m^2 radiant heat flux exposure

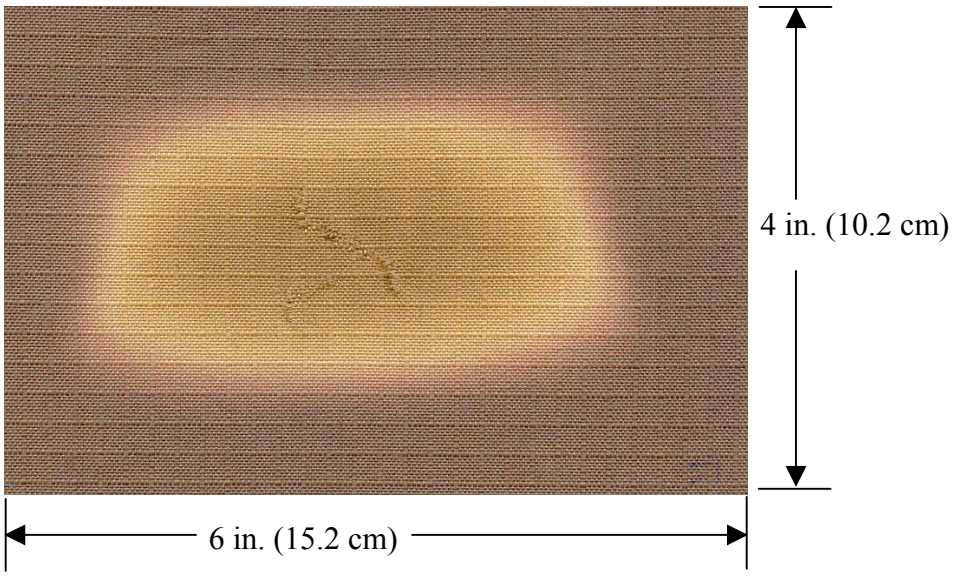

FIGURE 2.13: Outer shell fabric sample after 900 seconds of 10 kW/m^2 radiant heat flux exposure

The characteristic shape of the exposure on the fabric is due to the shutter apparatus and the shape of the aperture on the apparatus. With a battery of these fabric samples exposed, the research now switched to the analysis and assessment of the degradation. The next chapter will describe the destructive tests that were conducted to analyse these specimens.

CHAPTER 3: DESTRUCTIVE TESTING[4]

To examine the performance of the fabric specimens before and after the laboratory exposures, performance specifications were selected from requirements used for new garments. NFPA 1971 [3] provides a test matrix that gives a series of tests and minimum performance criteria for turnout gear. There are over 50 individual tests provided in NFPA 1971; most of these tests are destructive in that they require cutting of the samples and typically further destruction in the course of the testing. There are too many tests listed in the NFPA 1971 standard to conduct all of them in the course of this research, so only a sample was chosen. Tests were chosen based on the accessibility of testing apparatuses and an assessment of the tests' specific importance for the garments. Vogelpohl [21] identifies tear strength and tensile strength as tests that some of the retired turnout coats failed in her study, so these tests were considered appropriate. In addition to these destructive tests, non-destructive tests were also developed, which will be described in detail in Chapter 4. Destructive and non-destructive test results are then compared in Chapter 5.

The destructive tests were primarily chosen from those specified in NFPA 1971. Table 3.1 lists the tests employed in this research and the particular ensemble elements

[4] Some material from this chapter and Chapter 4 has been accepted for publication in the Journal of the American Society for Testing and Materials [34].

that were tested using each method. Descriptions of the destructive test methods are provided in this chapter, along with the results obtained for each test.

TABLE 3.1: Tests used to evaluate fabric specimens after exposures

Destructive Tests	**Ensemble Elements Tested**
Ensemble temperature measurements	All elements
Thermogravimetric Analysis	All elements
ASTM F 903: Standard Test Method for Resistance of Protective Clothing Materials to Penetration by Liquids[a] [35]	Moisture Barrier
ASTM F 1060: Standard Test Method for Thermal Protective Performance of Materials for Protective Clothing for Hot Surface Contact [36]	Thermal Liner
ASTM D 5034: Standard Test Method for Breaking Force and Elongation of Textile Fabrics (Grab Test) [37]	Outer shell
ASTM D 5733: Standard Test Method for Tearing Strength of Nonwoven Fabrics by the Trapezoid Procedure [38]	Moisture Barrier, Thermal Liner
Non-Destructive Tests	**Ensemble Elements Tested**
Optical Microscopy	Outer shell
Raman Spectroscopy	Outer shell
Digital Image Analysis	Outer shell
Colorimetry	Outer shell

[a] While a test for liquid penetration is not necessarily destructive, the standard requires the use of a standardized outer shell and thermal liner, requiring the tester to cut the moisture barrier out of an in-use ensemble.

The ensemble temperature measurements were made during the radiant panel exposures and during one other bench-top test exposure, the thermogravimetric analysis tests were conducted independently of the radiant exposure. Both tests involved observing unexposed garment ensemble specimens as they were subjected to a high heat flux level. All of the ASTM tests were conducted after the radiant panel exposures listed in Table 2.1. ASTM F 903 and ASTM F 1060 were performed before ASTM D 5733 and

ASTM D 5034 because the latter two resulted in catastrophic failure of the garment elements.

3.1 Ensemble Temperature Measurements

The fabric ensemble was subjected to 80 kW/m^2 radiant and convective heat for 10 seconds of heating followed by 50 seconds of cooling. The apparatus is described in ASTM D 4108 Standard Test Method for Thermal Protective Performance of Materials for Clothing by Open-Flame Method [39], and uses a single Meker burner to provide the high heat flux exposure. Compressed propane provides the fuel for this testing. This heat flux level is typical of the thermal protective performance testing mandated in NFPA 1971 although NFPA 1971 specifies an exposure that is produced by a combination of quartz tubes and flame burners. One type K 24-gauge thermocouple was placed between each of the layers, one was sewn to the flame side of the outer shell and one was sewn to the skin side of the thermal liner. An Agilent (Palo Alto, CA) 34970A digital data acquisition system recorded the temperatures with time. Figure 3.1 shows the results of one of these tests.

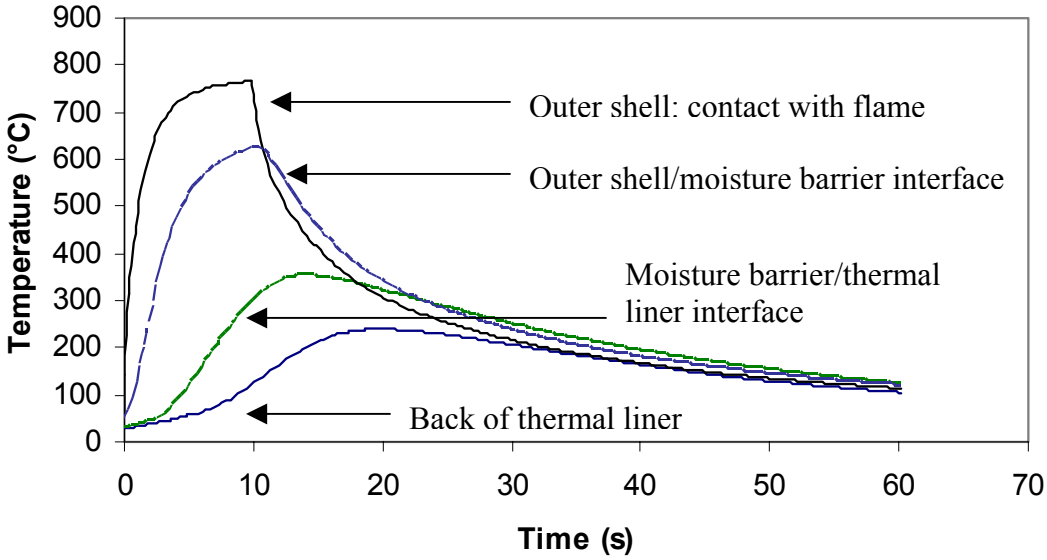

FIGURE 3.1: Ensemble temperatures during and after 80 kW/m^2 thermal flame exposure

The outer side of the outer shell obviously experienced the highest temperatures, as it was in direct contact with the flame. This curve has a sharper end point than the underlying layers because the flame exposure is removed abruptly, whereas in successive layers the heating continues due to conduction through the fabrics after the flame has been removed. This delayed heating means that in the inner layers the peak temperature comes after the removal of the exterior heat source. The cooling of the outer shell is also more rapid than for the other layers. This is because once the flame exposure is removed cool air begins to provide convective cooling to the fabric. The inner layers do not have that cool air source during the cooling phase of this test. In the field, fire fighters use a couple of methods to provide cooling: they will leave the area of high heat flux, spray themselves with cool water or open the coat to allow the outside air to reduce the temperature inside the coat [9].

While the inner surface of the ensemble is the closest thermocouple to the skin, the temperature indicated on the figure is not likely what the skin of the fire fighter would experience. This is because a uniform is typically worn underneath the turnout gear, and there are air gaps between the garment and the fire fighter that provide more insulation. While the skin may not experience these temperatures, the turnout gear certainly does. The implications of these temperatures on the layers of the turnout ensemble will be explored in future sections of this chapter. These data will be compared with thermogravimetric analysis results, to pinpoint the temperatures that result in the most degradation.

Temperatures were recorded in a similar manner (using a data acquisition device and thermocouples sewn onto the ensemble layers) during the radiant heat flux exposure (described in Section 2.3), measured at a sampling rate of one every second. The thermocouple that was recording the temperatures at the outer shell flame contact broke early in the testing, so no temperatures were measured at this position on the ensemble. Figures 3.2 to 3.6 give the results of the temperature measurements during the radiant heat flux exposures.

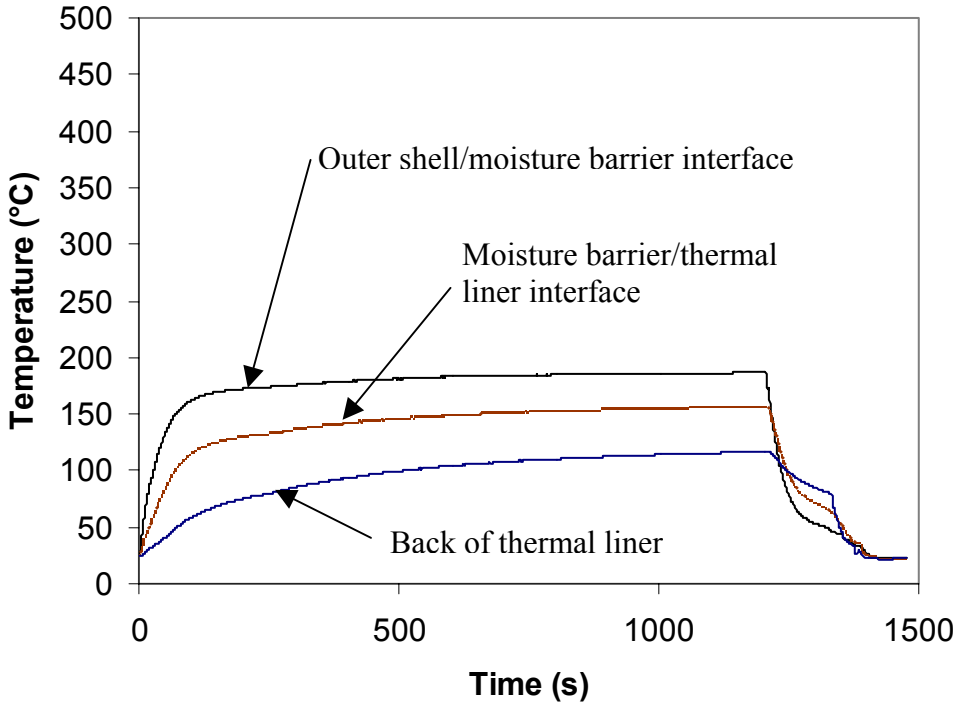

FIGURE 3.2: Temperature measurements during and after 5 kW/m^2 radiant exposure

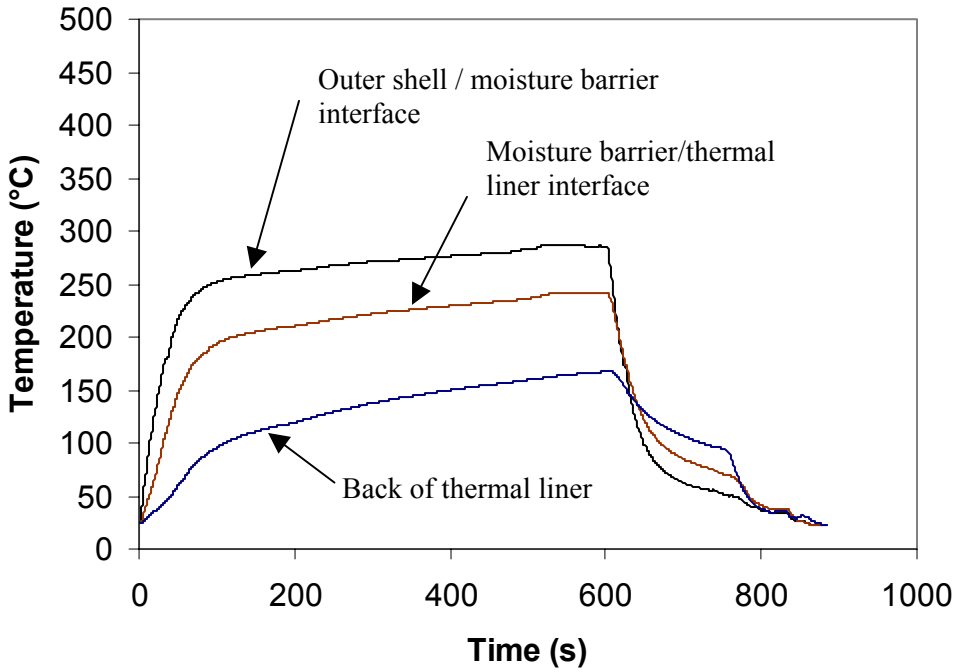

FIGURE 3.3: Temperature measurements during and after 10 kW/m^2 radiant exposure

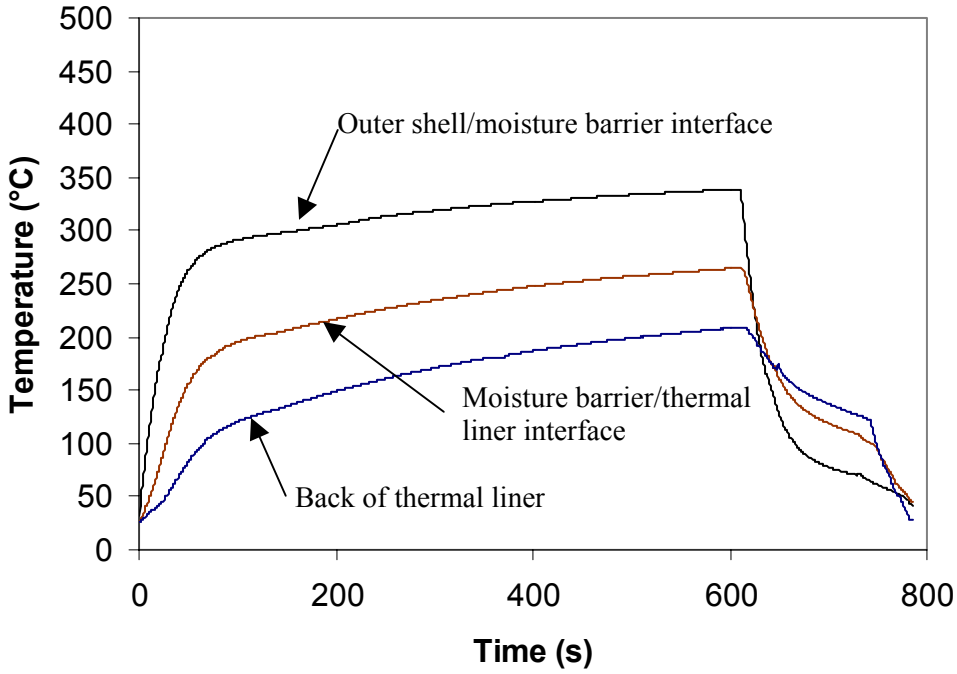

FIGURE 3.4: Temperature measurements during and after 15 kW/m^2 radiant exposure

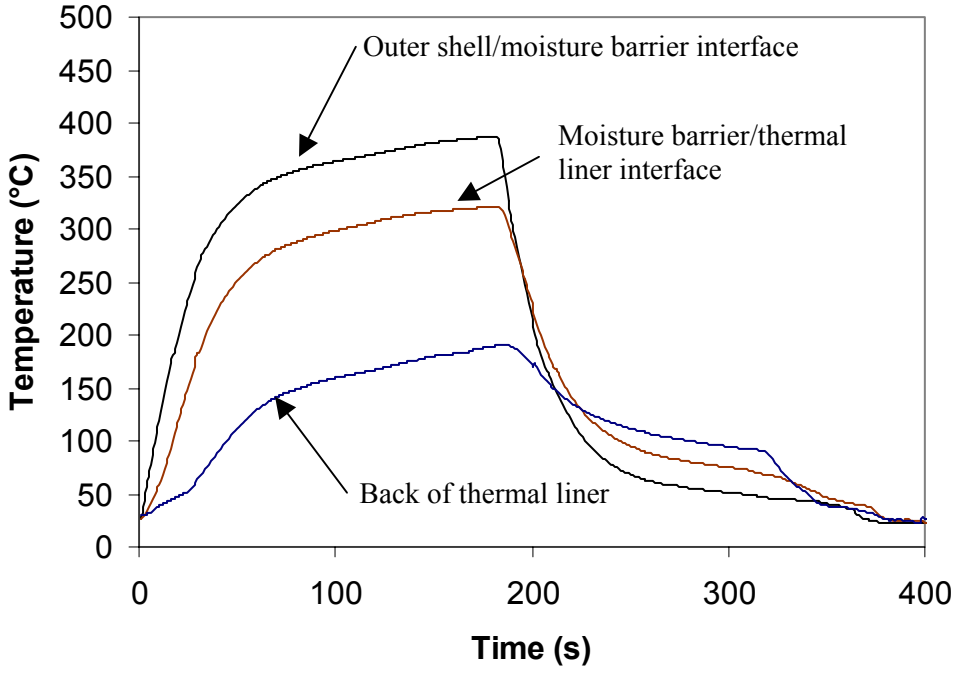

FIGURE 3.5: Temperature measurements during and after 20 kW/m^2 radiant exposure

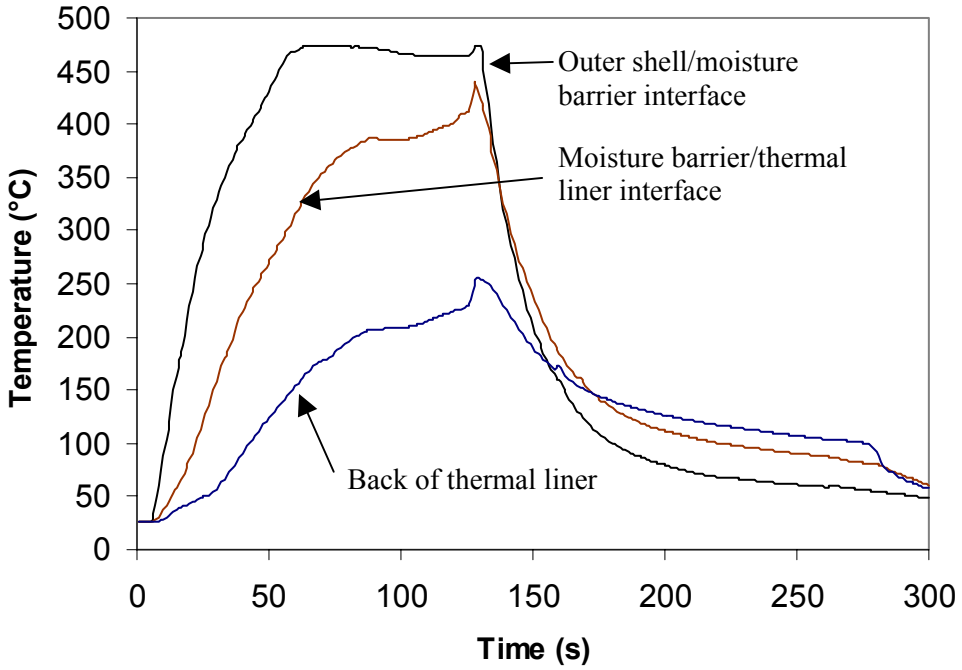

FIGURE 3.6: Temperature measurements during and after 30 kW/m^2 radiant exposure

The shape of the curves in Figure 3.6 is inconsistent with the other radiant exposure temperature measurements. Rather than rising smoothly with time, after approximately 60 seconds the outer shell/moisture barrier interface temperature plateaus then drops slightly. The two temperature curves rise irregularly until finally dropping off, though the shape of these curves follows that of the outer shell/moisture barrier curve. The odd shape of these curves can be explained by appealing to visual observations of the ensemble after 60 seconds of radiant exposure to a heat flux of 30 kW/m^2. After this exposure the outer shell has become very black (see Figure A.28) and consequently very weak. The outer shell has become very brittle and thin after this thermal exposures; the fabric is nearly entirely degraded at this point. This degradation reduces the thermal resistance of the fabric, a reduction that has ramifications for the subsequent

ensemble layers. Loss of thermal protection from the outer shell results in higher temperatures to the other layers.

These figures demonstrate an increase in peak temperatures with increasing heat flux. There is evidently a large temperature gradient across the thickness of the fabrics. The relative magnitude of the temperature gradients across the different layers indicate the greater insulating performance of the thermal liner, as there is a greater temperature gradient across the thermal liner than the moisture barrier. These figures will be used in the discussion of thermogravimetric analysis results in the next section.

3.2 Thermogravimetric Analysis

Thermogravimetric analysis is a test method that involves heating a specimen at a specified rate and recording the change in the mass of the specimen [40]. The temperatures at which major mass changes occur are determined using this method. For this research, a Mettler-Toledo (Schwerzenbach, Switzerland) Star system with TGA/SDTA85 module was used. It has two arms at the end of which are pans or crucibles that hold the samples. Testing was conducted in a nitrogen rich environment. The specimens were heated from room temperature to 575°C at a rate of 20°C/min.

The ensemble was divided into four different elements: the outer shell (60% Kevlar®, 40% Nomex®, dyed brown), the moisture barrier (polytetrafluorethylene based membrane layer), the thermal liner batting (undyed Kevlar®) and the thermal liner face cloth (Nomex®, dyed blue). Each element of the ensemble was tested in this manner;

results are shown in Figures 3.7 to 3.10. The mass changes in the fabrics are evident from the TGA plots. Plotted along with the TGA results are differential thermogravimetric (DTG) results for the same tests. This is the difference between the temperature near the sample and a reference program temperature. This creates similar data to differential scanning calorimetry as the data "indicates whether a weight loss measured by thermogravimetric analysis is an exothermic or endothermic process [41]." This information gives more evidence as to which temperatures are the most significant in the degradation of the fabrics. An increase in the DTG signal indicates an endothermic reaction.

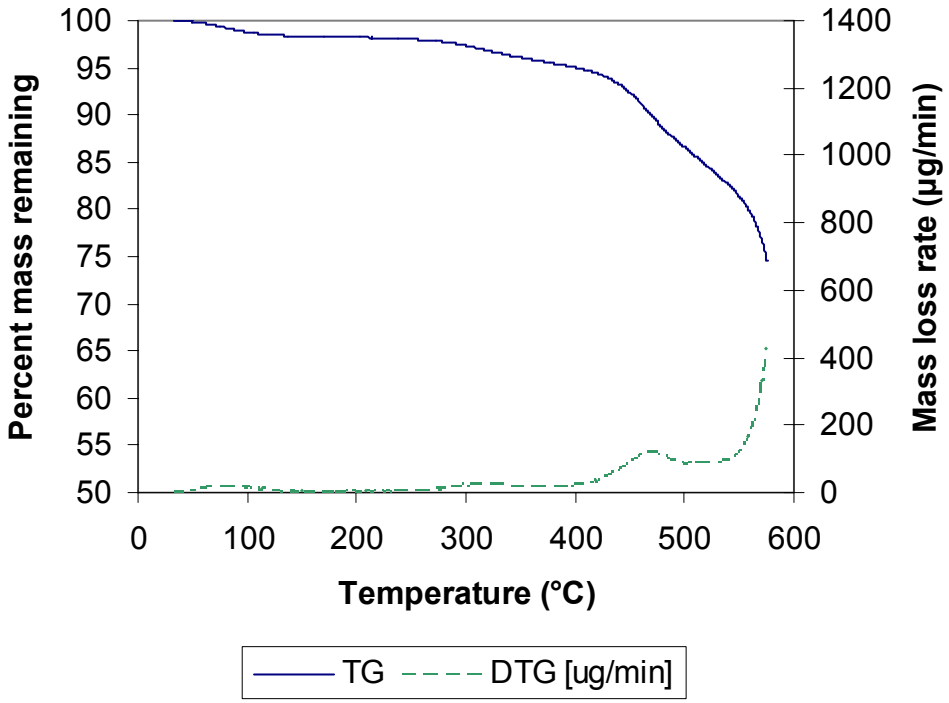

FIGURE 3.7: TGA curve for outer shell specimens (60% Kevlar®, 40% Nomex®, dyed brown) at 20°C/min heating rate, 28 minute test.

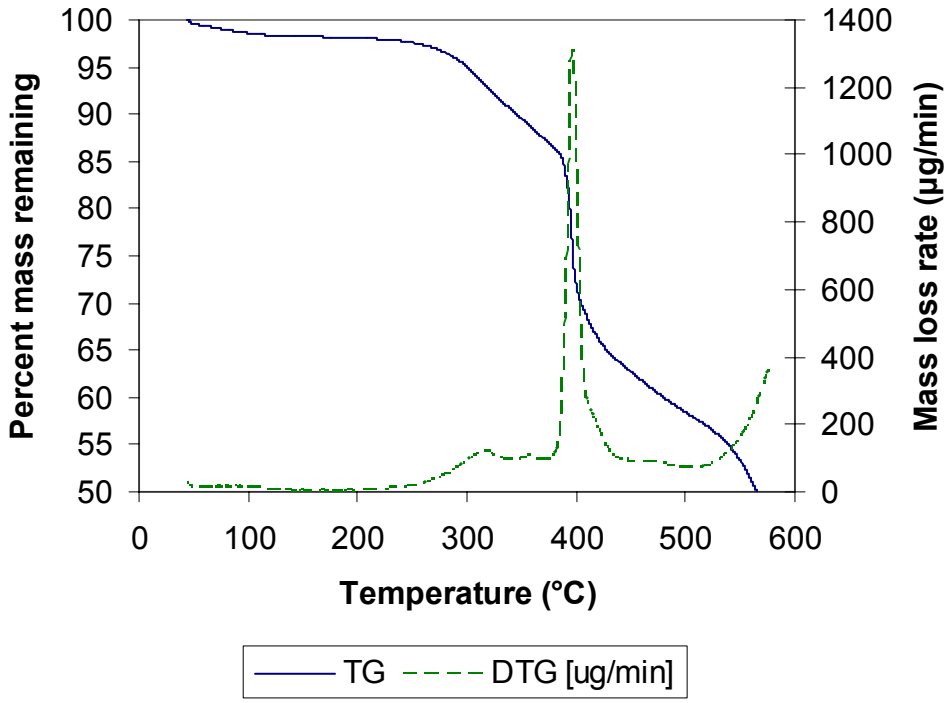

FIGURE 3.8: TGA curve for moisture barrier specimens (ptfe membrane) at 20°C/min heating rate, 28 minute test.

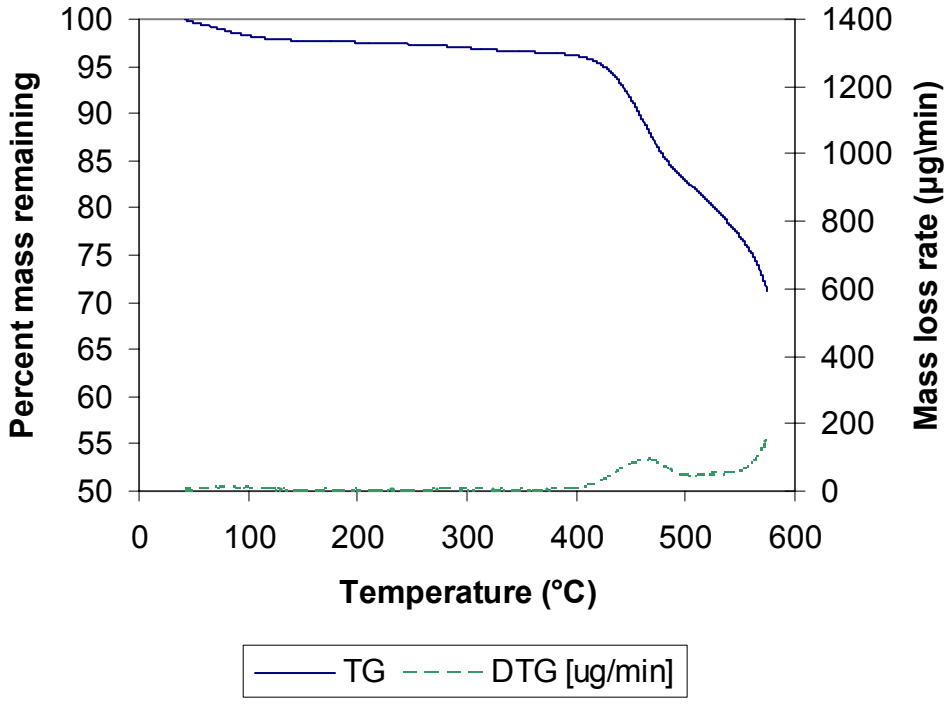

FIGURE 3.9: TGA curve for thermal liner batting specimen (undyed Kevlar®) at 20°C/min heating rate (28 minute test).

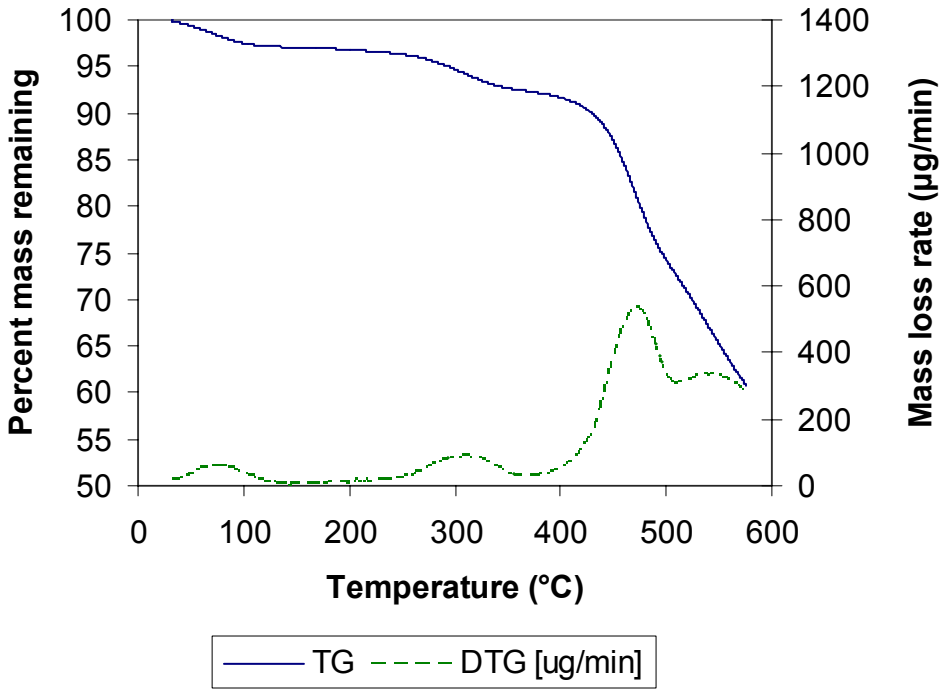

FIGURE 3.10: TGA curve for thermal liner face cloth specimen (Nomex®, dyed blue) at 20°C/min heating rate (28 minute test).

The first drop in mass, seen in all four TGA traces, occurs at approximately 100°C; this corresponds with the moisture in the fabric evaporating. Following these mass drops, curves for the outer shell (Figure 3.7), the thermal liner batting (Figure 3.9) and the thermal liner face cloth (Figure 3.10) are very similar. Due to the similarities in chemical structure in the materials used in these three layers, one would expect that the TGA curves would have similarities.

The batting material is of the natural Kevlar® colour, while the outer shell is dyed brown and the Nomex® face cloth is dyed blue. Examining the curves in light of this knowledge suggests that the mass drop and energy change at approximately 300°C is the result of the dye being removed. A comparison of the DTG curves in Figures 3.9 and 3.10 demonstrates the removal of the dye at approximately 300°C.

The largest decrease in mass for these three specimens occurs at approximately 420°C, as the polymers are experiencing changes in their structure. Charring has begun and some of the fibres are beginning to experience melting. The increase in the DTG curve at approximately 575°C for the batting and the outer shell indicates that the Kevlar® is starting to experience more significant degradation at this point. Kevlar® has a higher glass transition temperature than Nomex® [42], so this observation is logical.

A comparison between the TGA traces for the Nomex® and Kevlar® elements of the ensemble and the temperatures recorded during the radiant panel exposure will be useful. As noted above, temperatures near 300°C were required for removal of the dye in the face cloth, while temperatures of more than 400°C were required for degradation of the Nomex® and Kevlar®. As the temperatures recorded at the moisture barrier/thermal liner interface and at the inner surface of the thermal liner (Figures 3.2 to 3.5) only exceeded these critical temperatures for exposures of 20 and 30 kW/m^2, it is expected that the thermal liner did not experience significant degradation during the 5, 10 and 15 kW/m^2 exposures. Some degradation is expected to occur during the longer exposures to 20 and 30 kW/m^2 of radiant heat flux (Figures 3.5, 3.6).

The outer shell material actually experienced greater temperatures on the side closest to the quartz tubes of the radiant panel performance apparatus than is indicated in Figures 3.2 to 3.5. As previously mentioned, the outermost thermocouple on the outer shell broke, so the actual temperature on the front surface of the outer shell can only be estimated. Figure 3.1 shows that across the outer shell, a temperature gradient of

approximately 150°C is possible. The gradient across the outer shell in the lower heat flux exposures is likely less than for the case of 80 kW/m^2 exposure, but it is reasonable to suggest that for each of Figures 3.2 to 3.6, the actual temperatures experienced by the outer surface of the outer shell may be at least 100°C higher than at the outer shell/moisture barrier interface. Applying this assumption and comparing Figure 3.7, the TGA trace for the outer shell, with Figures 3.2 to 3.6, it can be suggested that significant degradation is expected to occur in the outer shell at heat fluxes of 15 kW/m^2 and higher. Lower level heat flux exposures of 5 and 10 kW/m^2 likely did not result in the outer shell reaching a temperature at which degradation of the material would occur. A 5 kW/m^2 exposure may not even produce temperatures high enough to cause dye removal in the outer shell (approximately 300°C), so one would expect little colour change in these exposures. This hypothesis is consistent with visual observations of the outer shell colour.

The moisture barrier is made of a different polymer than the rest of the layers of the ensemble; as a result the TGA trace is quite different. Significant decreases in mass occur at approximately 300°C and 400°C. These mass losses correspond to the breaking down of the fabric, and the blackening of the material. Visual observations of moisture barrier specimens after the radiant panel exposures found that the moisture turned brown during longer duration exposures to the mid-range (10, 15 and 20 kW/m^2) heat fluxes. Visual evidence of exposure to 30 kW/m^2 radiant heat flux included portions of the specimens turning black. Comparing the TGA trace from Figure 3.8 and the results from Figures 3.2 to 3.6, it is observed that only in the 30 kW/m^2 exposure did the moisture barrier experience temperatures of 400°C. This demonstrates that the

second drop in mass in the TGA curve would not have been experienced by the moisture barriers that had been subjected to heat fluxes of less than 30 kW/m^2.

3.3 Liquid Penetration Testing

Moisture barriers perform a number of functions, as mentioned in Section 1.2; therefore they are tested in a number of ways, one of which is to examine the penetration of liquid through the barrier. There are a number of different standards referenced in NFPA 1971 for testing moisture barriers. Examples include: Federal Test Method Standard 191A, Method 5512, Water Resistance of Coated Cloth; High Range; Hydrostatic Pressure Method [43], ASTM Standard Test Method for Resistance of Protective Clothing Materials to Penetration by Liquids (ASTM F 903) [35] and ASTM Standard Test Method for Resistance of Materials Used in Protective Clothing to Penetration by Synthetic Blood (ASTM F 1670) [44].

The emphasis on resistance to penetration by synthetic blood indicates the desire to protect service personnel from blood borne pathogens such as Hepatitis and Human Immunodeficiency Virus (HIV). Modern moisture barriers are often designed to prevent liquid penetration, but to also reduce the build-up of perspiration by allowing gaseous transport outwards from the skin through diffusion. Studies have shown that some membrane moisture barriers exposed to heat saw a reduction of pore size that reduced the vapour transmission but increased the liquid penetration resistance [45]. Equipment constraints limited the moisture barrier testing conducted: neither vapour transmission nor penetration by synthetic blood was evaluated in this study.

The NFPA 1971 mandated tests for the moisture barriers all have a pass or fail criteria. A penetration test has been failed when there is "any evidence of liquid on the liquid absorptive garment, as determined by visual, tactile, or absorbent towelling [3]." Due to equipment constraints, the test as specified in the standard could not be performed, so modifications to the test method were made. To test the moisture barriers, evidence of liquid transmission through the membrane in an hour of exposure was measured. Each moisture barrier was placed over a sheet of paper towelling, and then a standardized amount of water was placed in the centre of the specimen. After one hour of exposure the paper towel was observed for evidence of liquid, as evidenced by discoloration of the paper towel. Any liquid penetration through the moisture barrier constituted a failure in this test. As indicated in Table 3.2, the moisture barriers performed very well in this testing. All moisture barriers without any holes that were visible to the naked eye passed the test.

TABLE 3.2: Moisture barrier liquid penetration testing

Exposure (kW/m^2)	Time (s)	Pass/Fail
5	600	Pass
5	1200	Pass
5	3000	Pass
5	1800	Pass
5	2400	Pass
5	3600	Pass
10	120	Pass
10	240	Pass
10	480	Pass
10	600	Pass
10	600	Pass
10	600	Pass
10	720	Pass
10	900	Pass
15	90	Pass
15	120	Pass
15	150	Pass
15	240	Pass
15	360	Pass
15	600	Pass

Exposure (kW/m^2)	Time (s)	Pass/Fail
20	30	Pass
20	45	Pass
20	60	Pass
20	75	Pass
20	90	Pass
20	90	Pass
20	90	Pass
20	105	Pass
20	120	Pass
20	180	Pass
30	30	Pass
30	45	Fail[1]
30	60	Fail[1]
30	120	Fail[1]

1: Failure due to tears in moisture barrier

Moisture barriers that had been subject to the 30 kW/m^2 exposure were so brittle that they were broken merely in the removal of the ensemble from the radiant panel performance testing apparatus. This finding again complements the findings of Sections 3.1 and 3.2, specifically that the moisture barriers experience significant structural change during longer duration 30 kW/m^2 heat fluxes.

It should be noted that this portion of the study only looked at the effects of the heat flux exposures on one property of the moisture barriers. A more thorough analysis of the moisture barriers would include an investigation of the effects of thermal exposures

on the vapour diffusion characteristics of the barrier. The resistance of the barrier to synthetic blood could also be studied. Using the appropriate testing apparatus, one could determine whether moisture barriers continue to meet the standards specified by NFPA 1971 after being exposed to various heat fluxes and durations.

3.4 Conductive and Compressive Heat Resistance

To assess the influence of the heat exposures on the conductive heat resistance of the ensemble and the insulation it offers, ASTM Standard Test Method for Thermal Protective Performance of Materials for Protective Clothing for Hot Surface Contact (ASTM F 1060) [36] was used. NFPA 1971 uses this standard to determine the conductive and compressive heat resistance (CCHR) of the knee and shoulder areas of the turnout coat. In the standard, each test specimen is cut into 101.6 mm by 152.4 mm (4 in by 6 in.) rectangles. The entire ensemble is tested in the standard, but it was determined that the conductive exposure could significantly degrade the outer shell. This is a result of the dye being removed from the outer shell specimens at temperatures around 300°C. Outer shell samples were still required for the tensile testing described in Section 3.5 so it was determined that only the thermal liner would be tested. It was observed that this temperature of testing did not result in any noticeable degradation of the thermal liner if the undyed Kevlar® batting was placed on the hot plate, so the liners were still appropriate for use in the tear testing that would follow (Section 3.6). The standard uses a hot plate at a constant temperature to provide the thermal exposure, while a steel block provides the pressure on the specimen to reproduce the pressure of a knee compressing the sample or the straps of an SCBA system. The copper calorimeter described in Section 2.3 is placed between the steel block and the specimen to record

the heat flux through the sample. An Agilent 39470A Data acquisition switch unit recorded the time of the test and the temperatures of the hot plate apparatus and the copper calorimeter. Figure 3.11 illustrates the test apparatus.

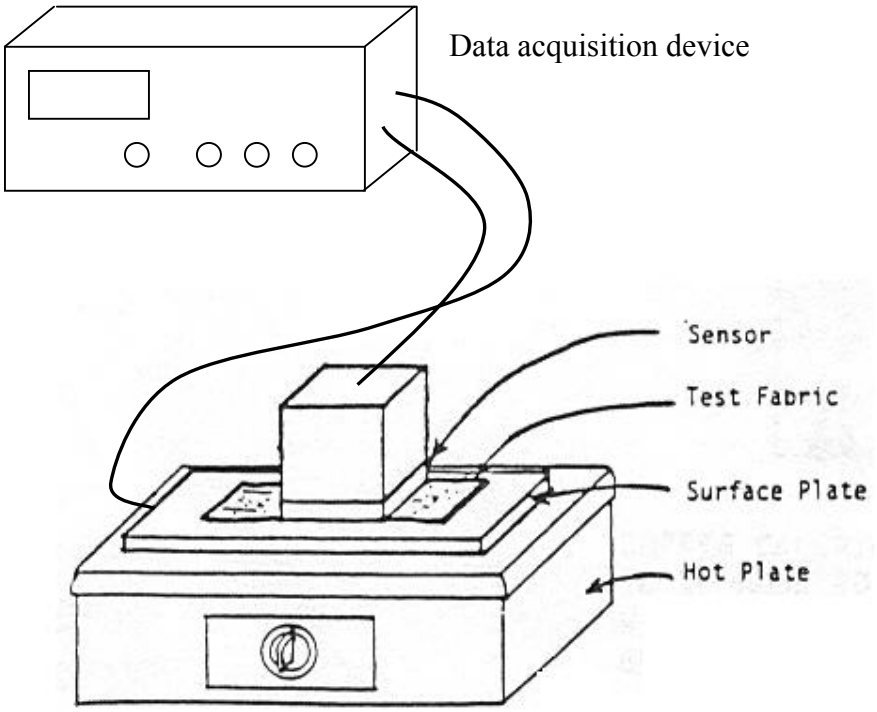

FIGURE 3.11: ASTM F 1060 apparatus [28] (used with permission)

NFPA 1971 changes the specification slightly as it calls for a constant hot plate temperature of 280°C ±5°C instead of the 200°C±3°C required by ASTM F 1060. The standard requires that combinations of layers that are to be used in the shoulder of a turnout coat and the knee area of a pair of turnout pants provide enough protection that a temperature change of 24°C will take at least 13.5 seconds. The time measured for a 24°C temperature rise is known as the Conductive and Compressive Heat Resistance (CCHR) rating. This phase of the research did not focus on the 13.5 second standard because it was desired to specifically examine the effects of thermal exposure on the

compressive heat resistance of the thermal liner, so it was a comparative study instead. The unexposed total ensemble was found to have a CCHR rating of 29.4, while the unexposed thermal liner was found to have a CCHR rating of 12.0, so it is clear that the thermal liner comprises a major portion of the compressive and conductive resistance. Figures 3.12 to 3.16 illustrate the results of this testing.

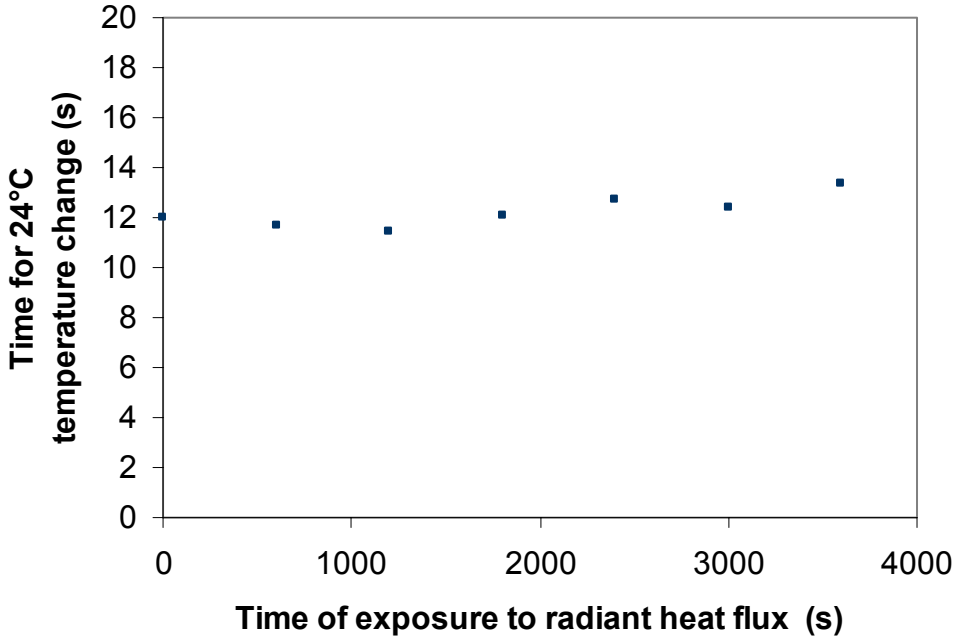

FIGURE 3.12: ASTM F 1060 testing after 5 kW/m^2 radiant exposure

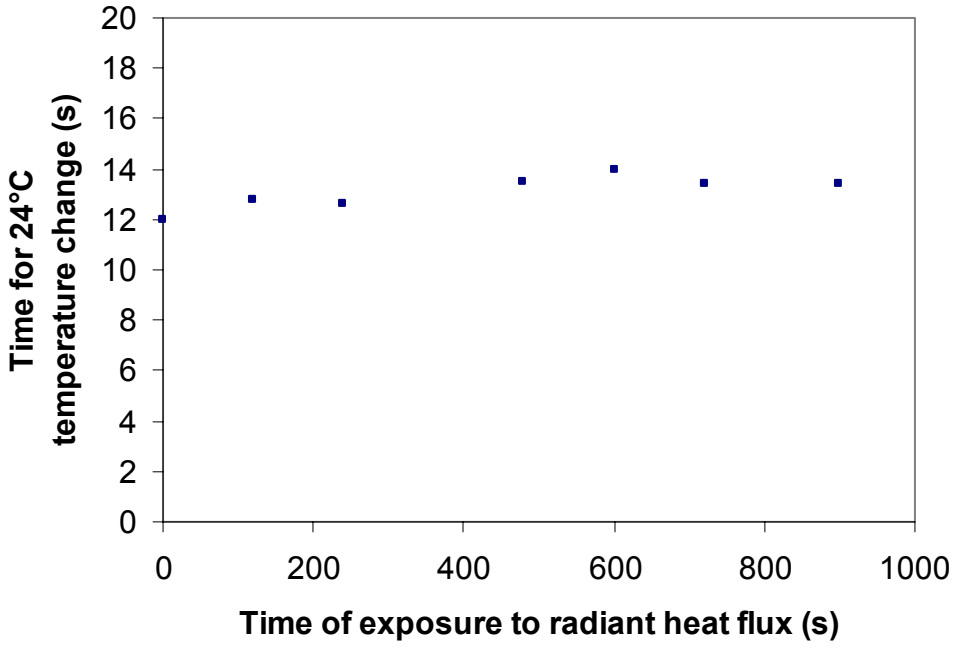

FIGURE 3.13: ASTM F 1060 testing after 10 kW/m^2 radiant exposure

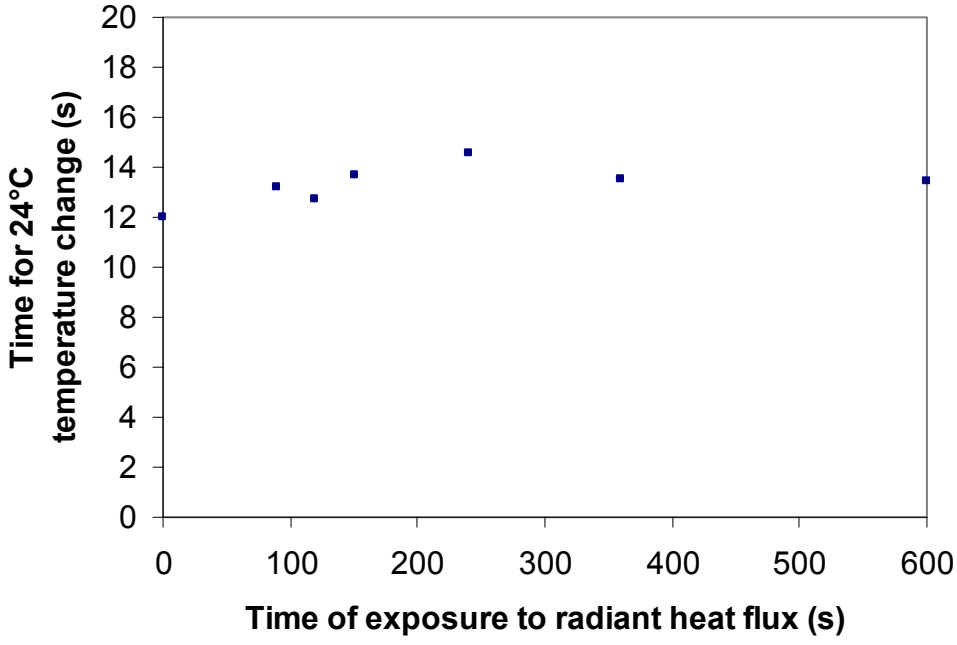

FIGURE 3.14: ASTM F 1060 testing after 15 kW/m^2 radiant exposure

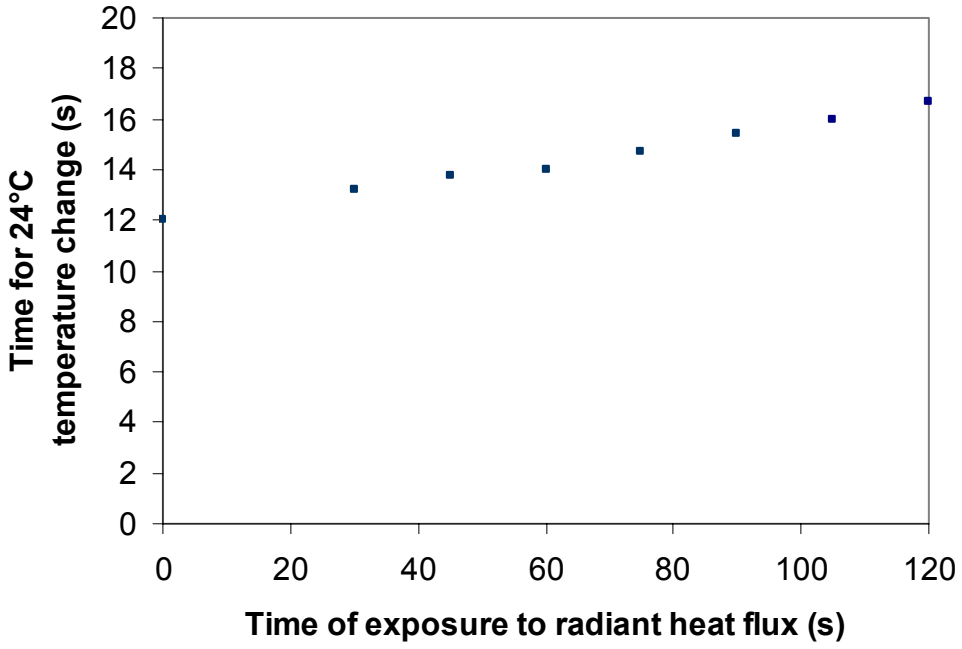

FIGURE 3.15: ASTM F 1060 testing after 20 kW/m^2 radiant exposure

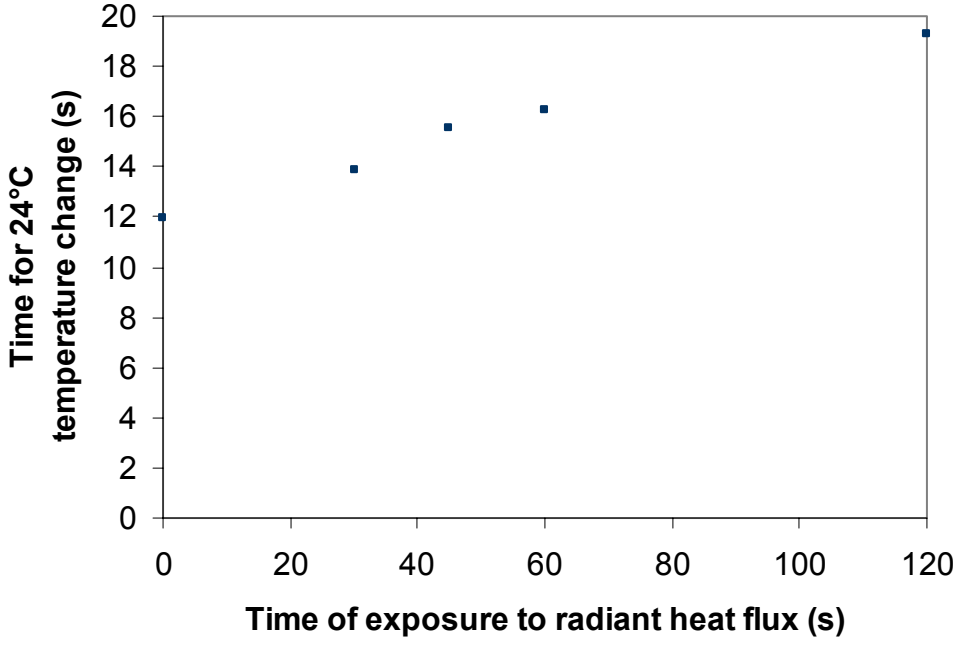

FIGURE 3.16: ASTM F 1060 testing after 30 kW/m^2 radiant exposure

As the results indicate, the compressive conductive resistance performance actually improves with greater heat exposure. The specimens get increasingly stiff following heat flux exposure, making the fabric more resistant to compression. This ensures that the air pockets that are created by the space in the fabric are maintained more consistently. The thermal liners do get more brittle, as the heat exposure increases, a factor that might reduce the effectiveness of the liner, but this test does not address that change in properties. The implications for this research suggest that the compressive conductive resistance of the thermal liners are not a critical concern in the thermal degradation of fire fighter's turnout gear.

3.5 Tensile Testing (grab test)

The NFPA 1971 standard for fire fighter's turnout clothing requires that an outer shell material must have a breaking force resistance of at least 623 N (140 lbf) when tested in accordance with ASTM Standard Test Method for Breaking Force and Elongation of Textile Fabrics (Grab Test) (ASTM D 5034) [37]. For this testing an INSTRON™ (Instron Corporation, Canton MA) 1100 tensile testing machine was used with a full scale load of 2000 N. Pneumatic jaws with an air pressure of 90 psi forced parallel plates together to hold the specimens. ASTM D 5034 specifies fabric samples of 101.6 mm (4 inch) by 152.4 mm (6 inch), which corresponds with the size of the specimens exposed with the radiant panel performance tester (Section 2.3). The standard also specifies a constant crosshead speed of 20 mm/min; this applies increasing tensile load on the fabric until it fails. With a nominal gauge length of 3 in. (7.6 cm), this creates a strain rate of 0.26 min^{-1}. A marking pen records the load on the specimen

as a function of time. All of the outer shell specimens that had been subjected to the radiant heat exposure (Section 2.2) were tested. The specimens with little visible signs of degradation broke at a relatively high load, while specimens with increased visible signs of degradation broke at lower loads.

Curves generated by this test are plotted in Figures 3.17 through 3.21 for fabric specimens that were exposed to heat fluxes of 5, 10, 15, 20 and 30 kW/m^2. The NFPA 1971 minimum requirement for new turnout gear, 623 N is superimposed on the figures to show the point at which the fabric will no longer meet this particular standard.

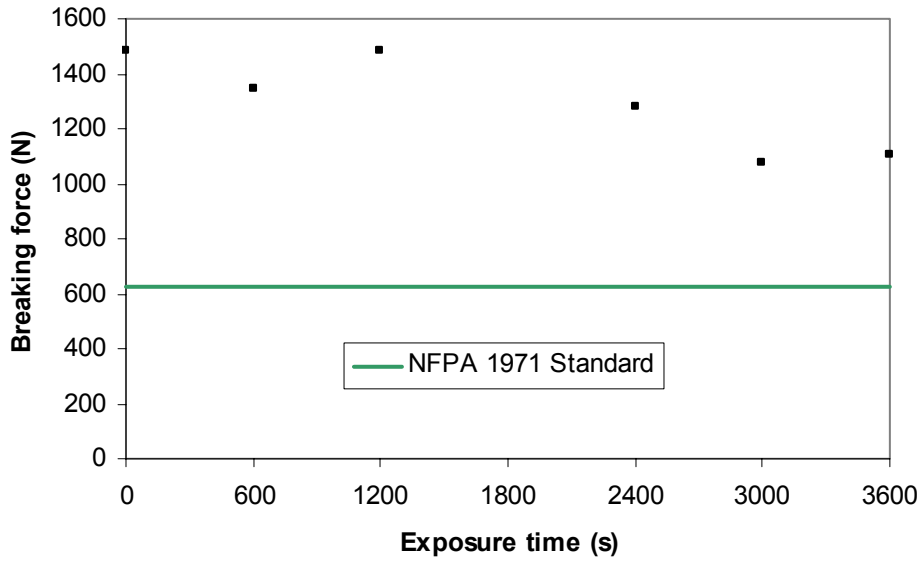

FIGURE 3.17: Tensile testing after 5 kW/m^2 radiant exposure

It is clear that even with one hour of 5 kW/m^2 radiant exposure on the ensemble, the outer shell met the performance requirement of 623 N of breaking force. This is an indication that for tensile strength loss to occur, the thermal exposure in these tests must be more severe than an exposure of 5 kW/m^2.

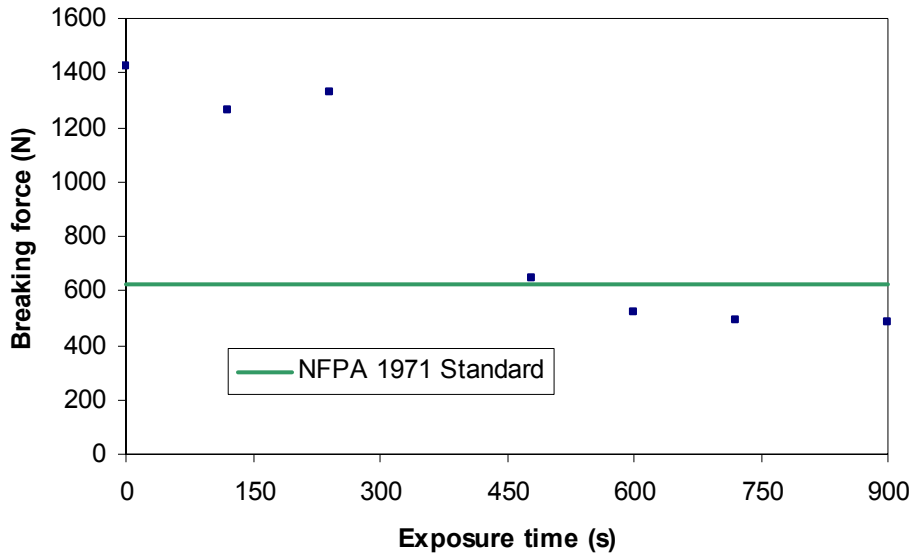

FIGURE 3.18: Tensile testing after 10 kW/m^2 radiant exposure

Figures 3.18-3.21 demonstrate that there is a distinct point in the exposure history of the fabric at which the outer shell will not meet the NFPA 1971 requirement for breaking force. In the case of an incident heat flux of 10 kW/m^2, an exposure of 480 seconds or more resulted in compromised performance. Figures 3.18 to 3.21 demonstrate the reduction of the exposure time for compromised performance. As the heat flux is increased in these exposures, the time before the NFPA 1971 standard is compromised

is made shorter and shorter, until the case of 30 kW/m^2 in which it takes less than 30 seconds to breach this performance barrier. The exposures of 30 kW/m^2 are included here, but for exposures of 60 seconds or more, the fabric was so weak that bending with the fingers was enough to break it. In fact none of the specimens exposed to 30 kW/m^2 exceeded the standard, though if exposures of less than 30 seconds were performed, it is estimated that the breaking force would likely be higher than the NFPA 1971 standard.

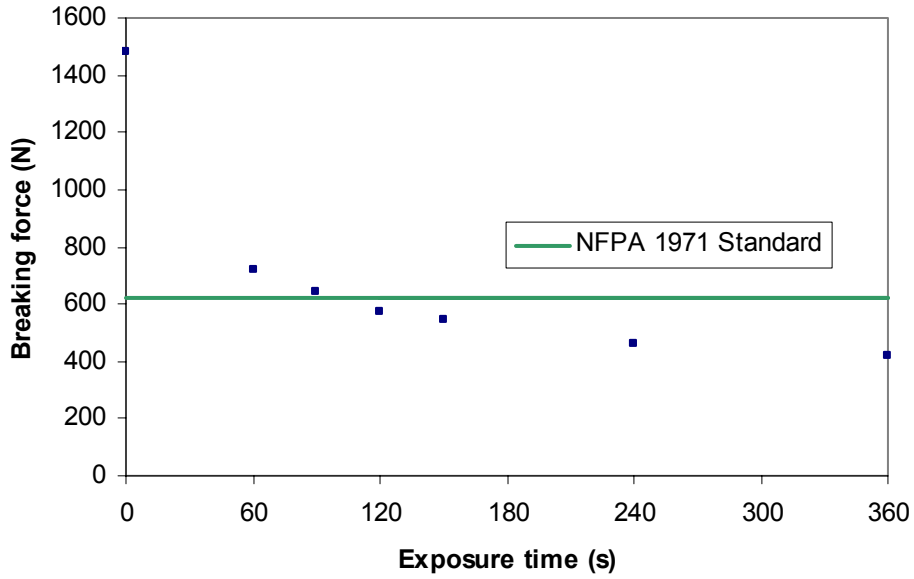

FIGURE 3.19: Tensile testing after 15 kW/m^2 radiant exposure

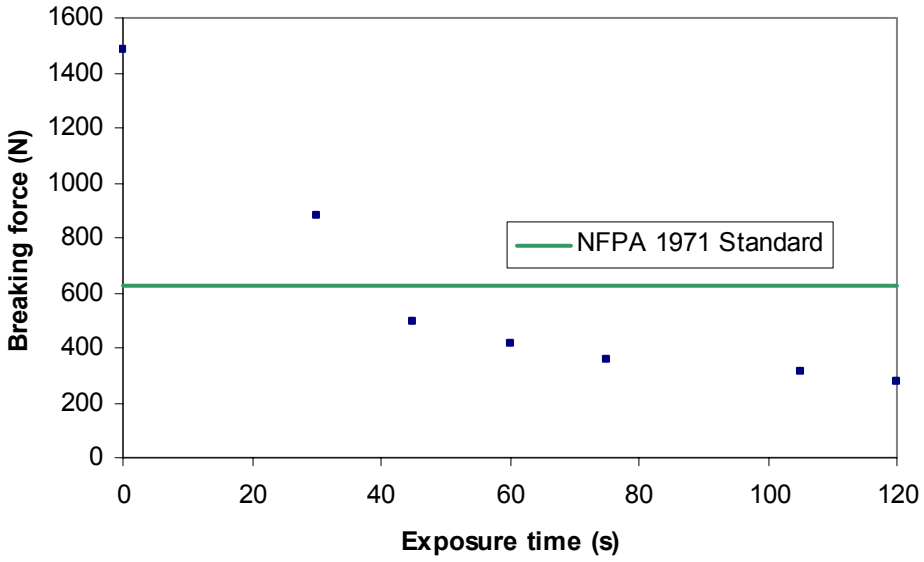

FIGURE 3.20: Tensile testing after 20 kW/m^2 radiant exposure

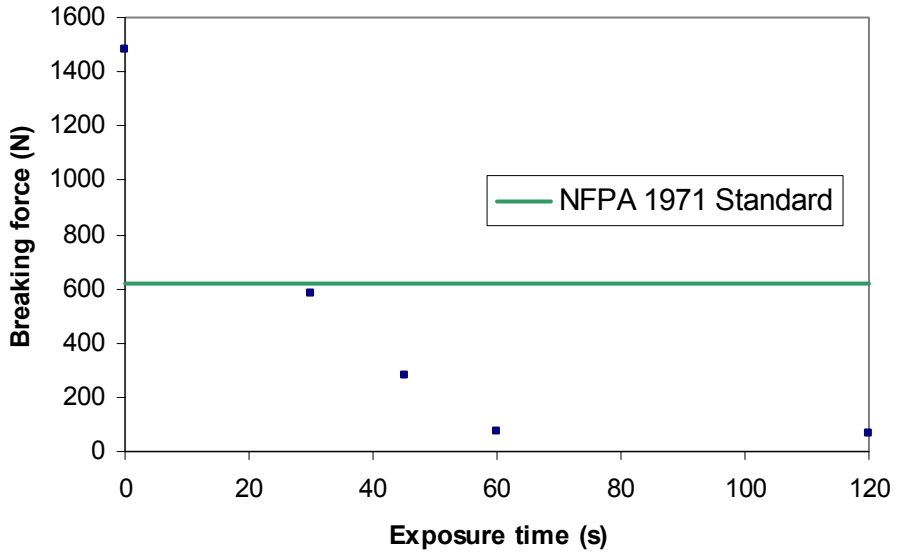

FIGURE 3.21: Tensile testing after 30 kW/m^2 radiant exposure

As the figures indicate, higher heat flux corresponds with shorter exposure time until performance compromise. This finding agrees with intuition, as one would expect high

heat flux to cause the most damage to the material. Heat fluxes of 30 kW/m^2 are the most severe of the exposures tested for this research and a fire fighter's turnout gear would be compromised in short order if this level of exposure were encountered in the field.

Examination of Figures 3.18 to 3.21 suggests that there is a point during each of the heat exposures at which the tensile strength is compromised such that it will not meet the NFPA 1971 standard. That point for each Figure can be determined by interpolating between the data points. Figure 3.22 demonstrates the results of these interpolations.

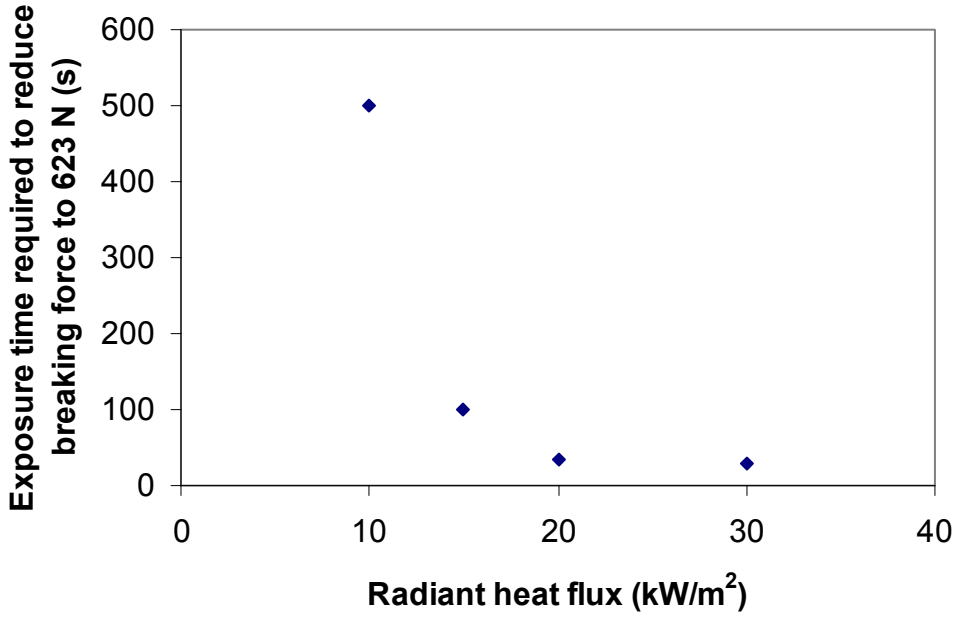

FIGURE 3.22: Time required for radiant heat flux to compromise NFPA 1971 breaking force performance of outer shell

If the values from Figure 3.22 are compared with the temperature measurement curves, Figures 3.3 to 3.6, it can be seen that these times correspond to a temperature of approximately 270°C at the outer shell/moisture barrier interface the temperature.

Applying the assumption that the outer surface temperature of the outer shell is approximately 100°C to 150°C higher than the measured interface temperature, an outer shell temperature of approximately 400°C is calculated. Comparison with the TGA trace for the outer shell in Figure 3.7, it can be seen that 400°C is approximately the temperature of the first major phase of degradation. This suggests that a test for tensile strength reduction should be able to indicate when this outer shell has reached 400°C.

3.6 Tear Strength Testing (trapezoid test): Thermal Liner

For the remaining layers of the ensemble, ASTM Standard Test Method for Tearing Strength of Nonwoven Fabrics by the Trapezoid Procedure (ASTM D 5733) [38] was used to examine the effects of degradation. This method is specified by NFPA 1971 to be used for each of the individual layers of the ensemble. The minimum tear strength for the outer shell is specified as 100 N (22 lbf); for the moisture barrier and the thermal liner, the minimum required tear strength is 22 N (5 lbf). ASTM D 5733 requires specimens 76.2 mm (3 inch) x 152.4 mm (6 inch) with an initial cut in the fabric of 15.9 mm (0.625 inch). Figure 3.23 details the template used to create the test specimens. The specimen is cut into the standard size and then notched with a pair of scissors as per the figure. Two lines are drawn on the specimen to create a trapezoid shape. The specimen is placed in the jaws such that these lines are parallel with the pneumatic jaws of the tensile testing machine. This orientation creates a loading situation that is favourable to tearing. A standard crosshead speed of 200 mm/min is used and the maximum force required to tear the fabric is recorded.

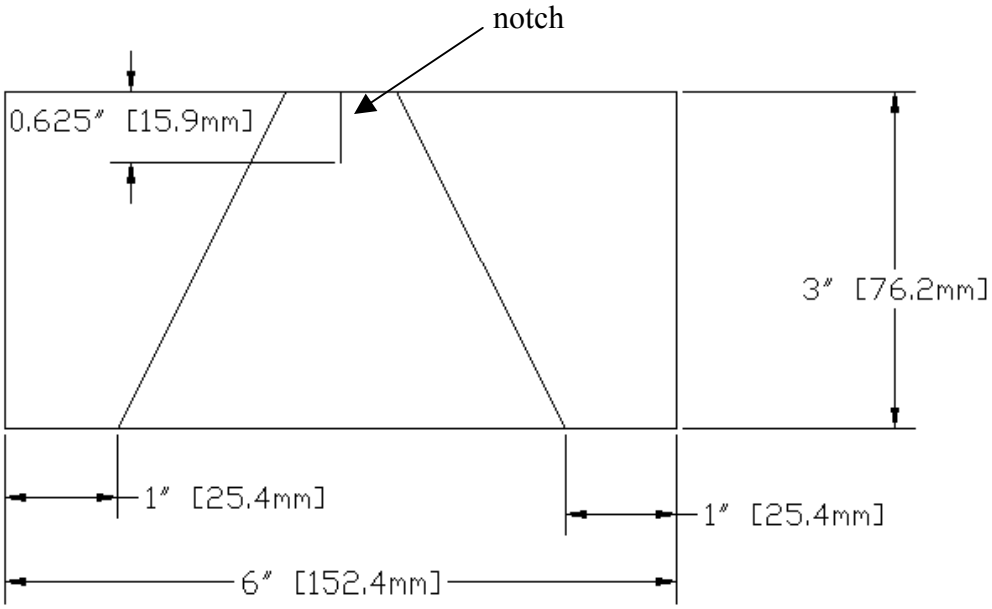

FIGURE 3.23: ASTM D 5733 [37] trapezoid test specimen specifications

For this research an INSTRON™ 1100 (Instron Corporation, Canton MA) tensile testing machine was used with a full scale load of 2000 N. Pneumatic jaws with an air pressure of 133.9 Pa (90 psi) forced two parallel steel plates, each 76.2 mm (3 in.) by 50.8 mm (2 in) by 4.8 mm (0.1875 in) thick, together to hold the specimens (see Figure 3.24).

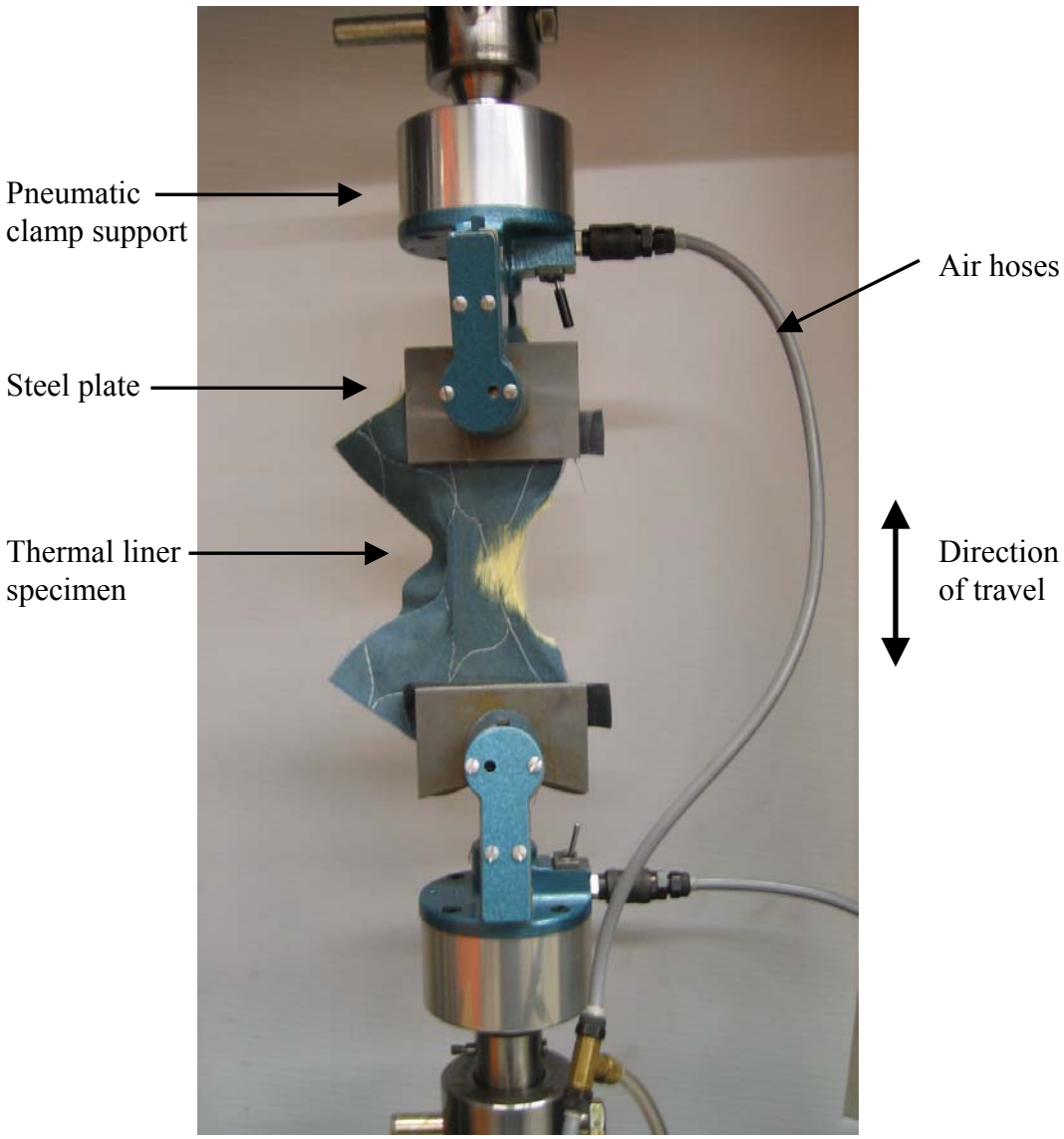

FIGURE 3.24: Trapezoid testing apparatus, thermal liner specimen shown

The thermal liner was tested first. It was assumed that the liner would hold up very well in this test due to a lack of visible degradation. Figure 3.25 gives the results for all of the thermal liners tested using this standard. As the figure demonstrates, the tear strength of the thermal liner was never reduced to a point approaching the NFPA 1971 specification. It is clear from this figure that the tear strength of the thermal liner was not adversely affected by the exposure to the heat fluxes used in this testing.

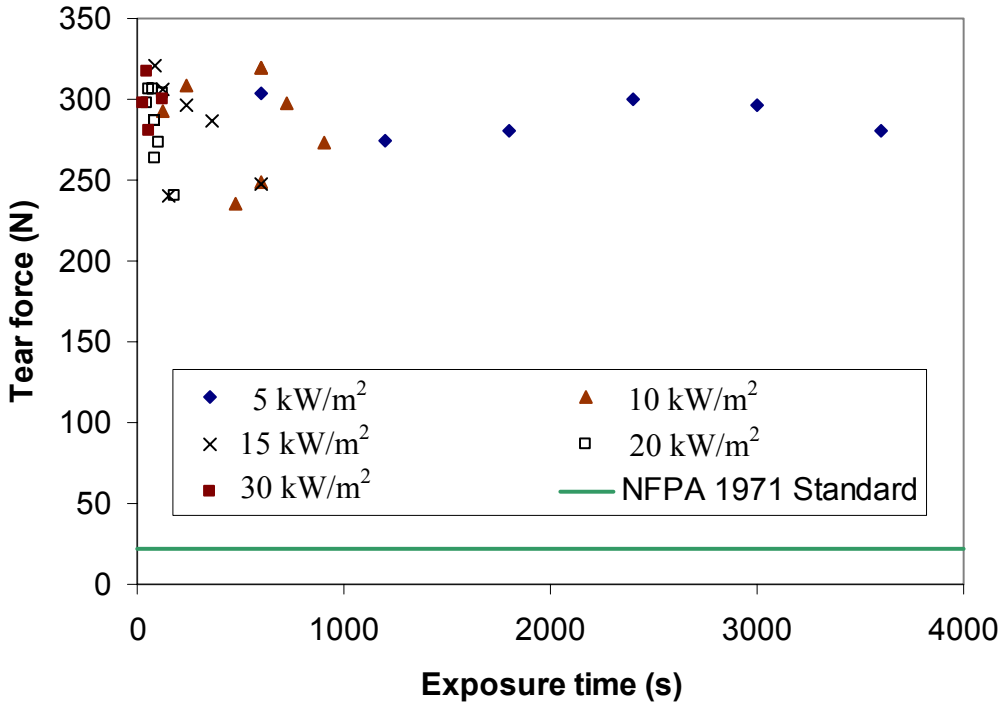

FIGURE 3.25: Tear strength testing results for thermal liner specimens after radiant exposure

3.7 Tear Strength Testing (trapezoid test): Moisture Barrier

The moisture barrier was tested with the same ASTM D 5733 standard. The radiant panel heat exposure left a characteristic mark (see Figure 3.26) on the fabrics, a result of the size of the quartz tube bank and the supporting apparatus. This heat affected zone did not extend the full width of the specimens. This created a situation in which the trapezoid testing may not have effectively tested the strength of the heat affected zone.

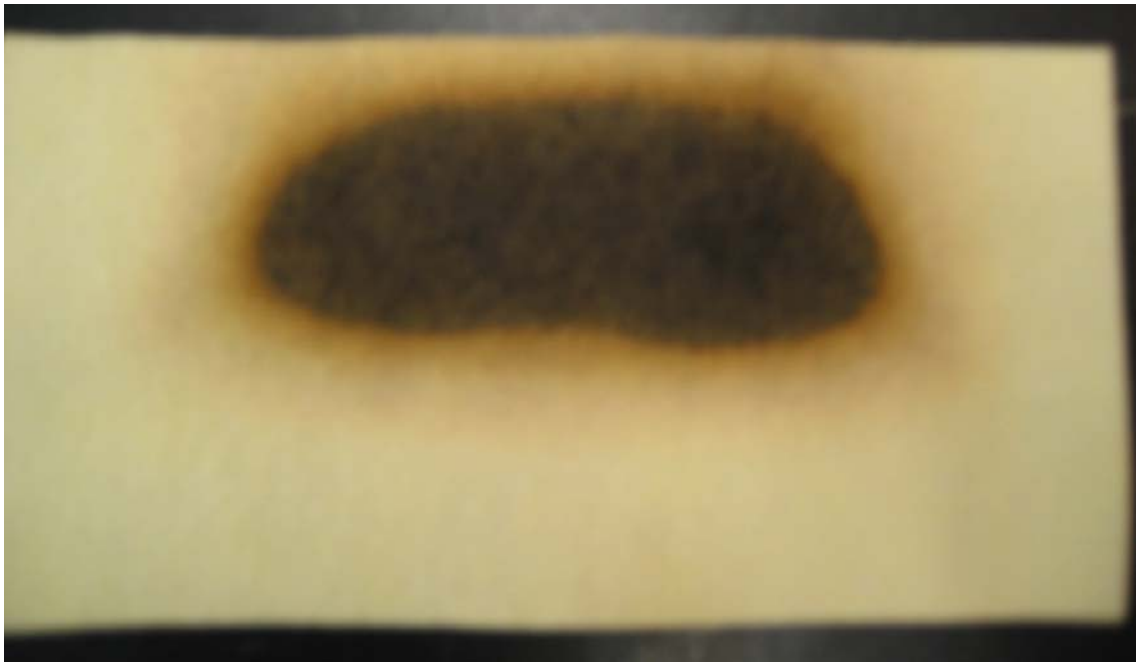

FIGURE 3.26: Heat affected zone on moisture barrier, characteristic oval pattern artifact of radiant panel exposure

Some measures were taken to reduce the error of this method, such as altering the size of the initial cut in the fabric to ensure the tear would start in the heat affected zone, and stopping the test when the tear had traversed the entire zone. Even with these measures, there is high degree of uncertainty in these results. The results will be reported here; some discussion of further tests conducted to reduce this source of error follows. Figures 3.27 to 3.31 give the results of this testing. The standard again calls for at least 22 N of tear force, only after the most severe exposure did the moisture barrier fail this test.

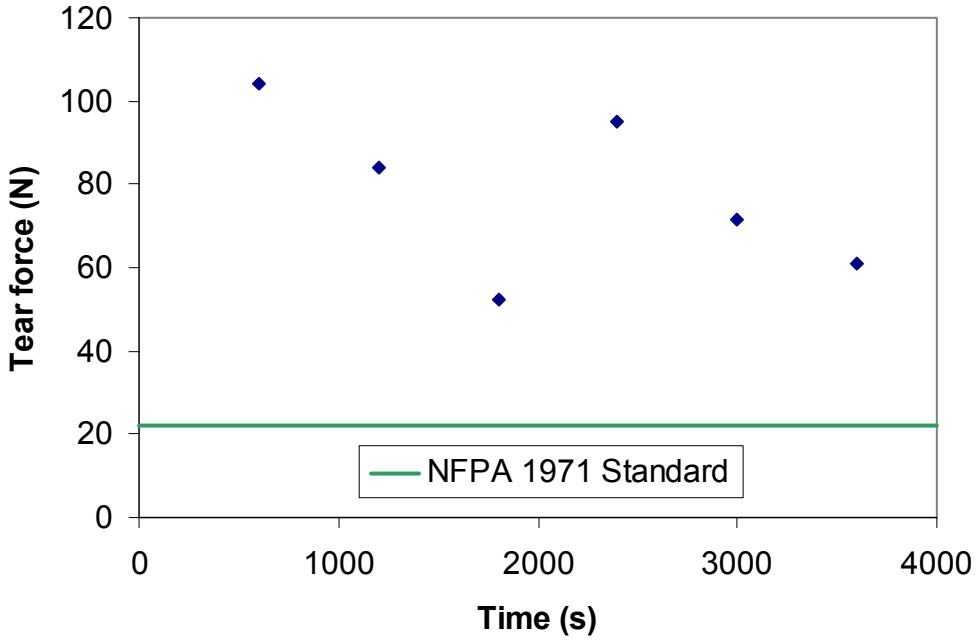

FIGURE 3.27: Tear strength testing of moisture barrier specimens after 5 kW/m^2 radiant exposure

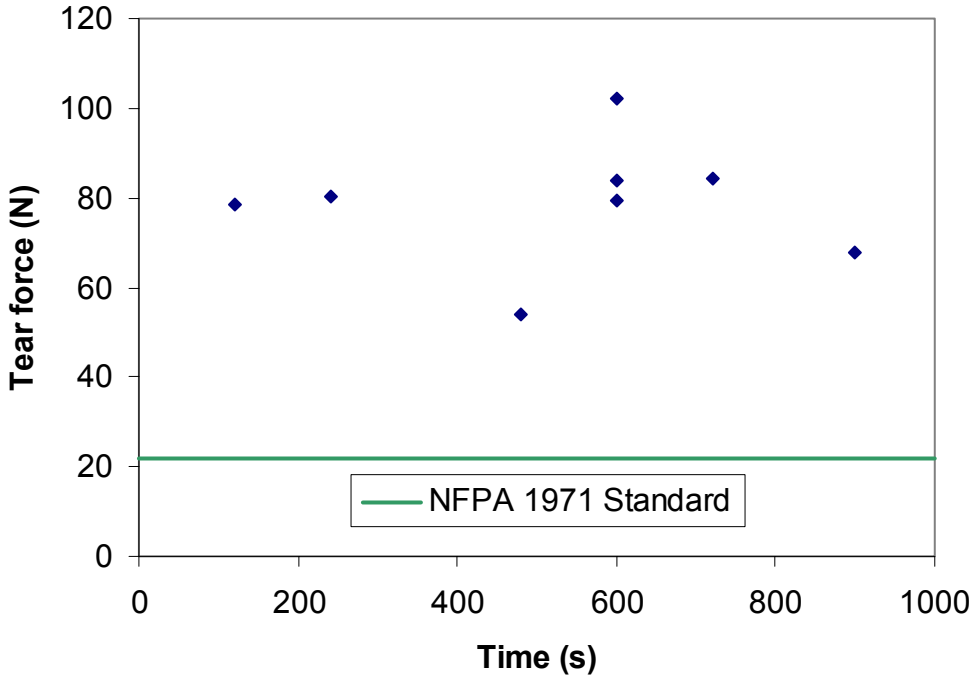

FIGURE 3.28: Tear strength testing of moisture barrier specimens after 10 kW/m^2 radiant exposure

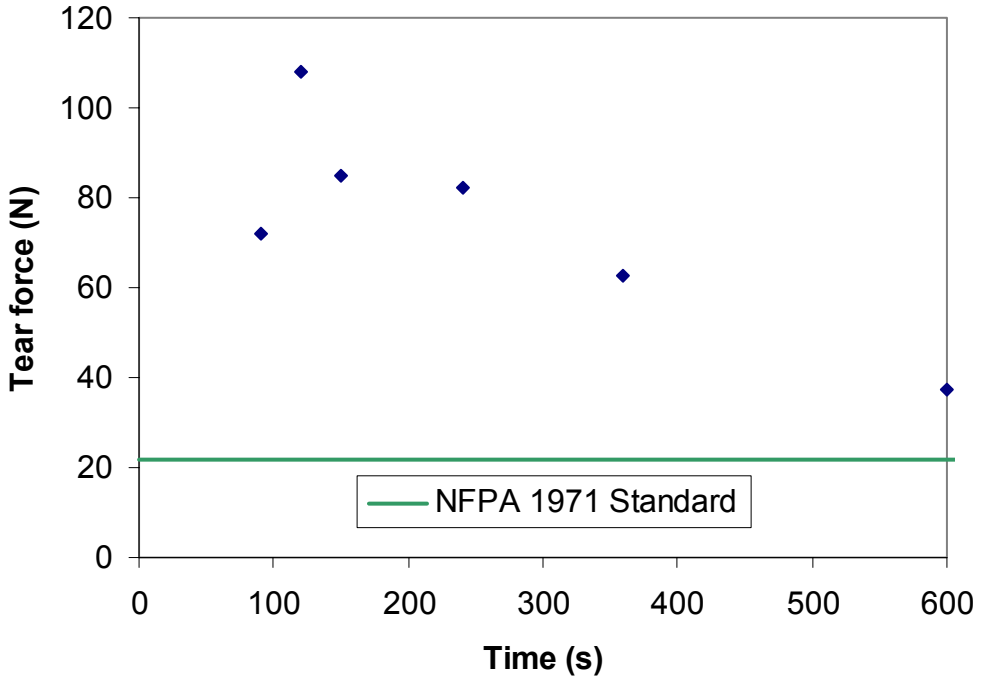

FIGURE 3.29: Tear strength testing of moisture barrier specimens after 15 kW/m^2 radiant exposure

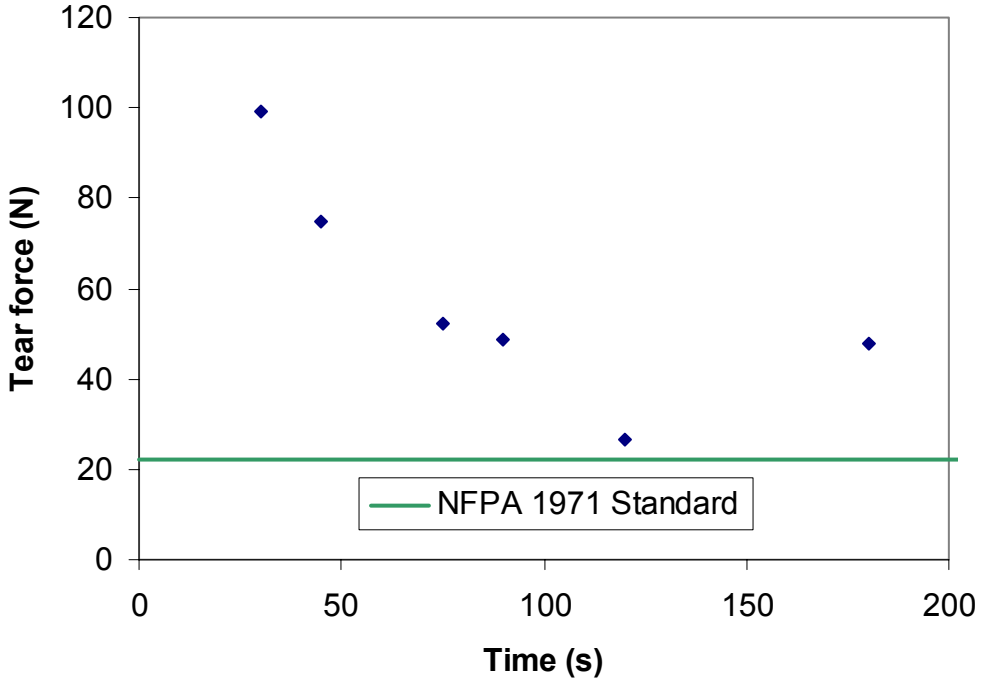

FIGURE 3.30: Tear strength testing of moisture barrier specimens after 20 kW/m^2 radiant exposure

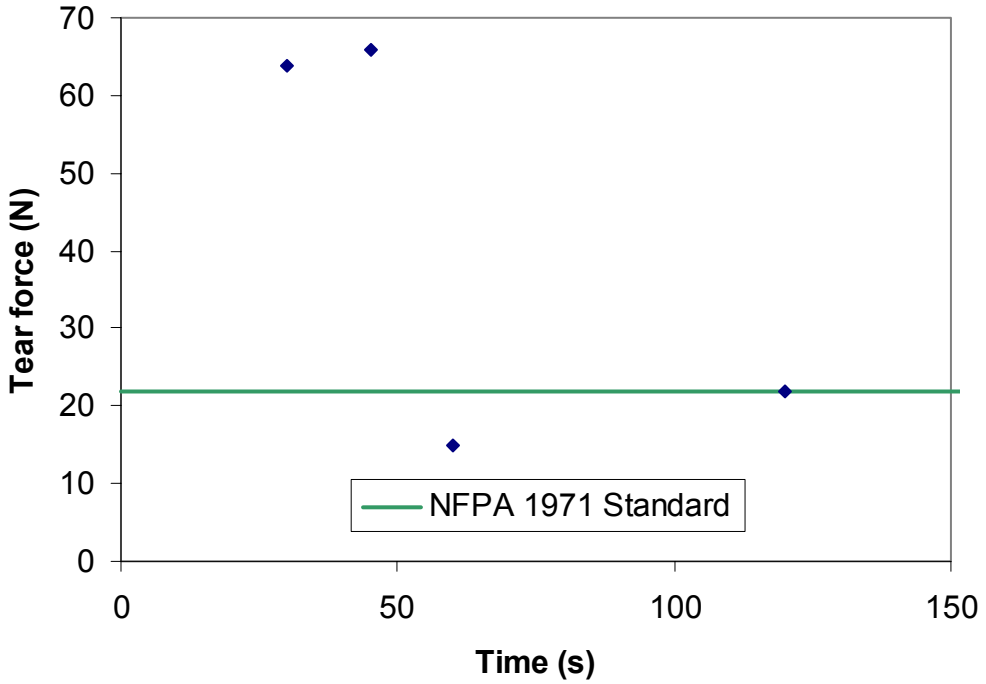

FIGURE 3.31: Tear strength testing of moisture barrier specimens after 30 kW/m^2 radiant exposure

The only moisture barriers that did not pass this tear test were the barriers that had been subjected to 60 seconds or more of 30 kW/m^2 radiant exposure. As was mentioned previously, there is some question about the reliability of these results. One suggestion to reduce this uncertainty was to expose the ensemble using a device larger than the radiant panel performance apparatus. One possibility is a cone calorimeter in which consistent heat flux is provided by an electrical resistant element in the shape of a cone. A 6 in. (15.2 cm) diameter cone will provide constant heat flux across the whole circle. Preliminary testing using the University of Saskatchewan's Fire Testing Technology Cone Calorimeter showed that the cone could provide constant exposure across the entire width of 6 in. (15.2 cm) x 4 in. (10.2 cm) ensemble specimens. Preliminary tear testing with these samples demonstrated a different shaped curve than with the radiant panel performance apparatus. Further research is required; for now it is enough to

suggest that this apparatus might be a better choice for further testing of this property of fire protective clothing.

3.8: Summary of Destructive Testing

This chapter described the various destructive tests that were conducted for this research. The first two sections detailed tests that were not mandated by NFPA 1971. Temperature measurements were made by recording thermocouple readings during heat exposures. These measurements were compared with results for thermogravimetric analysis, and some descriptions of the critical degradation temperatures. This provided a framework for the testing that was mandated by NFPA 1971. The moisture barriers were tested for their resistance to liquid penetration, and for their tear strength. Thermal liners were tested for their conductive and compressive resistance, and for tear strength. Outer shell specimens were tested for their tensile strength. Table 3.3 gives a summary of the findings from this chapter. The ASTM F 1060 standard is defined for the complete ensemble, but the testing only involved the thermal liner, so in this table, since the CCHR rating of the thermal liner increased with thermal exposure, all are considered to have passed the test.

TABLE 3.3: Summary of results of destructive tests

Heat flux (kW/m^2)	Exposure time (s)	ASTM F 903 (modified): Penetration of moisture barrier	ASTM F 1060: Conductive and Compressive Resistance Test	ASTM D 5034: Grab test (outer shell)	ASTM D 5733: Tear test (thermal liner)	ASTM D 5733: Tear test (moisture barrier)
5	600	Pass	Pass	Pass	Pass	Pass
5	1200	Pass	Pass	Pass	Pass	Pass
5	3000	Pass	Pass	Pass	Pass	Pass
5	1800	Pass	Pass	Pass	Pass	Pass
5	2400	Pass	Pass	Pass	Pass	Pass
5	3600	Pass	Pass	Pass	Pass	Pass
10	120	Pass	Pass	Pass	Pass	Pass
10	240	Pass	Pass	Pass	Pass	Pass
10	480	Pass	Pass	Pass	Pass	Pass
10	600	Pass	Pass	Fail	Pass	Pass
10	600	Pass	Pass	Fail	Pass	Pass
10	600	Pass	Pass	Fail	Pass	Pass
10	720	Pass	Pass	Fail	Pass	Pass
10	900	Pass	Pass	Fail	Pass	Pass
15	60	Pass	Pass	Pass	Pass	Pass
15	90	Pass	Pass	Pass	Pass	Pass
15	120	Pass	Pass	Pass	Pass	Pass
15	150	Pass	Pass	Fail	Pass	Pass
15	240	Pass	Pass	Fail	Pass	Pass
15	360	Pass	Pass	Fail	Pass	Pass
15	600	Pass	Pass	Fail	Pass	Pass

TABLE 3.3 (continued): Summary of results of destructive tests

Heat flux (kW/m^2)	Exposure time (s)	ASTM F 903 (modified): Penetration of moisture barrier	ASTM F 1060: Conductive and Compressive Resistance Test	ASTM D 5034: Grab test (outer shell)	ASTM D 5733: Tear test (thermal liner)	ASTM D 5733: Tear test (moisture barrier)
20	30	Pass	Pass	Pass	Pass	Pass
20	45	Pass	Pass	Fail	Pass	Pass
20	60	Pass	Pass	Fail	Pass	Pass
20	75	Pass	Pass	Fail	Pass	Pass
20	90	Pass	Pass	Fail	Pass	Pass
20	90	Pass	Pass	Fail	Pass	Pass
20	90	Pass	Pass	Fail	Pass	Pass
20	105	Pass	Pass	Fail	Pass	Pass
20	120	Pass	Pass	Fail	Pass	Pass
20	180	Pass	Pass	Fail	Pass	Pass
30	30	Pass	Pass	Fail	Pass	Pass
30	45	Fail	Pass	Fail	Pass	Pass
30	60	Fail	Pass	Fail	Pass	Fail
30	120	Fail	Pass	Fail	Pass	Fail

The next chapter examines the non-destructive testing that was conducted on these exposed fabric specimens.

CHAPTER 4: NON-DESTRUCTIVE TESTING

The financial demands on a fire department are vast, so any way to reduce the total cost of turnout gear without compromising safety would be a welcome improvement. Currently, testing of used turnout gear can be done either by conducting destructive testing or by using primarily visual methods to assess damage. As discussed in Section 1.3, NFPA 1851 directs users to routinely inspect their gear and to subject the gear to a more detailed inspection once every 12 months. The standard suggests that visual indications, such as charring and brittleness, should be used to identify degradation, but as was noted in Chapter 1, Slater [20] suggests that this may not be soon enough for maximum safety of the fire fighter.

Destructive testing can be used effectively if a number of garments have been exposed to similar conditions over their lifetimes and will behave in a similar fashion when tested. This is an impractical approach since it assumes a great deal about the exposures and still demands that at least one garment is destroyed, making it prohibitive for all but the largest departments. For these reasons, this research has turned to a preliminary study of the development of better non-destructive test methods to characterize the degradation of turnout gear.

The methodology of this part of the research was directed towards trying a number of different non-destructive test methods. Since neither NFPA 1971 nor NFPA 1851

provide a quantitative description of visual cues of degradation, it was determined that a systematic, quantitative analysis would prove useful. Since NFPA 1971 references a number of destructive tests, it was decided that successful non-destructive tests should provide some correlation with the destructive tests. This chapter details the process by which a group of non-destructive tests were selected, developed and performed, and describes the results of these tests. It was decided to focus on the visual properties of the outer shell for the non-destructive testing because this was the most accessible point on the turnout gear. Developing an enhanced visual testing method also serves to complement NFPA 1851 [4] and to help recude inconsistencies due to the subjective nature of some of the methods of inspection. In chapter 5, the results of the non-destructive tests will be compared with the results of the destructive tests described in Chapter 3.

Some ensemble systems allow for the removal of the moisture barrier and thermal liner but since this is not the case for every system, non-destructive tests were not considered for the moisture barrier in this study. The fabrics used in this study comprise an ensemble that is to be sewn together, so the only surfaces available to a tester are the outer surface of the outer shell and the inner surface of the thermal liner. The thermal liner exhibited only the most minimal damage when exposed to the radiant panel performance testing heat source described in Section 2.2, so it was decided to focus on the outer shell as the indicator of degradation. Four different non-destructive test methods were selected for this research: optical microscopy, Raman spectroscopy, digital image analysis and colorimetry. All of these methods use light to assess the changes in the outer shell fabric specimens resulting from radiant thermal exposures.

4.1 Optical Microscopy

If the effects of degradation can be seen with the naked eye, it was suggested that degradation should certainly be identifiable using microscopy. A number of samples were examined under a microscope and photographs were taken of the degradation. A Nikon Optiphot microscope was used with a Nikon 35 mm film camera and Kodak 400 film. Observations of the degradation were qualitative since a quantitative analysis was difficult to perform. The colour changes that were visible on a macro-scale were difficult to assess on the micro-scale because even the unexposed outer shell was multi-coloured (see Figure 4.1). Thermal exposure caused a darkening of the fibres and there were noticeably more dark fibres in the more exposed samples, but short of assessing the darkness of each fibre in the field of view, a quantitative analysis could not be performed. Figures 4.1, 4.2 and 4.3 illustrate a progression to increased degradation resulting from thermal exposure.

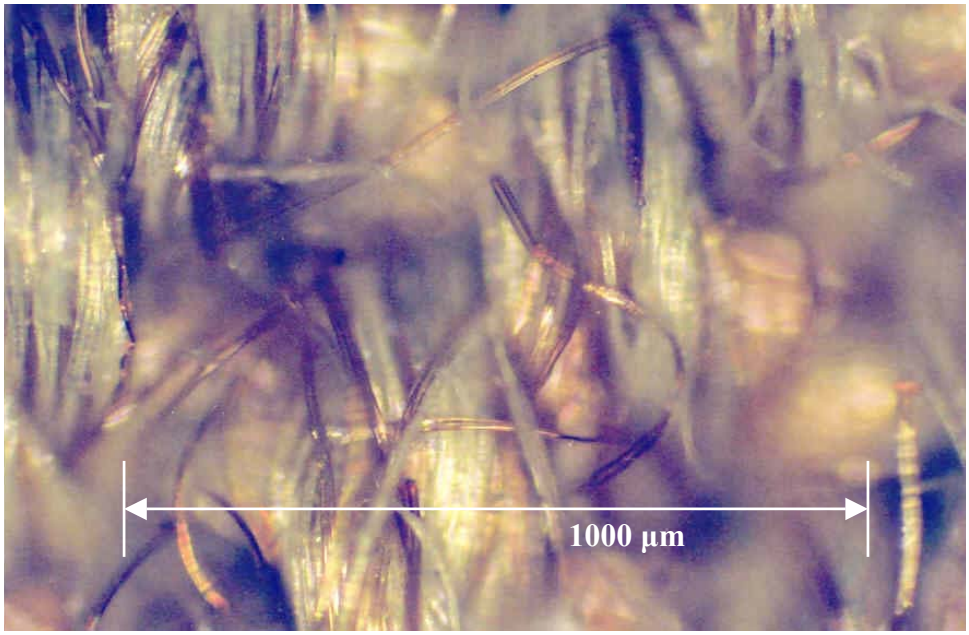

FIGURE 4.1: Unexposed outer shell specimen (magnification 100x)

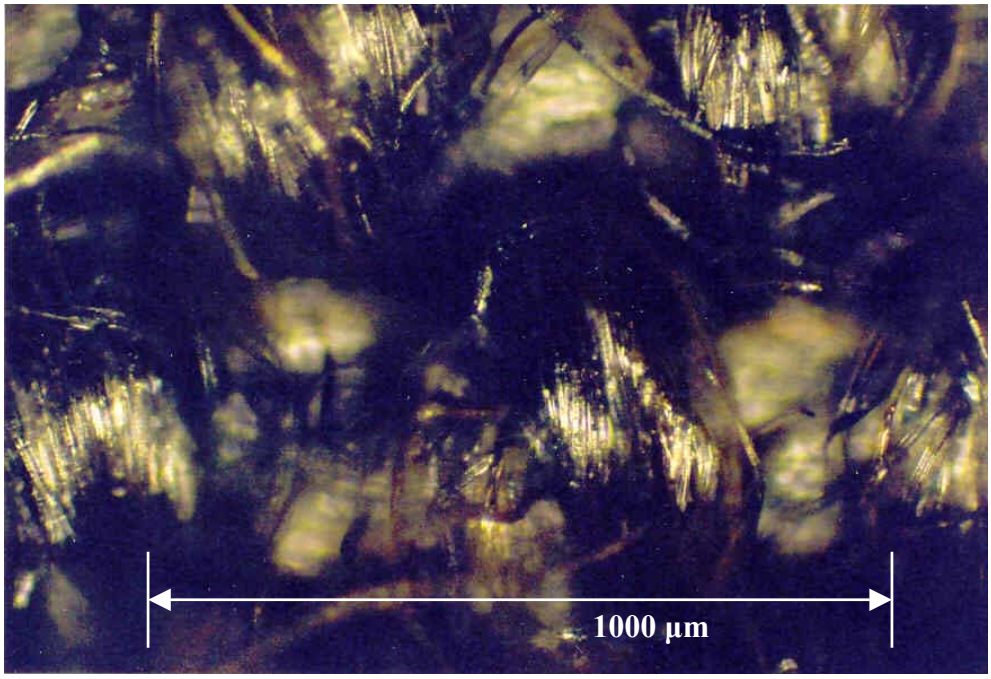

FIGURE 4.2: Outer shell sample after 120 seconds of 10 kW/m^2 radiant exposure (magnification 100x)

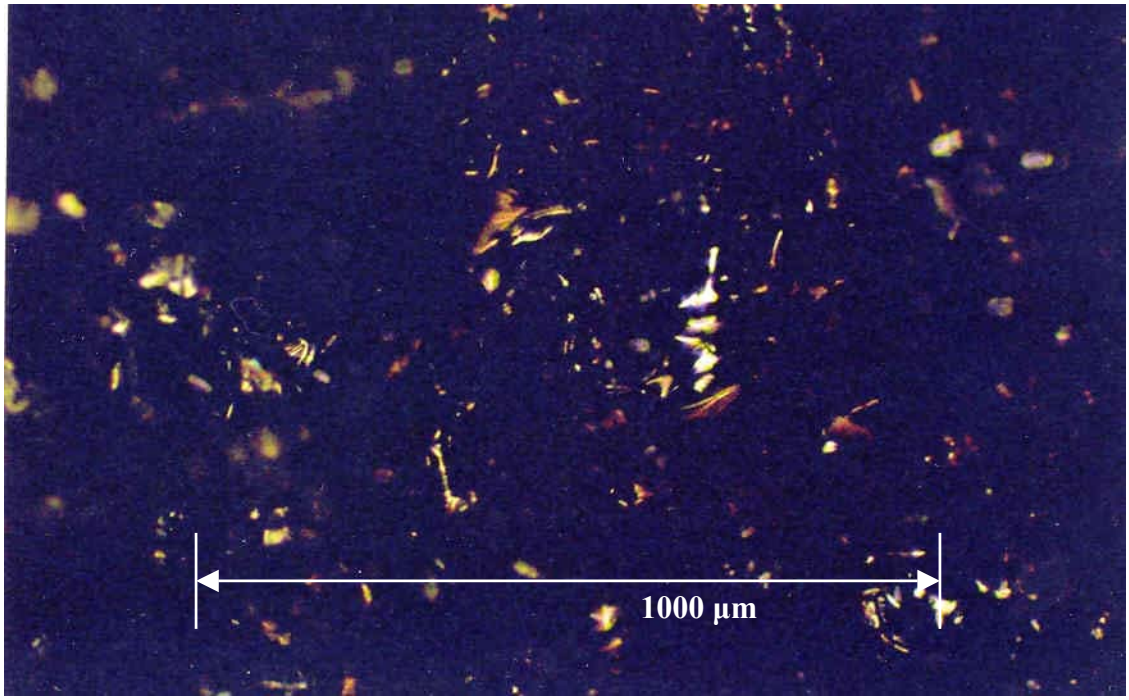

FIGURE 4.3: Outer shell fabric specimen after 120 seconds of 30 kW/m^2 radiant exposure (magnification 100x)

The highly degraded samples showed evidence of individual fibre strands joining with others and melting to form dark globules. These globules were shiny and smooth. The presence of these globules indicates a change in the structure of the fibres. The formation of the globules is expected to result in a change in the performance of the material as the movement and interaction of the individual fibres is reduced.

This study provided interesting images and information about the micro-scale changes of the fabrics, but more work was required to provide a quantitative measure of the degradation on the fabric. One possible method to improve this work would be to use digital image analysis to perform a count of dark fibres and light fibres. The respective percentages could give some indication of the colour change. While this technique was

not pursued, other digital image analysis was considered. This work is described in Section 4.3.

A number of different non-destructive evaluation techniques were considered for this research. There are a number of different methods that involve observing changes in the spectral characteristics of the molecules of the fabric samples. Examples of spectral techniques include infrared spectroscopy, Fourier transform infrared spectroscopy, mass spectroscopy, Raman spectroscopy. It was determined that due to time constraints, only one of these techniques would be explored, Raman spectroscopy. This technique is examined in the next section.

4.2 Raman Luminescence Technique

When monochromatic light is shone onto a molecule, there is a large amount of scattered light of the same wavelength as the incident light, but there is also a set of discrete frequencies above and below the incident wavelength. This scattering is known as Raman scattering. The Raman effect is caused when energy is added or removed to the molecules by changing their rotational and vibrational energies [46]. Raman spectroscopy is the process of observing the Raman effect as photons experience inelastic collisions with the molecules of the test subject.

Of all the various spectral characterisation techniques, Raman spectroscopy was chosen because it is frequently used to examine the excitation of fabric materials in the visual light spectrum. Another factor that contributed to the selection of Raman spectroscopy is the possibility of using remote sensing techniques. Fibre optics has made it possible

to conduct tests on in situ garments. If this technique proved promising, it would be possible to create a diagnostic test that could be portable and applied to fire fighting gear. Testing was conducted at the Saskatchewan Structural Sciences Centre at the University of Saskatchewan. Outer shell fabric specimens were placed in a Renishaw (Gloucestershire, UK) inVia Reflex Raman Microscope using two different incident lasers (wavelengths of 514 nm and 785 nm) to provide the light source. For the fabric specimens in this study it was determined that Raman spectroscopy would not be particularly useful since the fabrics responded to the two different incident lasers with a very high level of fluorescence. This created a poor signal to noise ratio that reduced the effectiveness of the method. Figure 4.4 illustrates the high level of fluorescence in a sample of unexposed outer shell material.

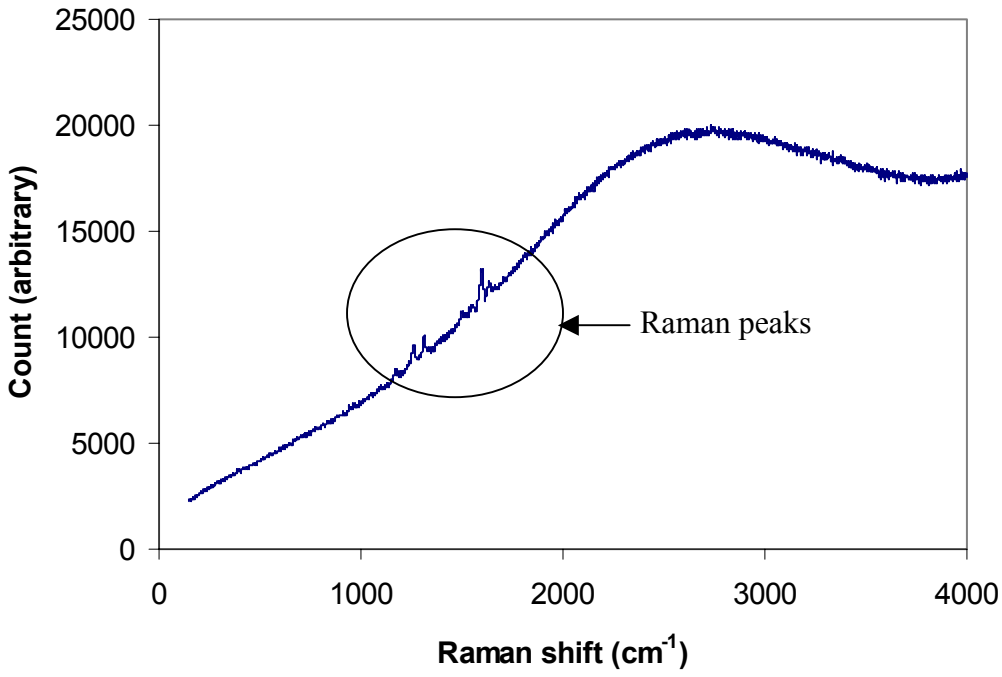

FIGURE 4.4: Raman spectrograph of outer shell material, excitation wavelength 514 nm

The x-axis is a measure of the frequency of the Raman shift from the excitation frequency, the y-axis is a measure of photons counted at that particular wavenumber. The actual count is not important to the study; in fact frequently counts are called arbitrary units. The important thing to observe is the relative intensities of the different features of the figure. The primary form of the curve is the fluorescence, but at wavenumbers of approximately 1200 to 1600 cm^{-1}, the Raman effect is seen. The size of these peaks demonstrate how much stronger is the effect of fluorescence than the Raman effect. Fluorescence is a common problem with Raman spectroscopy, a problem that may be solved by using a longer wavelength of excitation [47]. In the case of the materials used in this research, neither laser had a long enough wavelength to get good Raman spectra. Using ultraviolet excitation might resolve this issue, but in the absence of an ultraviolet laser, some other method was needed to test these materials.

An alternative method was devised using the same Raman microscope (a Renishaw (Gloucestershire, UK) Raman Microscope System 2000, with 514 nm excitation frequency) to quantify the luminescence of the fabric. In this method an incident laser of 514 nm illuminated the fabric and a continuous grating scan of the emitted light was conducted from 520 nm to 1000 nm. This produced a histogram of emitted and reflected photons in the visual spectrum. When this histogram is plotted with count versus the wavelength it gives a curve that identifies the important wavelengths for the reflectance of that material. It was hypothesized that the peak of this curve could be used as a diagnostic test to determine the level of degradation. Initial results were promising, as the peak wavelength appeared to shift slightly with increasing degradation. An example of the data produced by this method is given in Figure 4.5.

The peak is seen to shift from lower wavelength to higher wavelength as the exposure levels increase. Further examination of the repeatability of this method determined that the location of these peaks and shape of the curves were very inconsistent. For the same unexposed specimen, the location of the peak wavelength might shift 40 nm and the curve might have one or two large peaks (see Figure 4.6). Due to this inconsistency, the method was determined to be ineffective in precisely identifying peak wavelengths for the fabric tested, and therefore may be inappropriate as a diagnostic test of degradation.

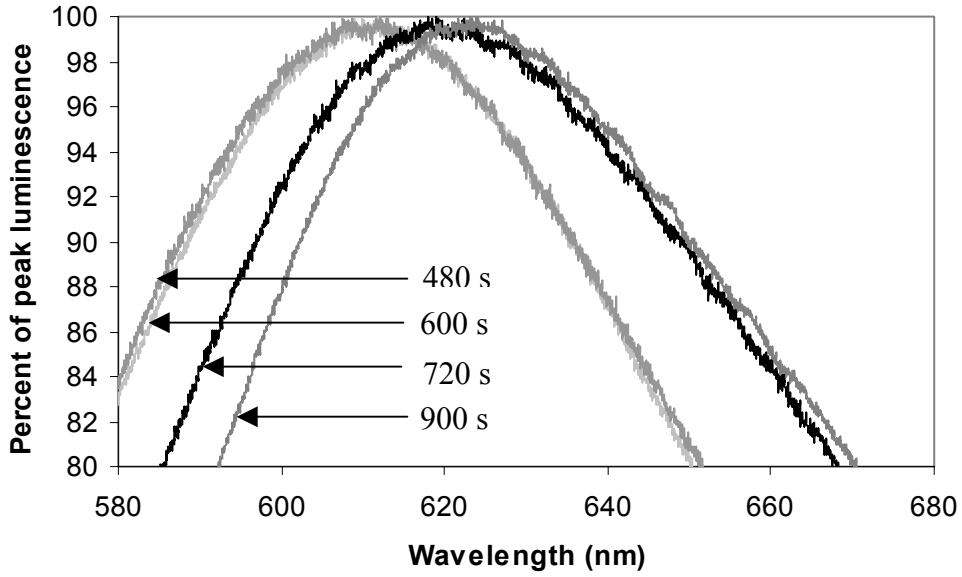

FIGURE 4.5: Raman luminescence spectra for outer shell fabric specimens exposed to a heat flux of 10 kW/m^2 for a range of exposure durations (view focused on 580 – 680 nm for clarity)

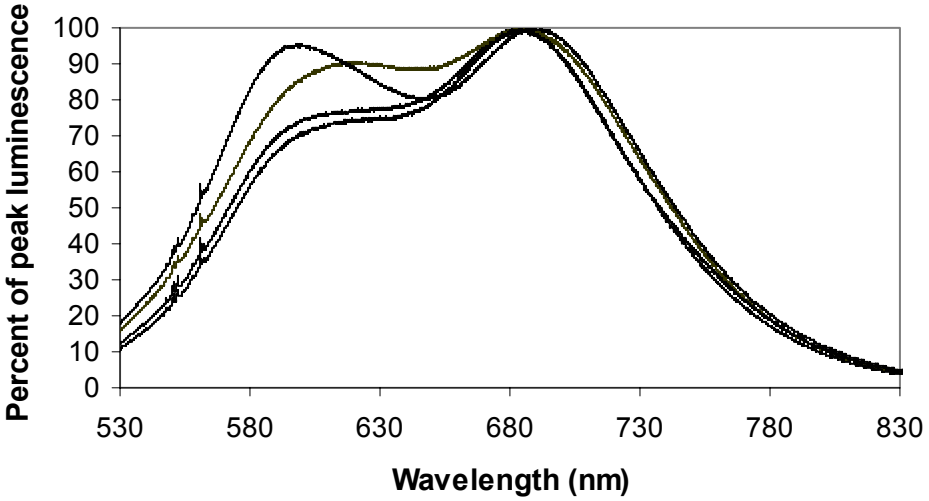

FIGURE 4.6: Raman luminescence method at different locations on the same unexposed outer shell fabric specimen

The focal point of the CCD of the Raman microscope can also be varied significantly. The objective lenses range from 5 x to 50 x, making the exact location of study somewhat variable. A study into the influence of objective size showed that the variability in the resulting curves could be a result of the objective chosen. Figure 4.7 illustrates the inconsistency inherent in this method, by comparing luminescence scans of the same location on the outer shell using two different objective lenses. The lens varies the size of the focal point: with the 5 x objective, a number of threads become the focal point, while with the 20 x objective an individual fibre on a thread is focussed on. The two curves are quite different both in shape and location of the peaks. This illustrates one aspect of the various analytical non-destructive techniques used throughout this research. Each of the techniques examines a different length scale. The 5 x objective of the Raman luminescence technique is effectively measuring the average luminescence of a number of yarns while the 20 x objective is directed at a single yarn.

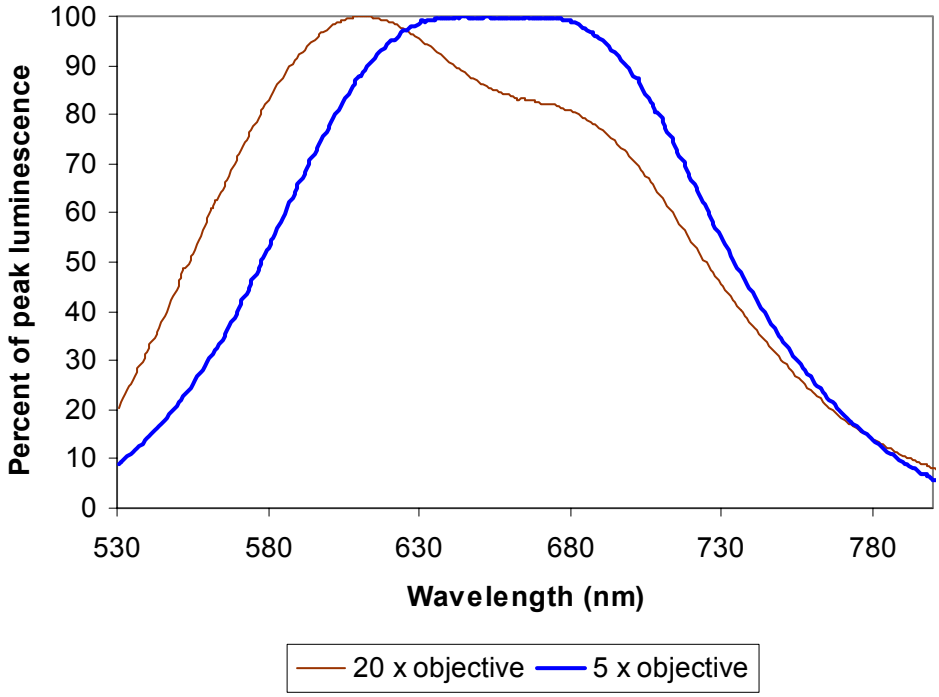

FIGURE 4.7: Raman luminescence spectra for outer shell fabric specimens exposed to a heat flux of 10 kW/m^2 for 120 seconds, two different objective lenses, same location

The inconsistency in the peaks of the unexposed outer shell fabric is thought to be caused by the variability of the dyeing process. Full saturation of the dye into a fabric is difficult to achieve in dyeing processes of technical textiles so the influence of incomplete dye saturation could alter the luminescence characteristics of the fibres, depending on the location of interest [48].

The appropriateness of this method may also be gauged by the relative cost of implementing such a system. Purchase of a new Raman microscope may cost in the order of $100,000 [49]. A fire department would not purchase a Raman system solely

for this purpose, but the lack of equipment availability may render testing inconvenient. An ideal non-destructive test for this application is one that does not require shipping of the gear; it is a test that can be conducted conveniently and in a short amount of time. These reasons also contribute to the rejection of the Raman luminescence technique.

4.3 Digital Image Analysis

Another technique to examine the fade of colour in the outer shell material was examined, this time using digital image analysis. In this technique, exposed outer shell fabric specimens were digitally scanned and the colors were compared and analyzed. Scanners, monitors and televisions all use a method of producing and recording colour known as RGB. This stands for the red, green and blue lights that are combined to create any colour required. The RGB system uses the colour cube as its fundamental model. The colour cube is a three dimensional space that has axes for red, green and blue. It is a Cartesian coordinate system with all of the values used consisting of positive coordinates: minimums at 0 units and maximums at 1 unit (see Figure 4.8 for an image of the colour cube). Any colour must have three components in order to exist in the colour cube. The number of bits used to represent the data will scale the method in which the number is stored, so if 8 bit data storage is used, 2^8 or 256 different colour intensity gradations can be distinguished. A zero level is black and a level of one is pure colour. If all three colors are pure then the resultant color is white.

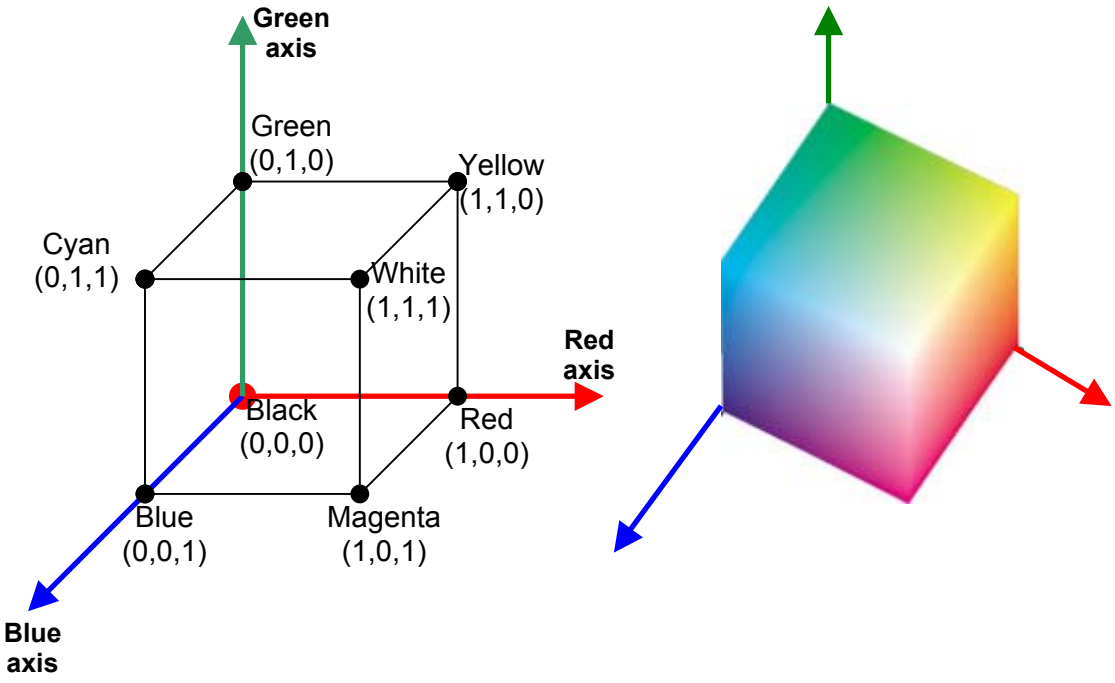

FIGURE 4.8: The RGB colour cube [50] (reprinted with permission)

Using a commercially available Hewlett Packard (Palo Alto, CA) Scanjet 4400c scanner, outer shell fabric samples were scanned with the "true color" setting and saved as a bitmap file. "True color" is based on three layers of 8-bit data, so 24 bit information for each pixel gives a possibility of 2^{24} or 16777216 colors. Files were saved as m x n x 3 matrices, with each m x n matrix filled with red, green and blue intensity levels respectively. A relatively low resolution is required for this procedure, so 150 dpi x 150 dpi was used, giving file sizes of approximately 3 Megabytes, and image sizes of approximately 800 pixels by 700 pixels.

Mathworks (Natick, MA) MATLAB® software was used to analyse the files. The program reads an image file from memory and stores it as an m x n x 3 matrix on which standard matrix operations can be performed. This particular procedure involves reading in the matrix of the fabric sample, selecting an appropriate interrogation area,

and then getting average values for the color intensity for each of the three layers. Figure 4.9 shows a representative scan, indicating a typical interrogation area used for this technique. The interrogation area in this case was chosen to be 100 pixels by 100 pixels. Using a scanning resolution of 150 dpi x 150 dpi, this corresponds with an interrogation area of 16.9 mm x 16.9 mm. A study of the sensitivity to pixel number indicated that the results were very similar when using 20 to 100 pixels for each side, but areas with less than 20 pixels per side had increased error.

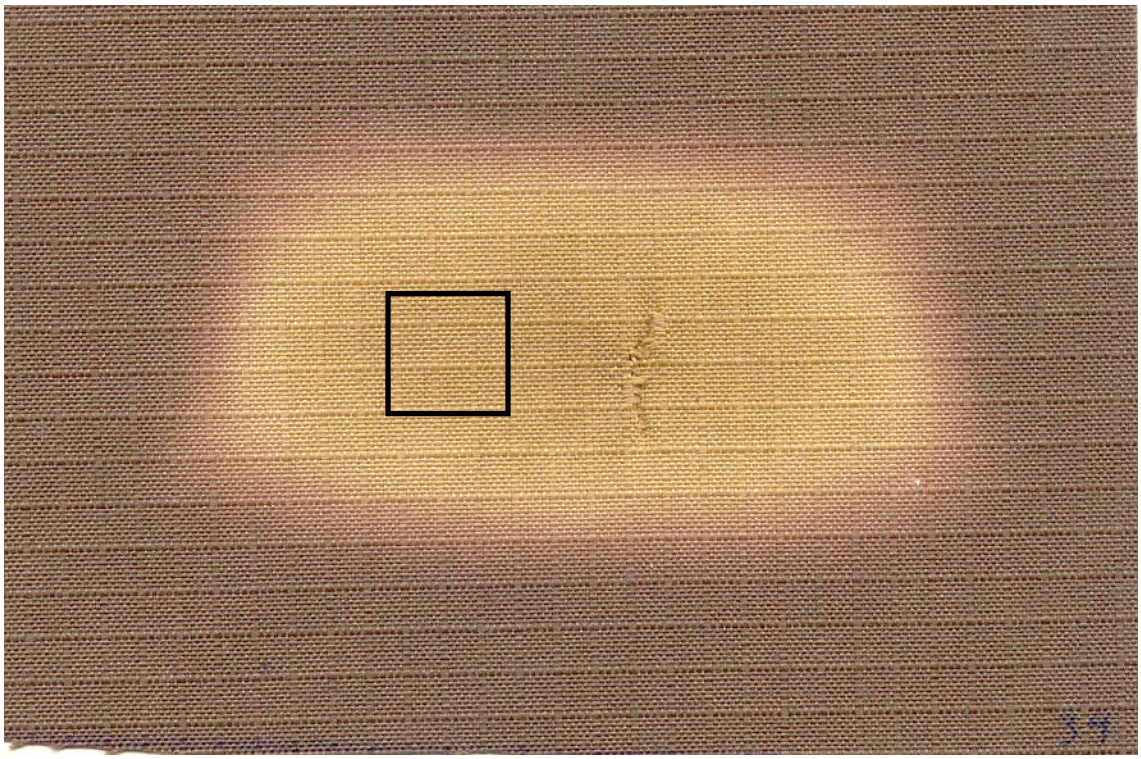

FIGURE 4.9: Digital scan of outer shell fabric specimen following 480 seconds of radiant heat exposure of 10 kW/m^2, interrogation area shown by black square

The interrogation area is selected through coordination with user input and a visual display to ensure that the area contains only the fabric that was exposed by the radiant

heat source (the heat affected zone). Once the interrogation area is selected, a new m x n x 3 matrix is created for that area. The average values of each m x n matrix are calculated and returned as single values for each of the red, green and blue layers, which represent the average values of the intensity levels of each colour. In Figure 4.10, the interrogation area from Figure 4.9 is converted from a 100 x 100 x 3 matrix to a 1 x 1 x 3 matrix, and shown as the summation of the red, green and blue values. The average values were then compared with color intensity averages for other heat flux exposures.

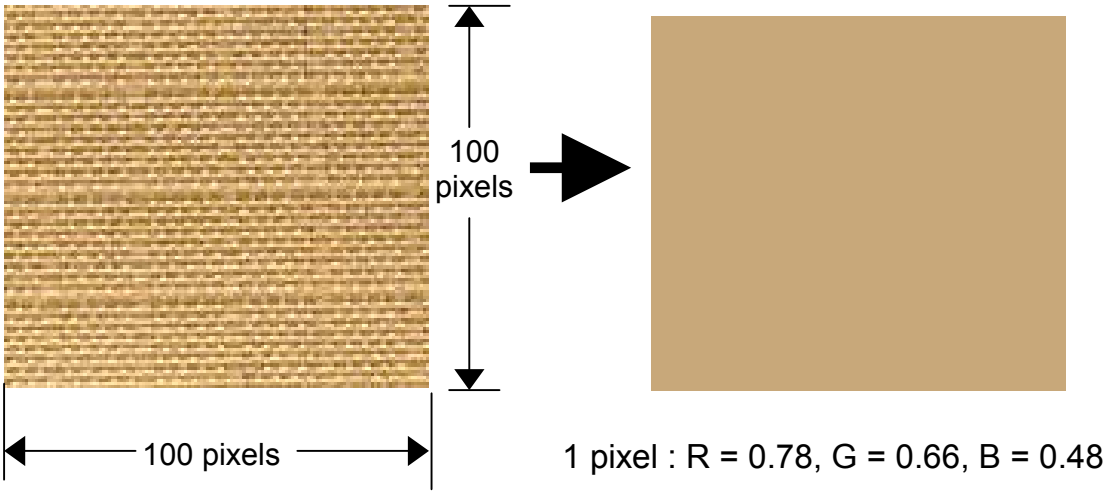

FIGURE 4.10: Interrogation area for 480 seconds at 10 kW/m^2 exposure, reduced to single colour by averaging values

The average RGB intensity values for the different samples are then input into a spreadsheet to compare the intensities with different exposure levels. Figure 4.11 illustrates one example of these results.

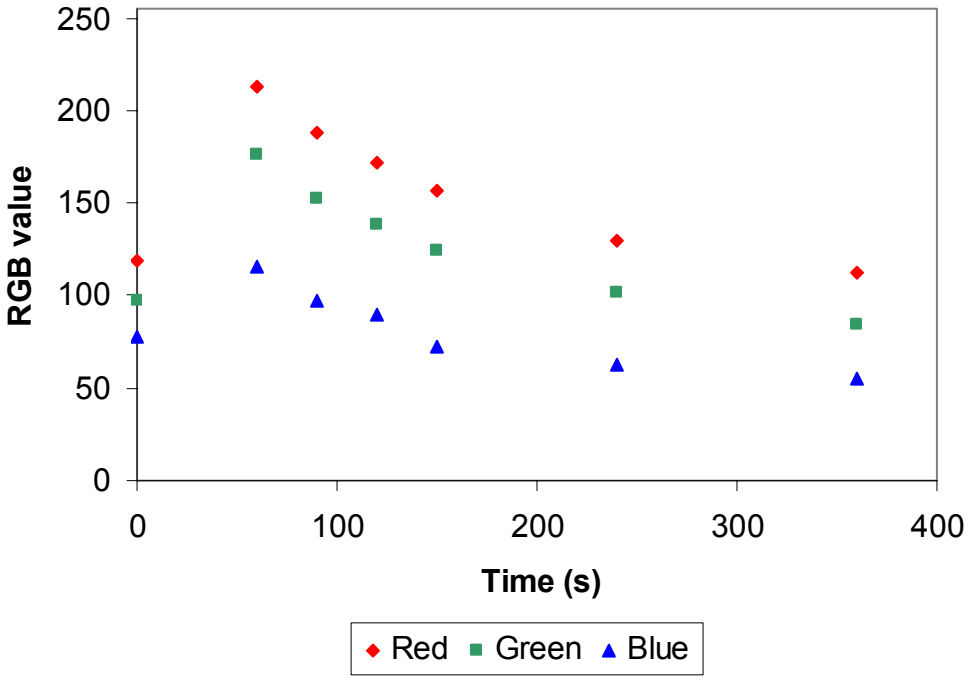

FIGURE 4.11: DIA results for outer shell samples exposed to 15 kW/m^2 radiant heat

It was decided that these data were not effectively expressed in this manner because RGB values are difficult to visualize, so a different colour model was chosen to represent the data. As was noted in Section 1.4, RGB is not an intuitive scale for the human eye, so in order to observe these data in a more intuitive manner, the CIE L*a*b system [25] was chosen. The CIE L*a*b system is a framework for plotting color in three spatial dimensions. It was designed by the Commission Internationale de L'Eclairage (CIE) in an effort to create a colour model more in keeping with the physiology of the human eye. The CIE L*a*b colour model is actually a Cartesian system (as portrayed in Figure 1.5) for quantifying colour but the limits of human colour perception reduce the image to a cylinder, so this is commonly how the model is portrayed. Figure 4.12 illustrates the colour model in its cylindrical form.

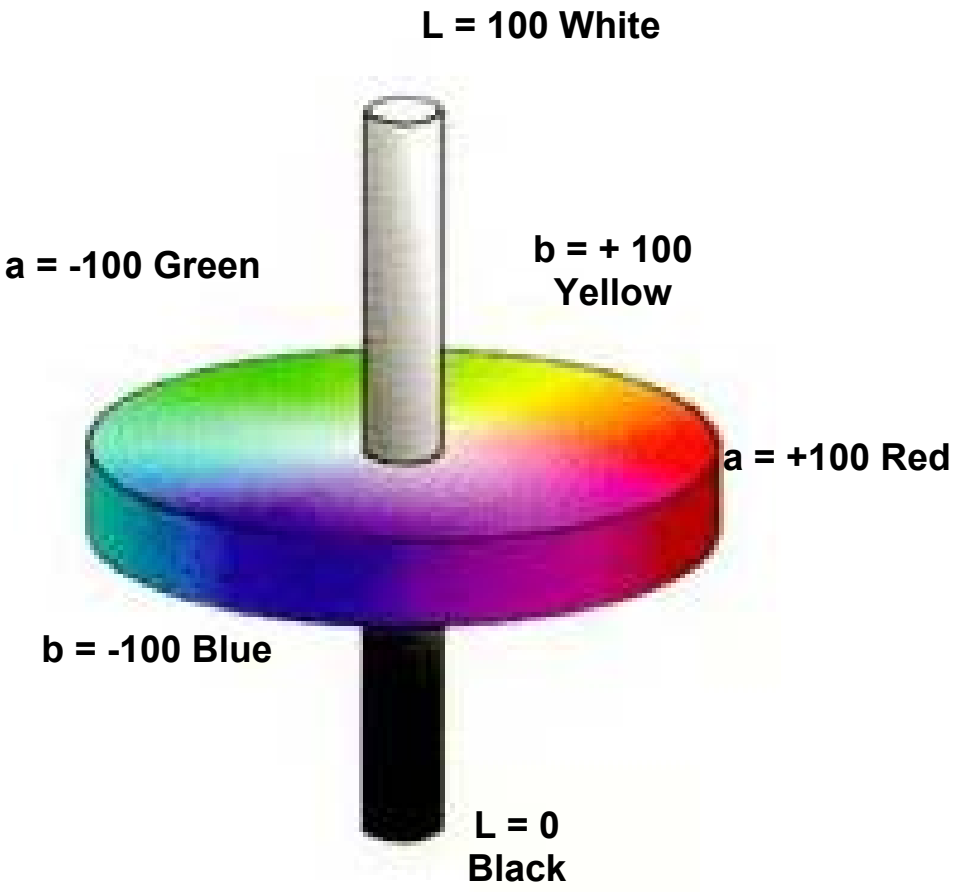

FIGURE 4.12: The CIE L*a*b colour model [51]

The “L” value refers to lightness from 0 to 100 (from dark to light), the “a” value is the placement on a continuum from green (-100) to red (+100) and the “b” value is the placement on a continuum from blue (-100) to yellow (+100).

One of the benefits of representing the colour data in this manner is that calculations of colour difference can be easily performed. The CIE developed the colour space with a mind to straightforward calculation of colour difference. Colour difference can be calculated as the Euclidean distance between two points in the colour space. This means that by determining the magnitude of the vector between two colours, a quantity

can be calculated that is the colour difference. Mathematically, the colour difference (ΔE) can be written as [52]

$$\Delta E = \left(\Delta L^2 + \Delta a^2 + \Delta b^2\right)^{1/2} \qquad (4.1)$$

where ΔL is the difference between the luminance values of the two points in question and Δa and Δb are the chromatic differences.

The RGB values determined by the MATLAB® scan method were converted into CIE L*a*b values using online conversion software [53] that employs a matrix conversion developed by the CIE [25]. The most obvious criterion to plot against is the exposure time, so there is a different graph for each heat flux level. The outer shell fabric specimens in this study have been dyed brown. This particular dye has been chosen as an appropriate compromise between visibility and reduction of the effects of soiling. As discussed in Section 3.2, when the fabric is subjected to certain thermal exposures the dye is consumed and the fabric fades to a bright yellow colour. After the yellowing, a charring process begins during which an increasing amount of the fabric turns black as thermal degradation occurs. The colour difference in CIE L*a*b space has been chosen to represent the color difference between an unexposed specimen and the specimen in question. Figures 4.13 to 4.17 show the results of the digital image analysis for the outer shell specimens. The highest colour difference values represent the yellowing of the fabric specimens. Lower colour difference values occur both near the original brown colour and after char has begun to accumulate on the samples. Figure 4.14 provides the clearest illustration of this rise and fall of colour difference. The highest value occurs at 600 seconds when the outer shell is the most yellow, after that point the

yellow turns brown and then black, a progression that is seen as a drop in the colour difference.

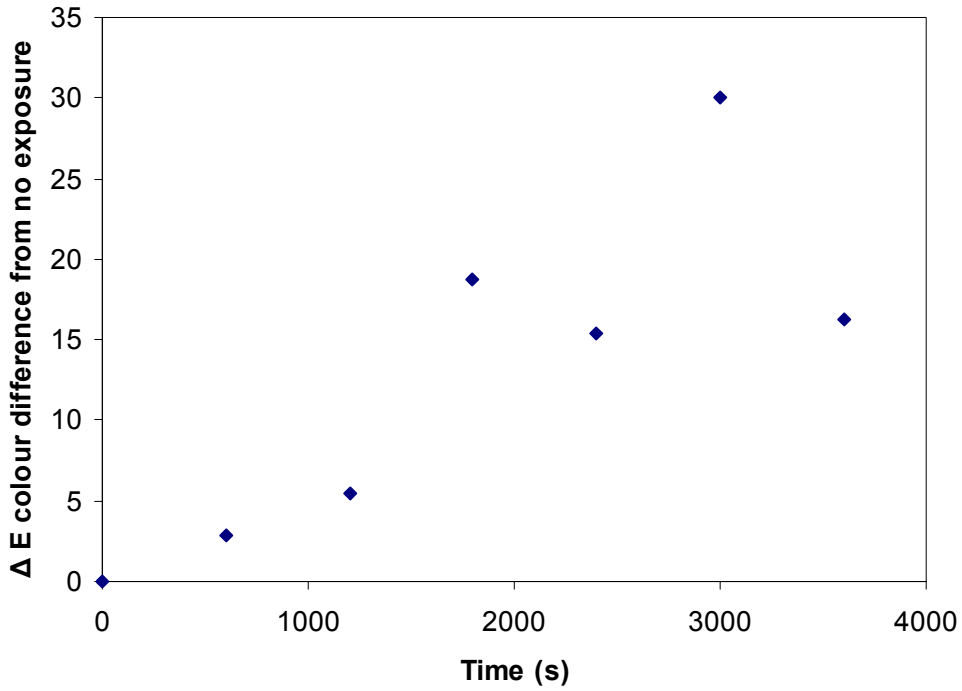

FIGURE 4.13: Digital image analysis for 5 kW/m^2 radiant panel exposure

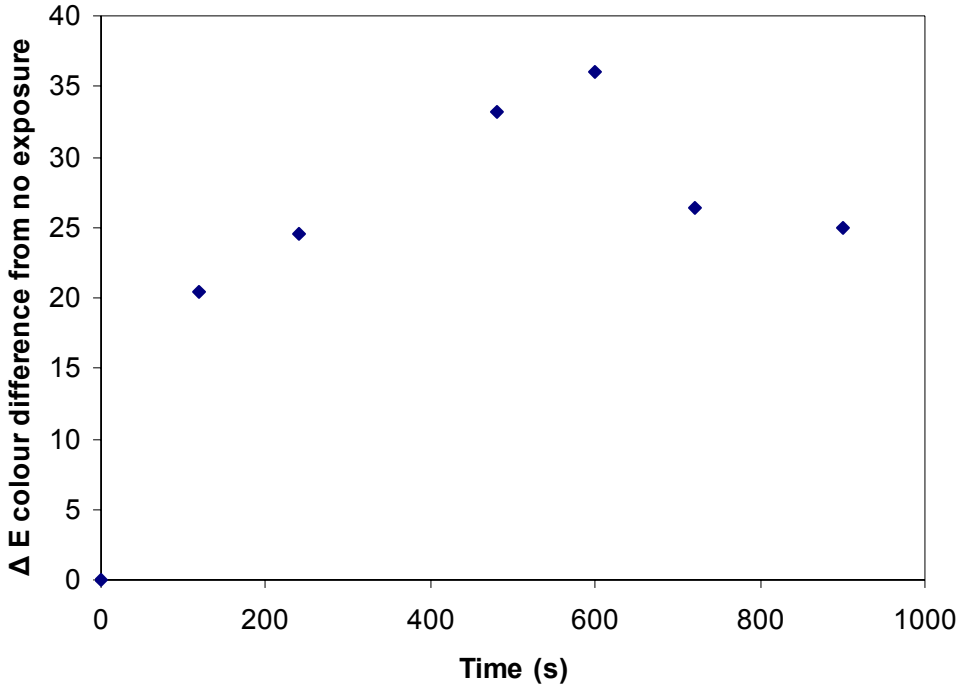

FIGURE 4.14: Digital image analysis for 10 kW/m^2 radiant panel exposure

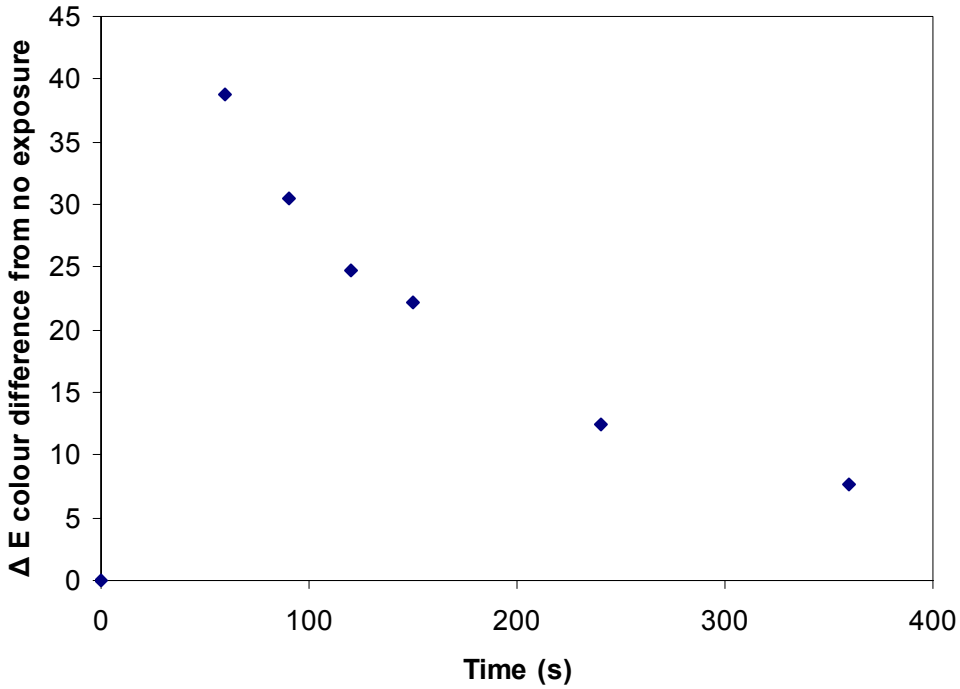

FIGURE 4.15: Digital image analysis for 15 kW/m^2 radiant panel exposure

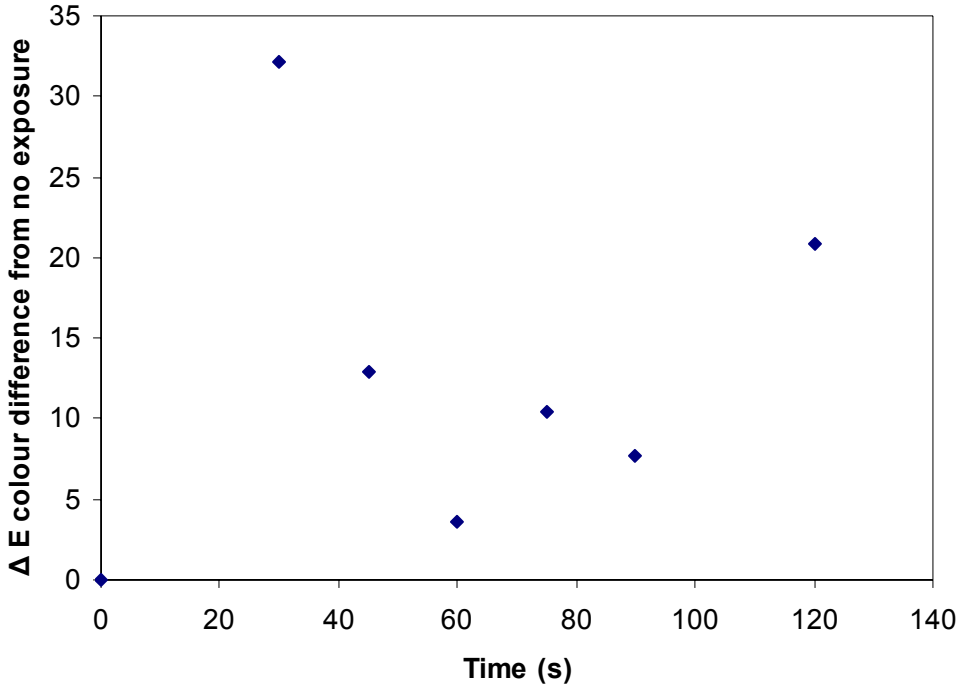

FIGURE 4.16: Digital image analysis for 20 kW/m^2 radiant panel exposure

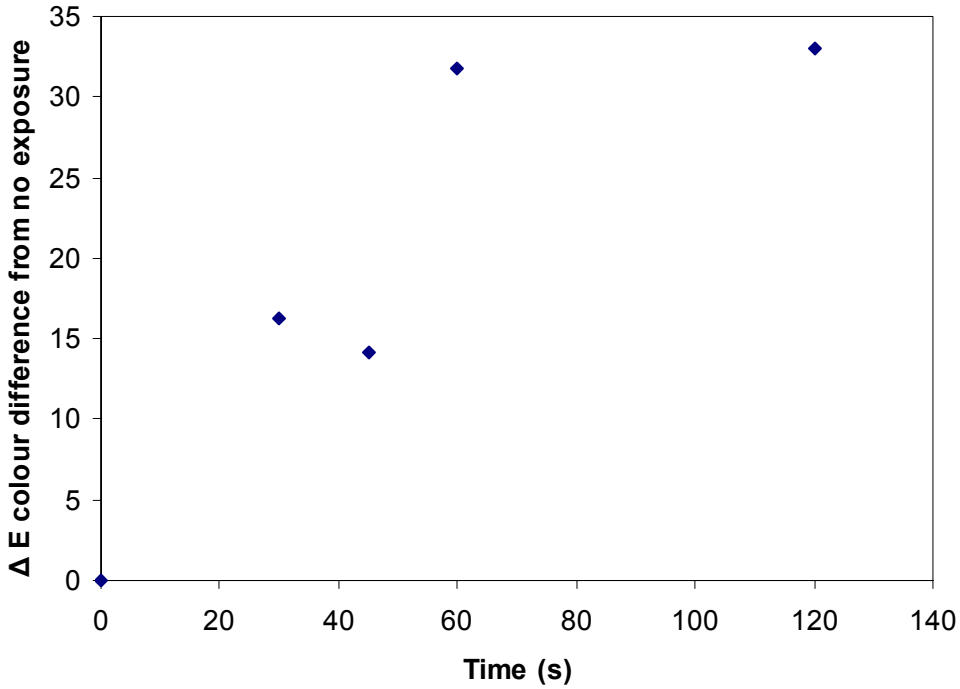

FIGURE 4.17: Digital image analysis for 30 kW/m^2 radiant panel exposure

One factor that will influence the adoption of various techniques for the fire service is implementation cost. The overall system would involve a PC, a scanner and some mathematics software. A PC and a scanner are very common pieces of equipment in any office, so potentially, the only cost would be the software. This testing apparatus also satisfies the desired criteria of convenience and ease of use. These reasons promote the choice of the digital image analysis technique for non-destructive testing of outer shell specimens.

The next chapter will compare the results of the digital image analysis with the results from the destructive testing. The correlation between the two methods should provide the basis for a diagnostic test that indicates the end of service life for a piece of turnout gear.

4.4 Colorimetry

The study of the measurement of colour is known as colorimetry. In colorimetric analysis, a standard light source is shone on a specimen and photoreceptors record the wavelengths of the reflected light. The results of the digital image analysis were considered to be successful, but some independent measure of colour changes was required. A colorimeter offers another method of analyzing the colour changes in the outer shell fabric resulting from heat exposure. For this study, a Hunterlab™ (Hunter Associates Laboratory, Reston, VA) Color Analyzer was used with a 10° standard observer, a D65 standard white reference illuminant, and an aperture of 6.35 mm (0.25 inch). Data is expressed in CIE L*a*b format as in the case of the digital image

analysis; this gives colour space coordinates for each fabric selected. Using the L*a*b colour measurement scheme, the difference in colours can be calculated as the magnitude of the vector between the coordinates.

In Figures 4.18 to 4.22, the unexposed fabric has been chosen as the reference point for calculating colour difference. This again demonstrates the increase in the magnitude of the vector colour difference as the yellow colour increases and the subsequent decrease as the char covers the fabric specimen.

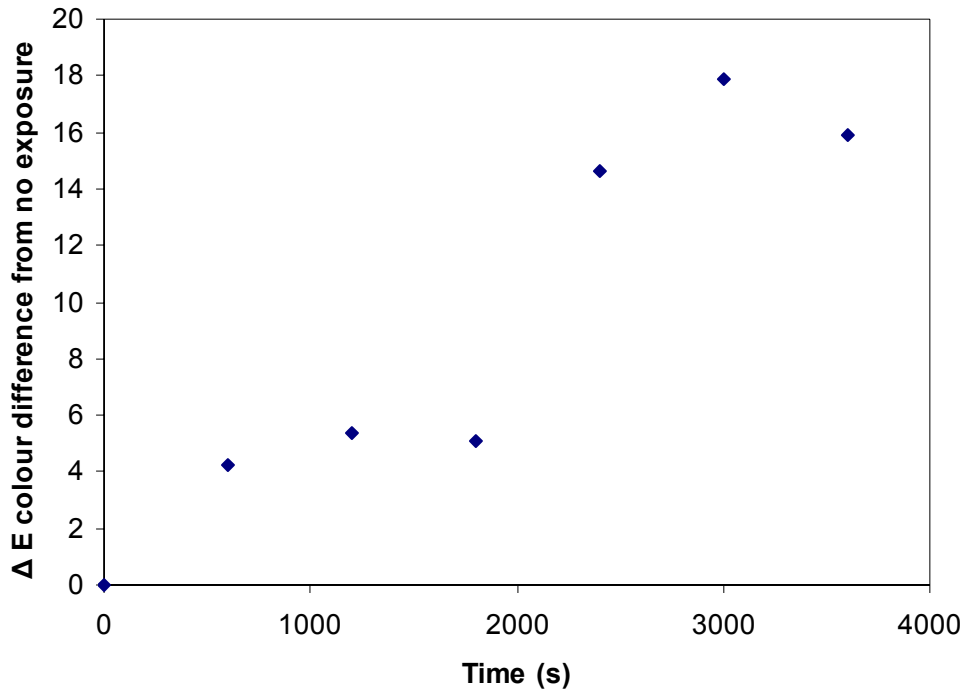

FIGURE 4.18: Colorimetric colour difference in outer shell samples subjected to radiant heat fluxes of 5 kW/m^2

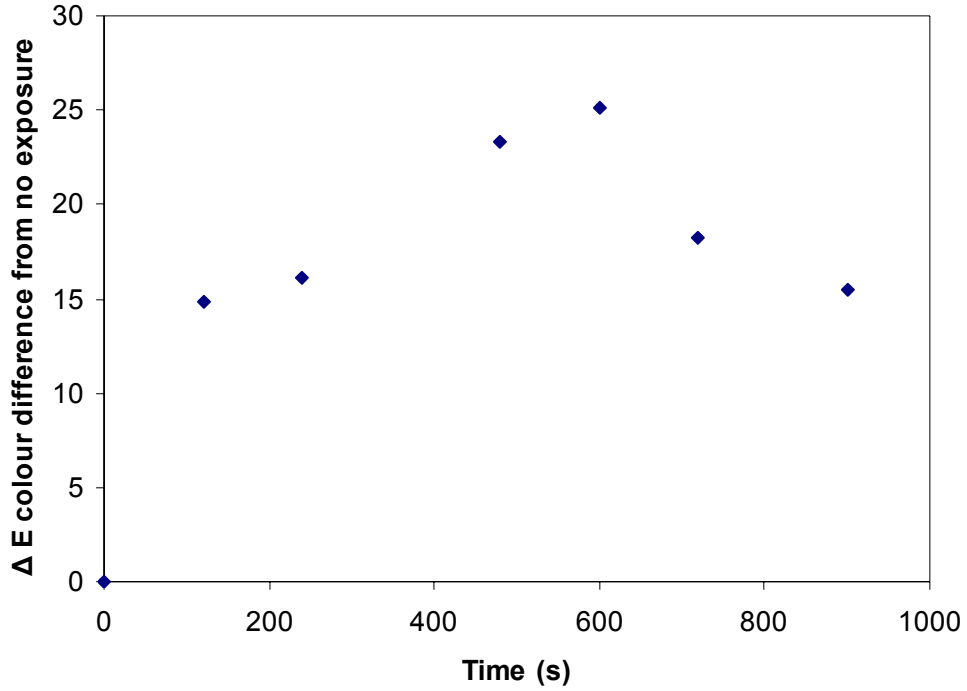

FIGURE 4.19: Colorimetric colour difference in outer shell samples subjected to radiant heat fluxes of 10 kW/m^2

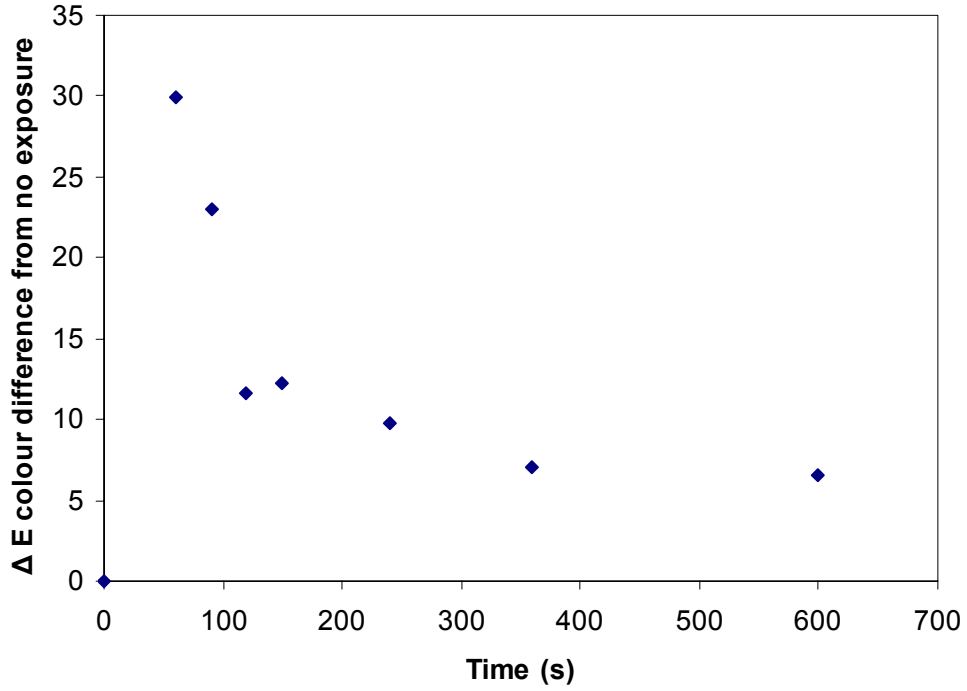

FIGURE 4.20: Colorimetric colour difference in outer shell samples subjected to radiant heat fluxes of 15 kW/m^2

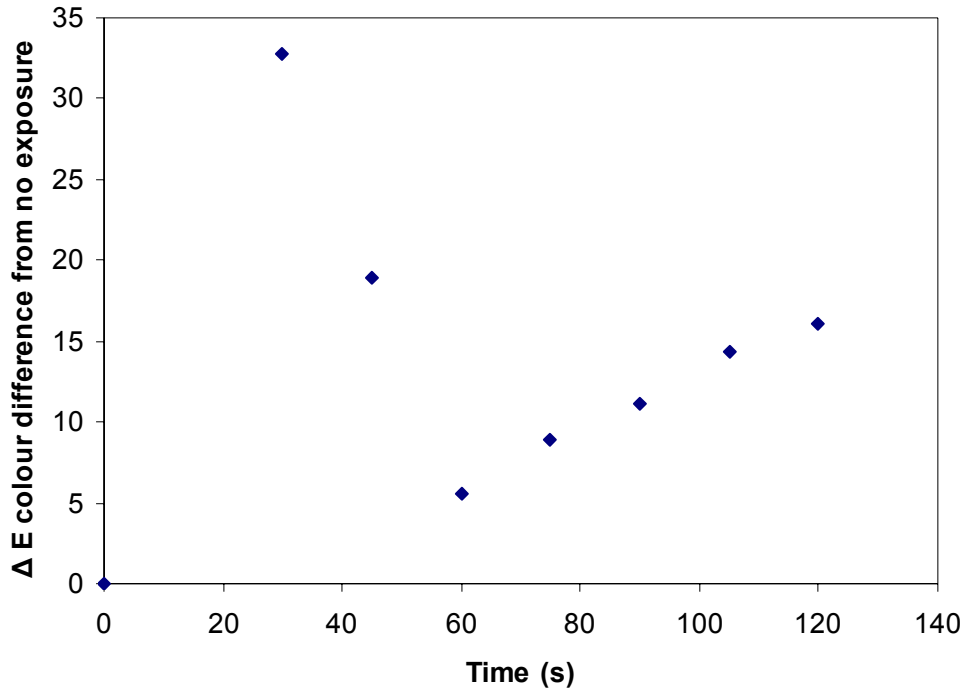

FIGURE 4.21: Colorimetric colour difference in outer shell samples subjected to radiant heat fluxes of 20 kW/m^2

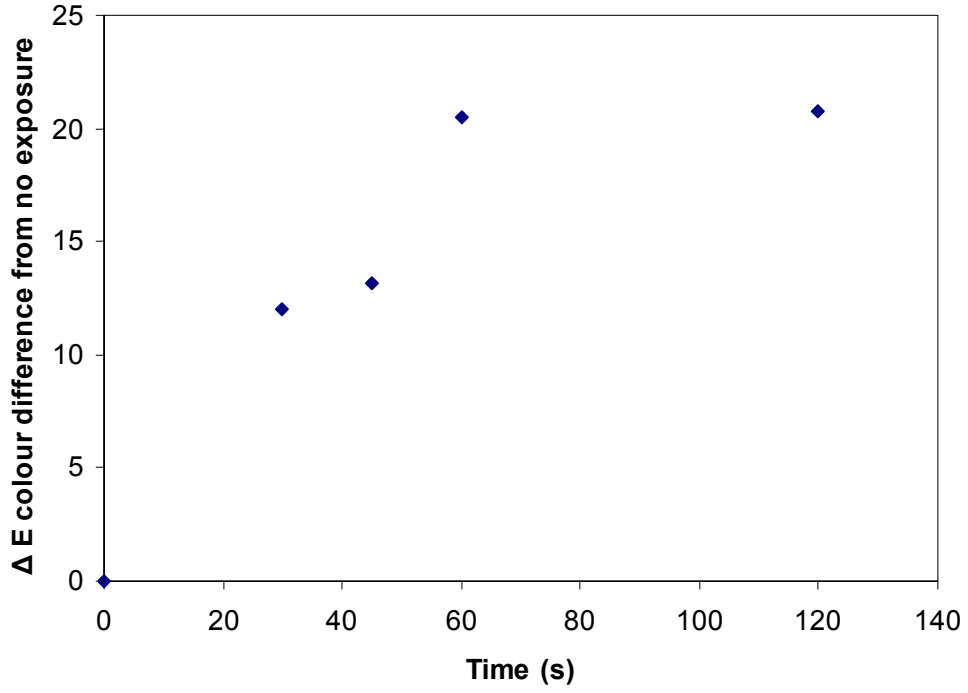

FIGURE 4.22: Colorimetric colour difference in outer shell samples subjected to radiant heat fluxes of 30 kW/m^2

A new colorimeter can cost up to $10,000 [54]. This cost, while less than the Raman microscope is still prohibitive to most fire departments and the use of a contracted laboratory would again result in a loss of testing convenience. Convenience and cost will be big factors in the adoption of a particular non-destructive test method, so a comparison between convenience and cost of the various methods presented in this study will be significant.

The next chapter will include a comparison of the digital image analysis technique and the colorimetry results. As mentioned previously, the potential benefit of these methods is in their use as diagnostic tests to predict performance of used turnout gear. Correlating these results with the destructive testing results will give an indication of the utility of these methods.

CHAPTER 5: CORRELATIONS OF DATA

The utility of these methods as non-destructive analytical tools is best assessed by comparing the results of the non-destructive test methods with the results from the destructive testing. In Chapter 3 it was shown that the destructive tests were inconclusive with regards to the thermal liner. Tear strength testing and compressive conductive performance testing demonstrated improved performance with radiant heat flux exposure. Even the most extreme exposure did not negatively affect the measured performance of the thermal liner so it was concluded that non-destructive testing should not focus on this layer of the ensemble.

The moisture barrier did demonstrate a loss of performance function after thermal exposure. While the moisture penetration was not compromised at any point in this testing, the tear strength testing demonstrated that the moisture barrier was susceptible to performance loss as measured in this fashion. That said, the moisture barrier did not show significant reduction in tear strength until the ensemble was exposed to 30 kW/m^2 radiant heat flux, an exposure level that coincided with very significant degradation of the outer shell.

Due to these factors, for this series of destructive tests, the outer shell performance is gauged to be the limiting factor in this ensemble. Since the moisture barrier is sewn into the garments and is inaccessible for examination, it was determined that

examinations into non-destructive tests of the outer shell would be sufficient. It should also be noted that only two aspects of the moisture barrier performance were tested in this study: liquid penetration resistance and tear strength. As will be discussed in Chapter 6, the effects of high heat fluxes on other aspects of moisture barrier performance such as vapour permeability, which may be measured using non-destructive tests, should be investigated.

5.1 Comparison of Digital Image Analysis and Colorimetry

The first test of the reliability of these methods is to compare the results from the digital image analysis and colorimetry. It is relatively straight forward to calculate the Eulerian colour difference between the two analytical techniques. Table 5.1 lists the different exposures and the colour difference between the two methods, as calculated in the CIE L*a*b space. The average calculated colour difference between the two methods is 4.58 units in the CIE L*a*b colour space. To provide some context for this number, the colour difference between the two methods for the unexposed outer shell was approximately 7 for DIA technique and 5 using the colorimeter. The colour difference between the two methods for the most yellow of the exposures was approximately 37 using the digital image analysis technique and approximately 35 using the colorimeter. These numbers correspond with a difference between the two methods of up to 100 per cent, obviously higher for lower values of ΔE.

While the measurements of colour difference are not particularly consistent between the two colour measurement techniques, it should be noted that the colour change trends are

very similar. A comparison of the colour difference data sets for the same heat fluxes shows this: Figures 4.13 and 4.18, Figures 4.14 and 4.19, Figures 4.15 and 4.20, Figures 4.16 and 4.21 and Figures 4.17 and 4.22 all demonstrate similar data trends.

TABLE 5.1: Comparison of colour measurement techniques

Heat Flux (kW/m^2)	Exposure Time (s)	Colorimeter ΔE	Digital Image Analysis ΔE	Difference between ΔE
30	120	15.11	22.19	7.08
30	60	14.69	21.82	7.14
30	45	11.02	12.63	1.61
30	30	7.29	11.51	4.22
20	120	13.18	20.85	7.67
20	105	12.25	7.67	4.58
20	90	4.01	4.26	0.25
20	75	8.36	10.37	2.01
20	60	4.97	3.58	1.39
20	45	13.69	12.87	0.82
20	30	27.15	32.19	5.04
15	600	5.53	3.46	2.08
15	360	4.70	4.30	0.40
15	240	5.64	5.67	0.03
15	150	7.69	13.75	6.06
15	120	19.57	19.21	0.36
15	90	17.69	24.21	6.52
15	60	24.24	32.93	8.70
10	900	10.30	16.90	6.59
10	720	12.74	18.75	6.00
10	600	19.98	27.17	7.18
10	480	17.80	26.94	9.15
10	240	14.50	23.20	8.70
10	120	13.59	19.93	6.34
5	3600	13.95	15.10	1.15
5	3000	12.91	23.85	10.94
5	2400	15.36	14.43	0.93
5	1800	4.86	17.58	12.72
5	1200	5.29	5.49	0.20
5	600	4.18	2.64	1.54
		average colour difference		4.58

In the analysis of whether to trust the colorimeter or the digital image analysis as the standard for these measurements, it is concluded that the colorimeter has a higher degree of accuracy than the DIA method. This is due to the nature of the colorimeter as a dedicated measurement of colour while the DIA uses a commercially available scanner, a tool that is designed to reproduce colour, not necessarily provide analysis of those colours. Thomson and Westland [55] note that the differences in colour measurement devices can lead to a problem in the comparison of results across media.

> Two physically different colour signals can be identical to the RGB system but not to the CIE observer, or conversely two physically different colour signals can be identical to the CIE observer but not to the RGB system. In fact, unless the device sensors happen to be equivalent to the CIE colour matching functions of the standard observer, there will be no one-to-one correspondence or mapping between device space and CIE xyz space, … this limits the usefulness of these devices.

Some work was done to examine the possibility of achieving an independent standard for measurement and the potential for a transfer function between the two colour measurement systems. Colour swatches were prepared on paper using an inkjet printer (see Figure 5.1), and the colours were measured using the two different methods. The colour difference between the colour values determined using each of the methods was then calculated. Since there is no independent reference, the ΔE colour difference reveals the differences in the methods, rather than in the colours.

The differences in the results for these tests were even more pronounced than the differences in the results for the outer shell fabric testing. As Table 5.2 indicates, the largest discrepancy was with primary colours such as red. This is positive in terms of the outer shell studied during this research, which is dyed brown.

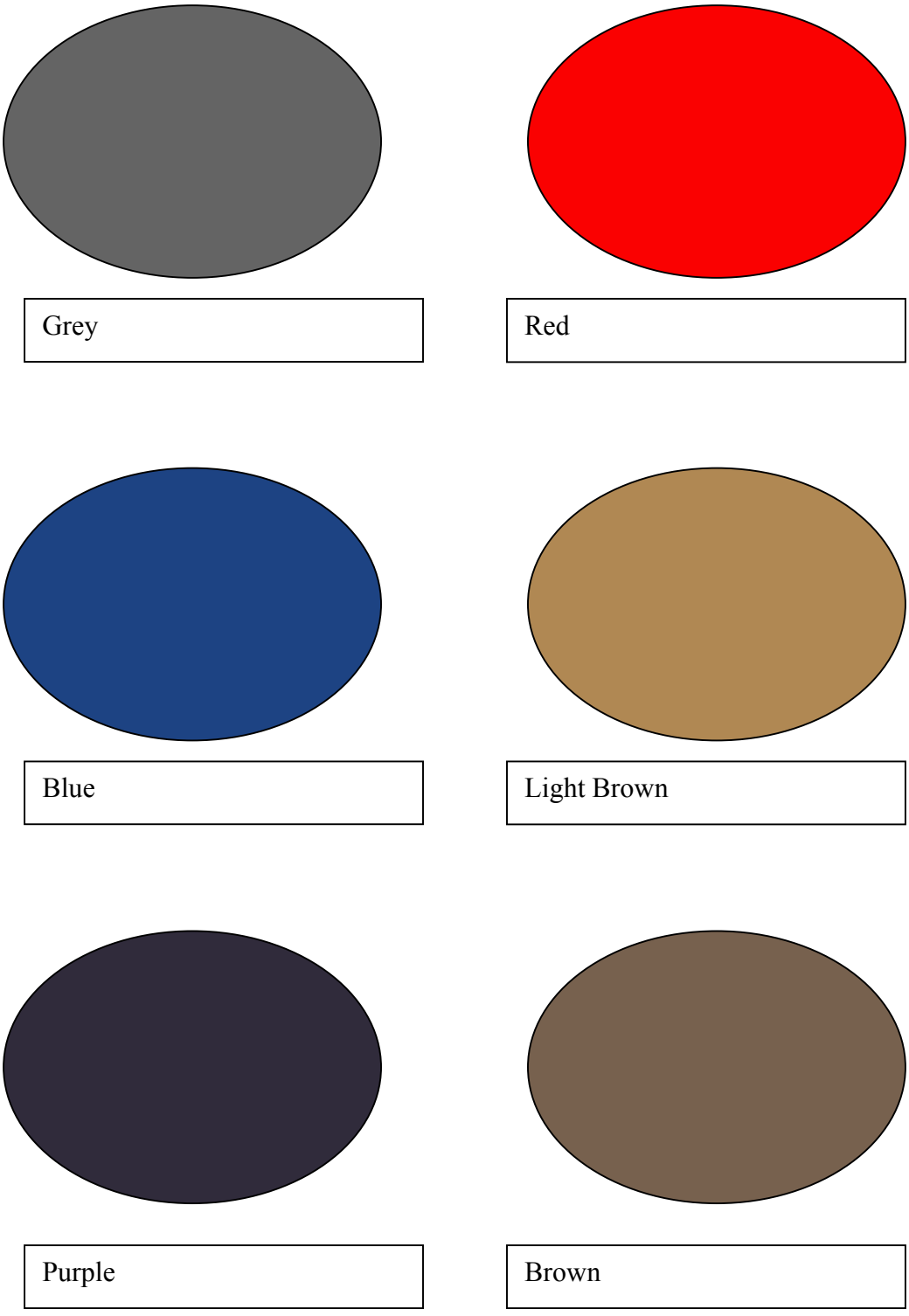

FIGURE 5.1: Colour swatches used for testing colour assessment methods

TABLE 5.2: Assessment of colour measurement techniques

	Colorimeter			DIA			
Colour Description	**L**	**a**	**b**	**L**	**a**	**b**	**Δ E (Eqn 4.1)**
Grey	40.70	-3.44	-4.99	51.61	7.37	-9.08	15.89
Red	37.53	49.56	16.30	53.87	79.02	51.37	48.63
Blue	31.41	-2.27	-41.07	36.78	12.11	-53.78	19.93
Light Brown	56.06	4.20	20.08	72.06	12.73	36.53	24.48
Deep Purple	22.85	1.47	-14.45	20.75	20.38	-36.16	28.87
Brown	39.20	2.04	4.22	51.49	17.18	6.08	19.59
					Average Colour Difference		26.23

These results suggest that the discrepancy between the two methods is systemic, but in the hardware and the software, rather than in the method. The results also suggest that the development of a transfer function to relate the two methods would be a complex task, outside of the scope of this research. If either method is to be used for the assessment of in-use turnout gear, it is critical to select one method and one set of measurement tools and consistently employ that method. A set of colour swatches could be used for calibration for the method selected, to provide a spectrum of heat exposures, with the expectation that every fabric should be placed somewhere between unexposed and total degradation.

The remainder of this chapter will examine the correlation between the performance of the outer shell of this ensemble with the results of the non-destructive testing using colorimetry and digital image analysis. Correlating in this manner should give an

indication of the possibility of these methods as beneficial non-destructive tests that could be used for the assessment of in-use garments.

5.2 Comparison of Outer Shell Tensile Test Results and Colorimetry

The outer shell samples were subjected to tensile testing as per ASTM Standard Test Method for Breaking Force and Elongation of Textile Fabrics (Grab Test) (D 5043) [37], as described in Section 3.5. When the results from the tensile testing of the outer shell samples are plotted against the colorimetry results, a pattern emerges that could be used to diagnose the breaking strength of a given outer shell from its colour.

Figures 5.2 to 5.6 illustrate the correlation between the colour change, measured by the HunterLab colorimeter and represented in Eulerian distance (see Section 4.3) between points in CIE L*a*b colour space, and the force required to break the specimens when tested in accordance with ASTM D 5043. The distance is measured from the colour data of a sample with no exposure, so the zero point in the colour difference can be considered to be the point of no exposure. A curve has been hand drawn on the points to indicate the trajectory of the colour change. It is the same curve drawn on each of the Figures; it has been drawn once all of the points had been plotted on the same curve. Figure 5.7 plots all of the colorimetry results on the same graph; the trajectory of the colour change is evident on this plot.

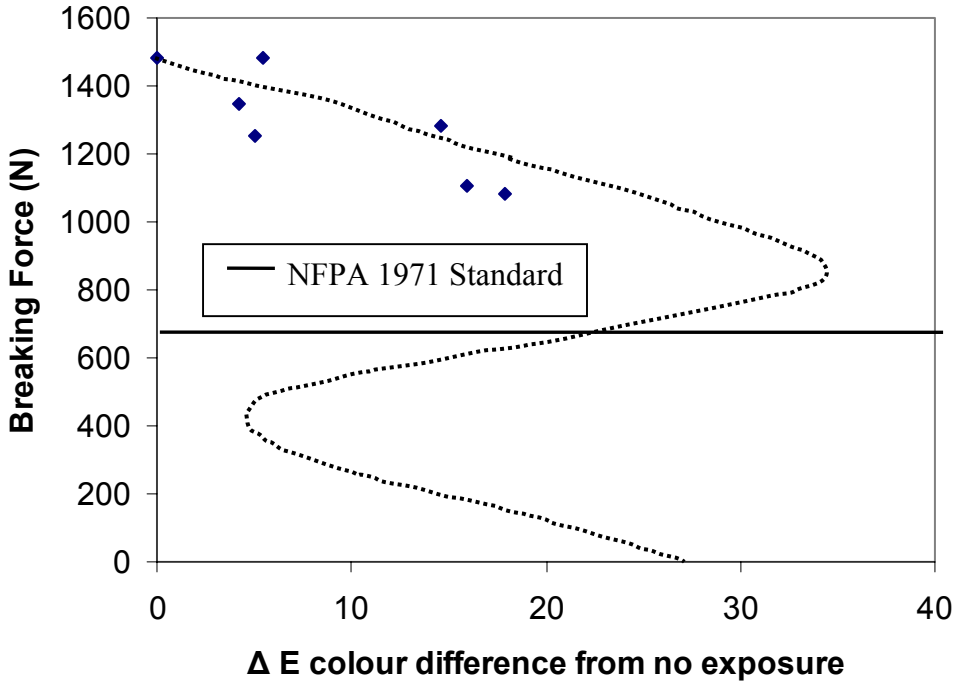

FIGURE 5.2: Comparison between tensile test performance and colorimetric colour differences for outer shell after radiant panel exposure of 5 kW/m^2

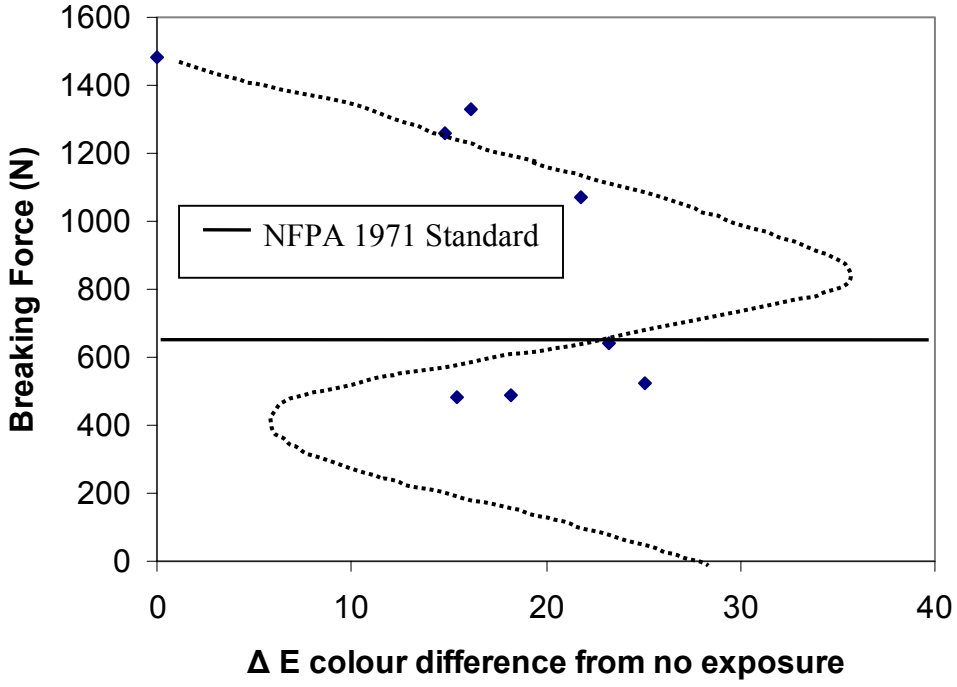

FIGURE 5.3: Comparison between tensile test performance and colorimetric colour differences for outer shell after radiant panel exposure of 10 kW/m^2

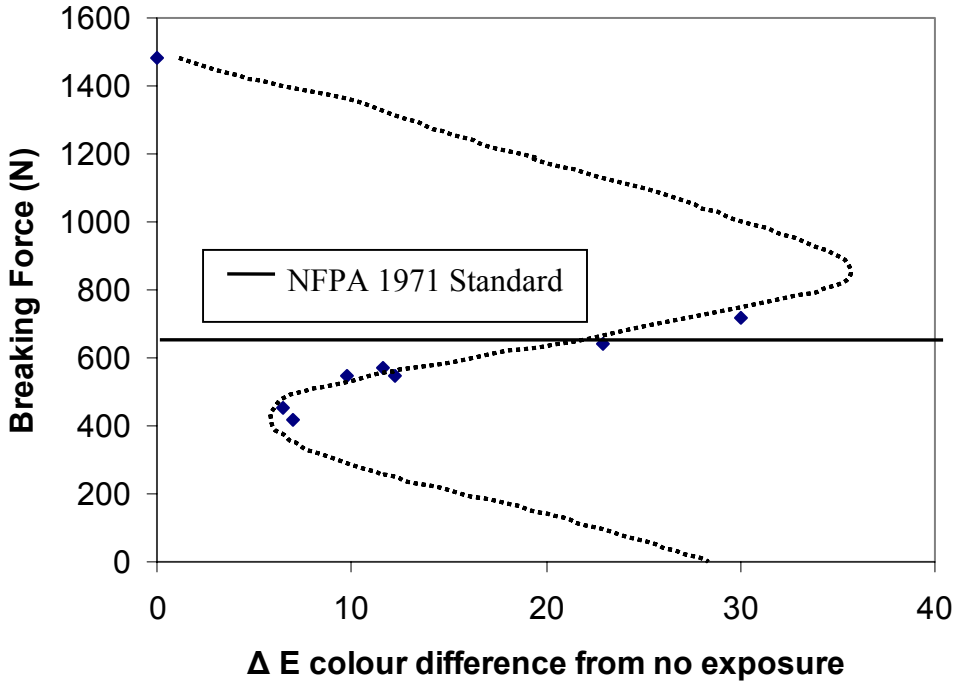

FIGURE 5.4: Comparison between tensile test performance and colorimetric colour differences for outer shell after radiant panel exposure of 15 kW/m^2

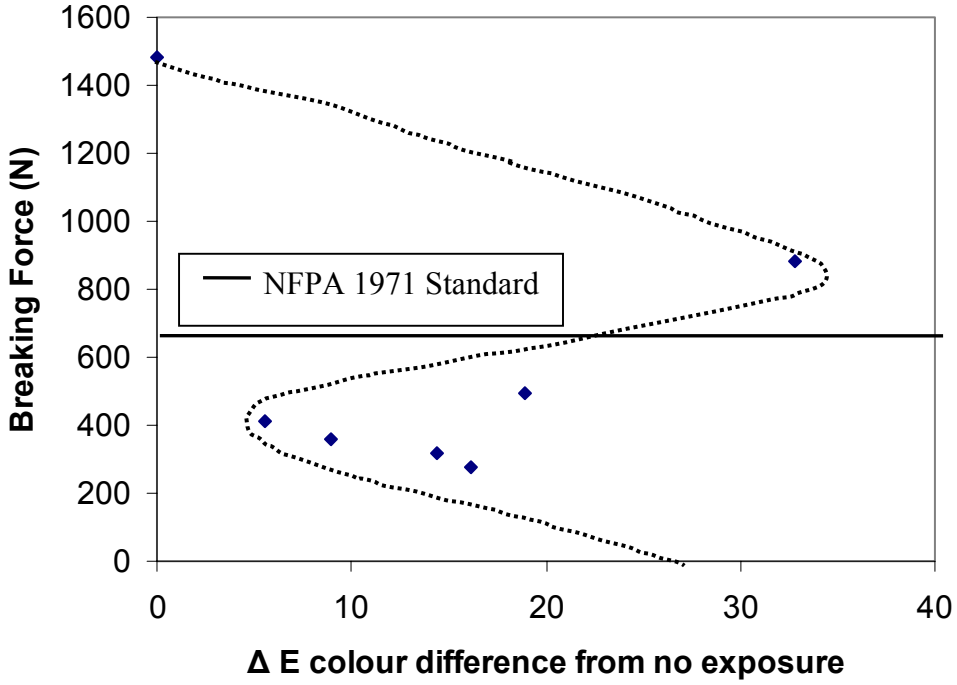

FIGURE 5.5: Comparison between tensile test performance and colorimetric colour differences for outer shell after radiant panel exposure of 20 kW/m^2

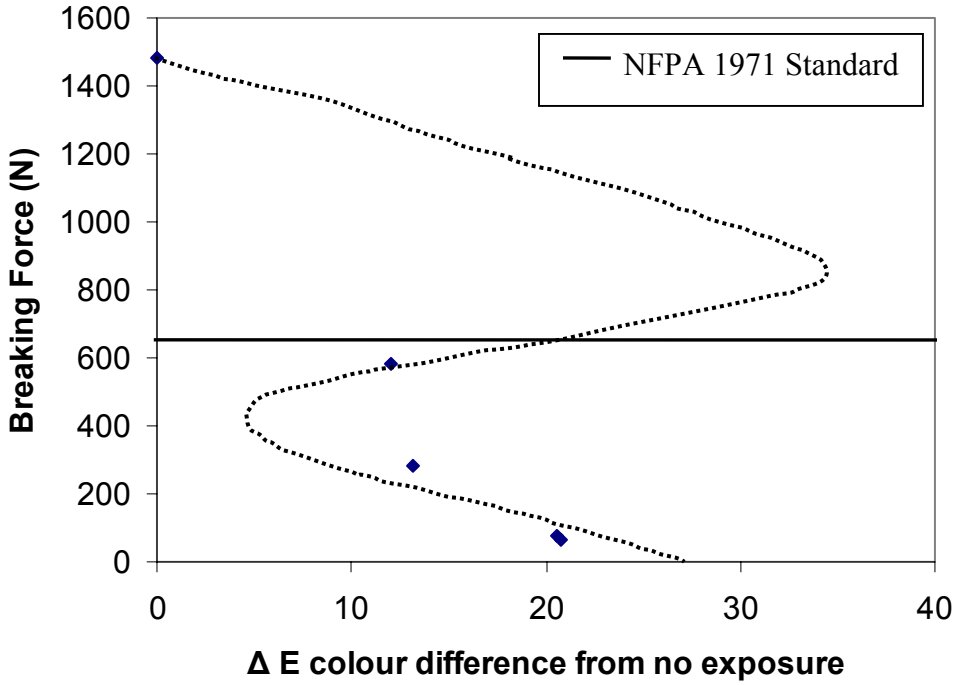

FIGURE 5.6: Comparison between tensile test performance and colorimetric colour differences for outer shell after radiant panel exposure of 30 kW/m^2

Figures 5.2 through 5.6 give important results, but perhaps the best way to see the use of this method is to combine all of these data into one graph. Figure 5.7 displays all of the specimens in terms of their colour difference from the case of no thermal exposure and their measured breaking force. Superimposed on the data in Figure 5.7 is the path of degradation as it is evidenced by colour change. This line is drawn to suggest how the method could be used to assess degradation of in-use turnout gear. The trajectory of the curve represents large changes in the colour of the fabric. Fabrics that have high levels of breaking force have experienced little degradation and consequently little colour change.

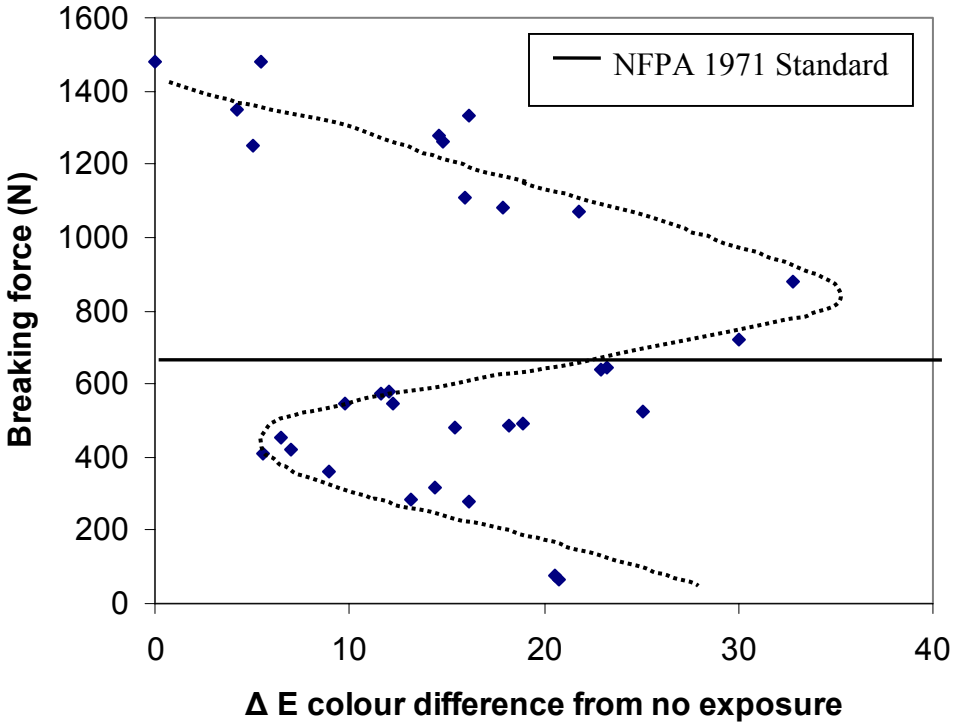

FIGURE 5.7: Combined colorimetry results for all outer shell specimens

The low colour difference numbers at the upper left of the figure indicate fabric that is still very close to the original brown colour. As the colour change increases, the breaking force decreases. The maximum colour difference corresponds with the case when the fabric is the most brilliant yellow. After this maximum the plot descends again as the fabric starts to turn brown again from charring. This creates a local minimum in the graph as the brown colour due to charring is similar in colour to the original brown. To an experienced practitioner the difference between these two browns is noticeable due to subtle differences in texture and appearance, but due to the relatively simple nature of the analytical technique, the test cannot distinguish between the two. After a minimum colour difference magnitude at approximately 400 N of breaking force the colour difference increases again. This is due to changes in the

appearance of the char that forms on the surface of the specimen. The fabric begins to blacken and become shiny as the individual fibres join together to form globules of carbon.

The trajectory of the curve includes three sections that could be confused if the colorimetry results were used without some experience. A measurement of 20 L*a*b units of colour difference could correspond with the case of the very start of degradation of the outer shell, with a breaking force of approximately 1100 N. Similarly, it could correspond with the brown as the char has begun to form, with a breaking force around 600 N; and finally it could correspond with a highly degraded fabric that is extremely brittle as in the case of the 60 second exposure of 30 kW/m^2. This is a result of the colour difference calculation: when measuring from a point in three-dimensional space, any point on a spherical shell of a particular radius will be the same difference from the original point. To the experienced practitioner these three states are noticeably different, so any test that used this method to assess degradation would involve some intuition on the part of the tester.

5.3 Comparison of Outer Shell Tensile Test Results and Digital Image Analysis

While the previous data has demonstrated the use of the colorimeter, it also raises some questions about the use of a test that could be affected by the texture and other non-colour related aspects of the fabric's appearance. The promise of using digital image analysis is that with minimal cost output the model could become more complex, by adding texture and shape analysis to the program. For this research, only the colour

changes were assessed, but with more work the technique could be enhanced with other analytical tools. The digital image analysis has a rather inexpensive set of requirements: a scanner, a PC and some analytical software. The National Institute of Standards and Technology (Gaithersburg, MD) has produced a free software package for digital image analysis called Scion Image (PC) and NIH Image (Macintosh) [56], so the cost constraint of the software portion of the method could be minimized. This research used MATLAB mathematical analysis software because it was available and familiar, but similar techniques could be implemented with other software packages.

Figures 5.8 to 5.12 show the correlation of the results from the tensile testing and the digital image analysis. The plots show the same patterns as the results from the colorimeter. The 5 kW/m^2 exposure shows little colour change; the 10 kW/m^2 exposure produces the largest colour difference as the fabric has faded to yellow. The higher heat flux exposures have reduced breaking force, and the colour difference drops to a minimum, then begins to rise again. Figure 5.13 provides an indication of all of the data from this testing when it is presented together. The curve descends initially from high breaking force at low colour difference, to a maximum colour difference at the point where the fabric is most yellow in colour. The curve then shows a trend to reduced colour difference as the char increases and the required breaking force is reduced. These results indicate that garments could be tested with a scanner and digital image analysis software and similar curves could be used to predict the performance of the garment in tensile testing.

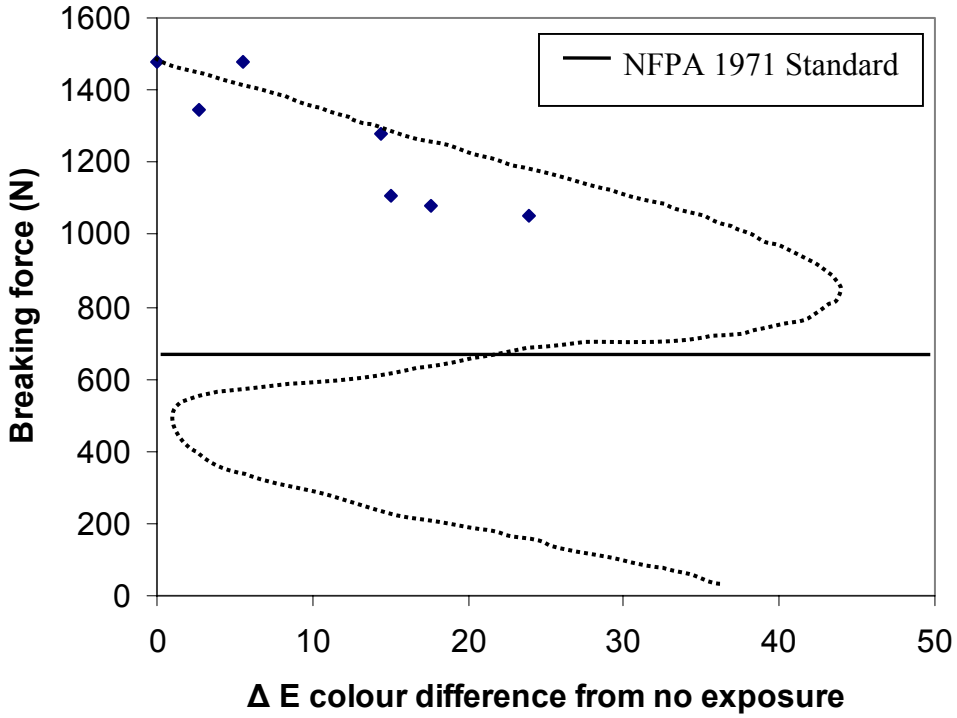

FIGURE 5.8: Digital image analysis comparison with tensile test performance, after 5 kW/m^2 radiant exposure

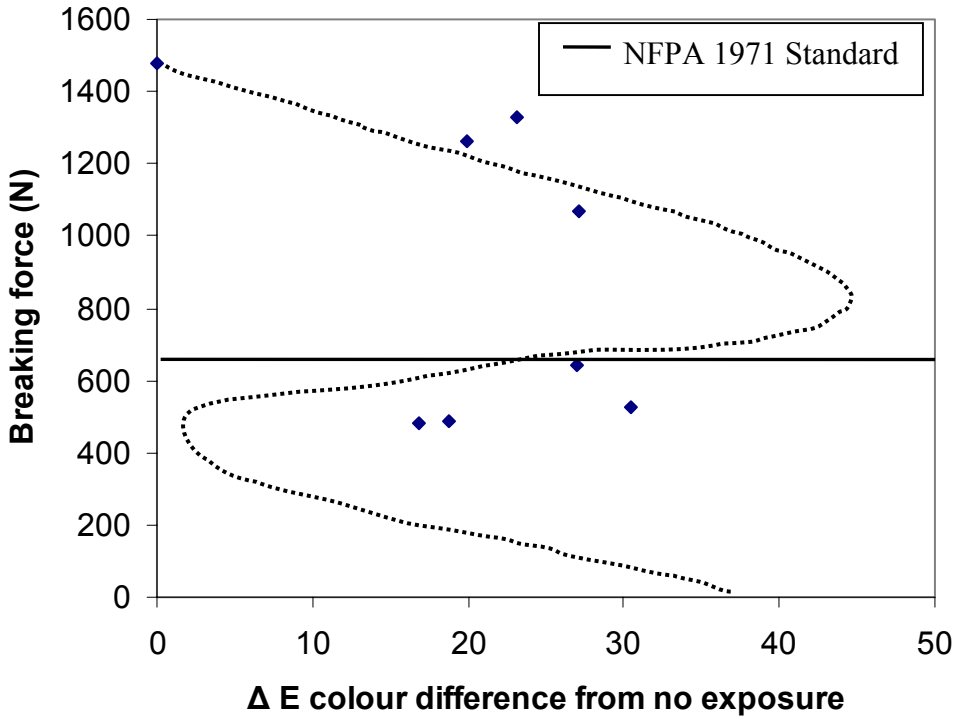

FIGURE 5.9: Digital image analysis comparison with tensile test performance, after 10 kW/m2 radiant exposure

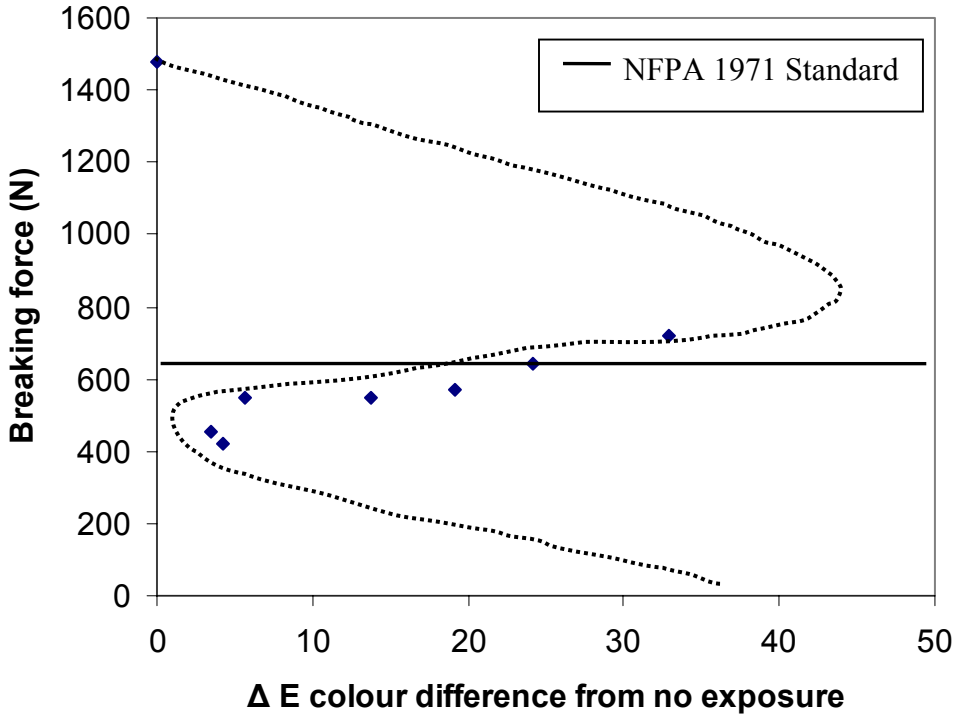

FIGURE 5.10: Digital image analysis comparison with tensile test performance, after 15 kW/m^2 radiant exposure

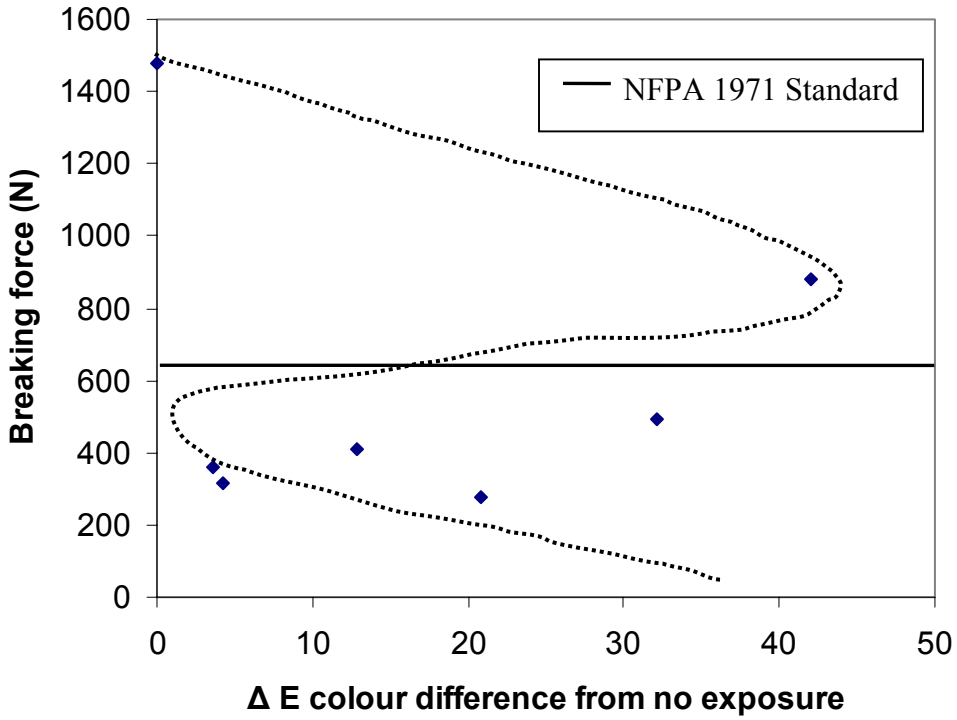

FIGURE 5.11: Digital image analysis comparison with tensile test performance, after 20 kW/m^2 radiant exposure

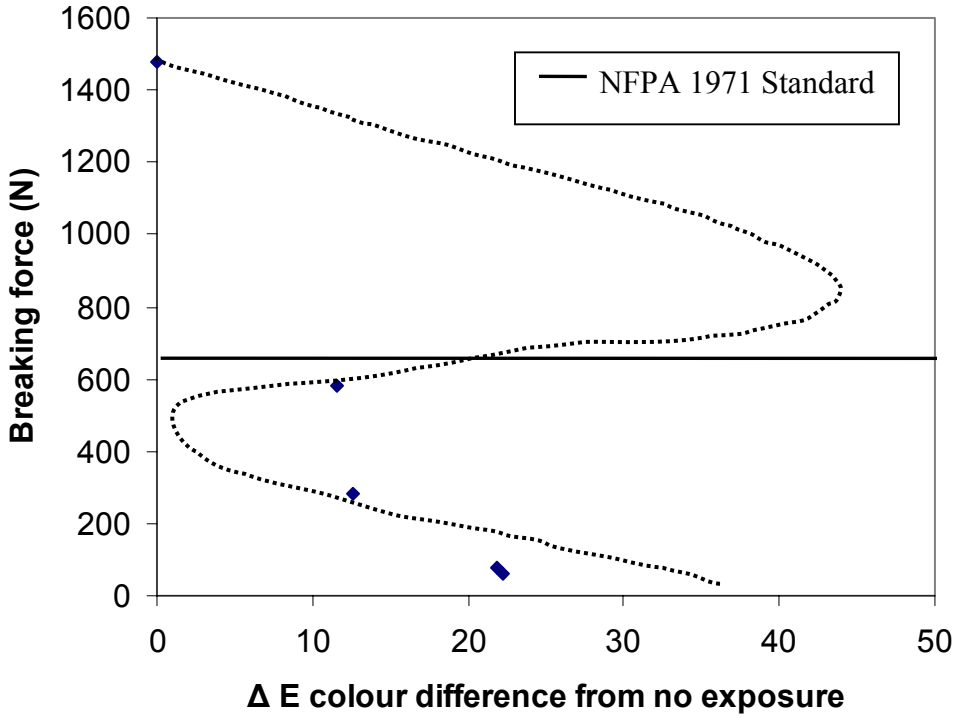

FIGURE 5.12: Digital image analysis comparison with tensile test performance, after 30 kW/m^2 radiant exposure

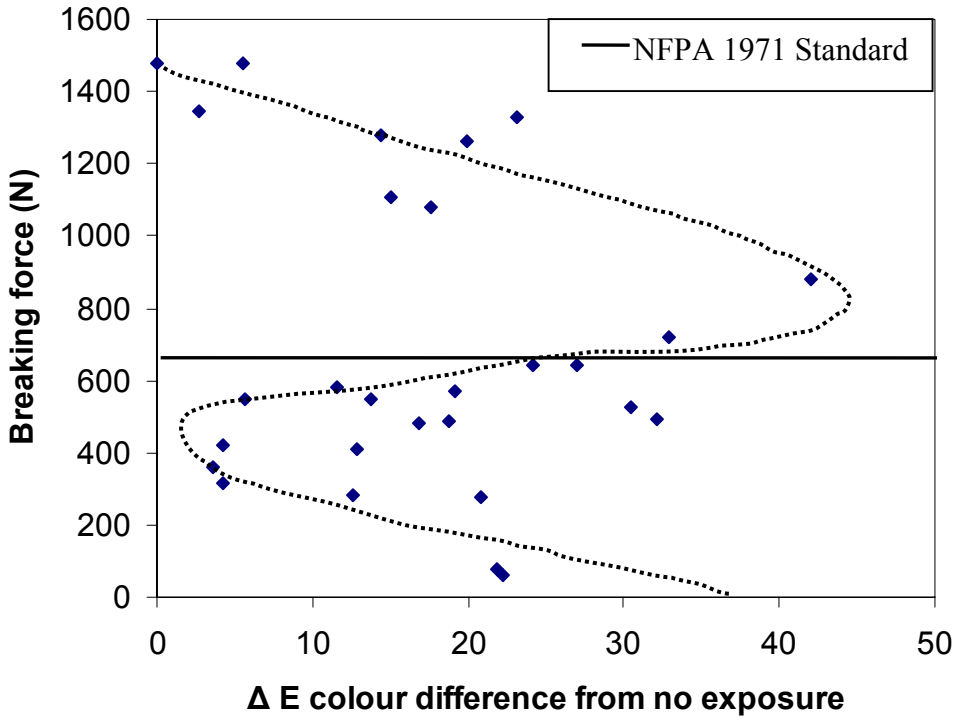

FIGURE 5.13: Digital image analysis colour difference as an indicator of breaking load for outer shell fabric specimens radiant heat flux exposures

The results of this technique are very similar to the colorimetry results. This is expected since both techniques are measuring colour change as an indicator of thermal degradation. The superimposed trajectory curve could be used again to place a test fabric along the curve to predict its breaking force. This technique has potential because the breaking force of a sample from in-use turnout gear could be predicted from similar curves that relate changes in the magnitude of the vector colour difference to the breaking load. This technique would require only a simple computer scan and some computational analysis. Again the need for more information than just the colour difference is noted, as there are a number of regions in Figure 5.13 that have different breaking force values for the same colour difference. The digital image analysis technique offers more promise in resolving this problem, as the knowledge of an experienced practitioner could perhaps be coded into the analytical program. Properties that could be added to the program include texture and reflectivity. The shapes of the fabric weave could also be determined through pattern recognition. Neither the sensitivity of this analysis to soil on the clothing nor the variability of different scanners has been assessed to date, but the promise of the technique is noted.

For an analytical test to be developed, some baseline data would have to be measured for every fabric and colour that is to be tested. Curves similar to Figures 5.7 and 5.13 would be required, so new specimens would have to be tested for colour difference and tensile strength. Since loss of tensile strength has been linked to the maximum temperature that the outer shell has achieved (TGA results from Section 3.2 combined with ensemble temperature measurements in Section 3.1 and tensile test results from Section 3.5), baseline testing could perhaps be conducted with one representative heat

flux. When a degradation curve is generated, this could then be used to test every garment that uses that same outer shell material and colour. This suggests the possibility of creating a library of degradation curves for various outer shell materials.

There is scatter in the data for this method, a fact which indicates that more work should be completed to clarify the consistency of the method. One reason for the scatter that has been suggested is the problem with the colour brown. Brown is a colour that cannot be easily described using these colour models, since it "cannot be produced by a combination of any three primaries. It can only be produced by a yellow color surrounded by brighter areas…we perceive something as brown instead of yellow when we think that its reflectivity is very low" [25]. Another variation on this problem is the fact that the char is black and increasing levels of char look like brown until the fabric is entirely black. The possibility exists then that the data would be more consistent with other dye colours in the outer shell. Some preliminary work was conducted to examine the possibility that other fabric colours would be better suited to these analytical methods. In his thesis work Torvi [57] examined the effect of flame on outer shell materials. Outer shell material made of blue dyed Nomex® was cut into specimens and subjected to 80 kW/m^2 flame exposure. Using a pneumatically controlled shutter Torvi was able to control the time of the exposure to a half second precision. He exposed fabrics to a Meker burner for times from 0.5 to 10.0 seconds in 0.5 second increments. The fabric specimens from that research were scanned and subjected to the digital image analysis to determine whether different colours would reduce the scatter in the data. Figure 5.14 plots the results of this preliminary study. The data form a very smooth curve with a marked shift in colour difference after 1.5 seconds of flame

exposure. This is a promising result; future work should further clarify the question of the appropriateness of alternative colours by conducting all of the destructive tests on this alternate fabric. This would answer the question of whether the scatter in the colour difference versus breaking force plots are due to the initial colour and the particularities of brown, or if there are other reasons for the scatter.

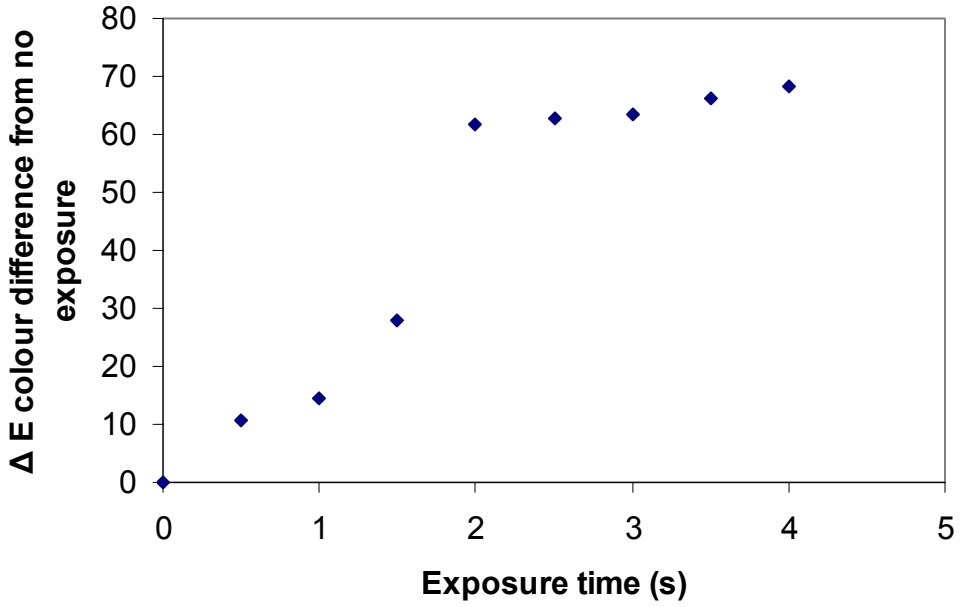

FIGURE 5.14: Digital image analysis of blue Nomex® subjected to 80 kW/m^2 flame exposure

The digital image analysis technique offers the most promise of the methods studied for this research in terms of incorporating more sophisticated assessment algorithms because of its relative simplicity and the use of common equipment. DIA also offers reduced capital cost and increased convenience over Raman Spectroscopy and colorimetry. Using free software, the only cost of implementing a DIA system for non-

destructive evaluation of thermal exposure on outer shells of turnout gear would be the development of a diagnostic program.

In this chapter two similar methods for assessing colour fade on outer shell fabric materials were compared. The digital image analysis technique and the colorimetry technique were used to create a distinctive curve for this brown outer shell material. The promise of the method was demonstrated, though it was noted that the data had a lot of scatter. It was suggested that a more thorough examination of digital image analysis techniques would improve the results of this testing. Preliminary tests of a blue material were conducted, with promising results that suggest that the dyes of other colours than brown may be better suited to this type of analysis. The next chapter discusses the implications and limitations of this work and draws some conclusions from these results.

CHAPTER 6: SUMMARY, CONCLUSIONS AND FUTURE WORK

6.1 Summary

This study was designed to explore the possibilities of using non-destructive test methods to assess the service life of fire fighter's turnout gear. The current standard for new gear, NFPA 1971 defines a number of tests that should be conducted on new gear, but has no mention of gear that is in service. The standard for the maintenance of fire fighter's protective clothing, NFPA 1851 does not provide quantitative tests to decide when to retire the gear. The gap left between the two standards has been noted in the literature, and it has been therefore the focus of this thesis work.

A study of the conditions that fire fighters face in the field involved recording heat fluxes and temperatures during two different live fire exercises. Observations were made of the comfort level of the fire fighters with different heat flux intensities. The influence of long duration, low intensity heat exposure on the performance of turnout gear has not been well studied to date. The results of this testing were used to define some useful heat flux levels for study of relatively low heat flux intensity with increased time duration. A radiant panel performance (RPP) testing apparatus (as described in ASTM F 1939 [28]) was selected to provide repeatable exposure levels for artificially aging turnout gear specimens. The fabric ensembles were exposed using the RPP apparatus, and then subjected to a series of destructive and non-destructive tests.

Temperatures at three locations of the ensemble were recorded during the radiant exposure of the fabric ensemble specimens. This provided an indication of the protection that each layer provided, and the temperatures that each layer will experience during the heat fluxes in question. To this information, thermogravimetric analysis was added. This testing gave an indication of critical temperatures that would result in degradation for each of the ensemble layers. The mass changes that each layer experienced at different temperature exposures were noted and compared with the temperatures recorded during the exposures. Interpretation of later results was made possible by the TGA data.

This research was concerned with the influence of thermal degradation on the performance of fire fighter's protective clothing. Some representative tests were selected from NFPA 1971 to demonstrate the performance of the clothing. Thermal exposure was limited to radiant heat flux; the degrading effects of conductive or convective heat fluxes were not considered. Based on the available research, this assumption was considered to have validity. There is a large body of literature that points to ultra-violet light exposure and laundering effects as having a significant influence on the lifetime of the fabrics that comprise the clothing. To limit the scope of the problem, these latter two factors were ignored.

Testing of the thermal liners demonstrated strong performance with increased radiant thermal exposure. Tear strength testing demonstrated that the thermal liners when new easily meet the NFPA 1971 standard of 22 N when tested according to ASTM F 5733. Even as the thermal liners experienced more thermal exposure, at no time did their tear

strength come close to the limit imposed by the standard. One factor to note is that the temperatures reached by the thermal liner were considerably lower than those experienced by the outer shell, as Figures 3.1 to 3.6 indicate. This is not surprising, but it does give an indication of why the thermal liner held up so well.

A second destructive test was performed on the thermal liner. The exposed liners were then tested for their compressive and conductive heat resistance according to ASTM F 1060. The NFPA 1971 standard for this test requires that the complete ensemble take at least 13.5 seconds to experience a temperature increase of 24°C when placed on a hot plate at 280°C ± 5°C. Since the outer shell material demonstrated a high degree of degradation during preliminary testing, and more testing was required of the outer shells, it was decided to use only the thermal liner for these tests. The conduction resistance provided by the thermal liner was nearly 50% of the overall conduction resistance, so this was considered to be an acceptable compromise of the standard. The thermal liners actually demonstrated an increase in CCHR rating with increased thermal exposure. It was suggested that this is a result of increased hardening of the Kevlar® fibres in the thermal liner batting, enforcing the air pockets to remain even under the influence of an external pressure source. Since the thermal liner's performance increased with thermal exposure, it was decided to focus on other elements of the ensemble for the non-destructive testing.

Moisture barriers were tested only for liquid penetration and tear resistance. The function of modern moisture barriers is to provide protection from any liquids on the outside of the turnout gear, but the moisture barrier is also required to allow moisture

vapour to escape through the garment. It is thought that this reduces the overall heat stress on the fire fighter. This research did not consider the effects of thermal exposure on the vapour diffusion performance of these moisture barriers.

Liquid penetration testing was performed on the moisture barriers. Standards call for the moisture barrier to provide enough protection that there is no penetration of the barrier for one hour. All of the moisture barriers in this study that were structurally sound when tested for their liquid penetration resistance passed this test. This result was justified by a study that demonstrated that the pore sizes of ptfe moisture barriers are reduced with thermal exposure [45]. This fact likely increases the liquid penetration resistance but decreases the vapour diffusion performance.

Tear strength testing was also performed on the moisture barriers in this study. NFPA 1971 calls for 22 N of tear strength. It was observed that a characteristic of the radiant panel performance tester that was used to expose the fabrics in this study is the production of an oval shaped heat-affected zone that does not cross the entire fabric specimen. It was seen during this testing that this heat affected zone influenced the tear strength of the fabric, and so it was concluded that this test was inappropriate for assessing the influence of thermal exposure on the tear strength of these moisture barriers. Some preliminary work was conducted to assess the viability of different exposing apparatuses for this testing. It was observed that using a 6 in. (15.2 cm) cone calorimeter, an exposure that spans the breadth of the specimen could be achieved. The shape of the tear strength curve changed as a result of this different exposure. Further work should exploit this benefit of the cone calorimeter.

Outer shell specimens were tested to determine whether their tensile strength was reduced as a result of thermal exposure. It was found that certain radiant thermal exposures did indeed reduce the tensile strength of the outer shell below the minimum acceptable standard of 622 N as required by NFPA 1971. Only one destructive test could be performed on the outer shell specimens, so the results of the tensile strength testing formed the basis for the correlation between the destructive tests and non-destructive tests performed on the outer shell.

Since the performance of the thermal liner was not negatively affected by the thermal exposure in the tests that were conducted, it was determined not to use the liner for non-destructive tests. The moisture barriers demonstrated no loss of liquid penetration function in this testing, and the tear strength testing was determined to be problematic. In a similar fashion, the moisture barrier was rejected for non-destructive evaluation in this study. The outer shell is the most accessible layer anyway, so this choice is the most appropriate. As will be discussed in Section 6.2, more work should be conducted to evaluate the effects of thermal exposures on other properties of the moisture barrier.

Exposed outer shell specimens were tested using four different non-destructive testing techniques. Optical microscopy was used to make observations of the effects of thermal exposure on the appearance of the outer shell fabrics. Increased exposure was seen first as a change in colour of individual strands in the fibre, then as the fabric was further exposed, fibres began to melt and fuse together. This fusion formed globules of

polymer that were shiny and smooth. It was decided that an observational method would not produce quantitative results, so other methods were considered.

Raman spectroscopy was chosen to test these fabrics because it has been used for other in-situ fabrics with success. With remote sensing technology, turnout gear could be tested without destroying the garment. It was determined that Raman spectroscopy would not work for this material, the fluorescence was simply too great to retrieve meaningful results. Two different laser wavelengths were used, but still the fluorescence created an unmanageable signal to noise ratio. Using an ultra-violet laser was suggested, to potentially reduce the fluorescence, but due to equipment restraints, this was impossible during the timeframe of this research.

Another technique was devised using the Raman microscope. It was suggested that the absorbance of the material that was causing problems in the fluorescence could be used as an analytical tool. The luminescence of the outer shell materials was measured, as light from the laser was reflected and absorbed and emitted from the outer shell fabric. This technique showed promise, but it proved highly erratic and consequently was rejected. It was postulated that inconsistent dye on the fabric strands caused the erratic results for this method. Some preliminary work was conducted to assess the consistency of the method with other outer shell colours. This work was promising, but more study is required before this method can be affirmed.

A colorimeter was used to measure the colour of the outer shell fabric specimens, and to quantify the fade of the colour. This created more promising results, as the colour could

be compared with the breaking strength for each specimen. A characteristic curve for each fabric could be generated and used to provide data for a diagnostic test of degradation. More work is needed to assess the level of scatter in the data, but the technique was considered to have some promise.

A technique for measuring colour was devised using a digital scanner and mathematics software. The results for this testing were very similar to the colorimetry results, which is to be expected since both techniques measure the change in colour of the outer shell specimens. The correlation between this testing and the breaking strength of the outer shell could be used to create a simple method of assessing degradation in outer shell fabrics.

The correlations between the digital image analysis technique discussed in Chapter 4 and the destructive testing discussed in Chapter 3 have limitations. The correlations are accurate insofar as the scope of the project allows, they do not consider the colour changing influence of sunlight or laundering or even soil on the fabric. The digital image analysis technique itself as a measure of colour fade is independent of the mechanisms that cause the fabric to fade. More work is required to verify whether fade caused by sunlight and laundering has the same performance implications as the colour fade caused by purely radiative thermal exposure as tested in this research.

6.2 Conclusions

This research examined the possibility of using non-destructive test methods to assess the degradation of in-use fire fighter's protective clothing. It was determined that colour fade could be used to observe degradation in the outer shell fabric. Destructive tests were used to compare exposed fabric specimens with the criteria specified for new gear in NFPA 1971. It was determined that the outer shell was the ensemble element that was most susceptible to performance reduction due to degradation. The outer shell was tested for its breaking force. The breaking force of the outer shells was reduced to the minimum acceptable level at different times of exposure, depending on the heat flux to which they were exposed. It was observed that the breaking force was compromised when the temperature of the outer shell reached approximately 400°C.

Non-destructive tests were used to provide a quantitative measure of the degradation of the outer shell specimens. Raman spectroscopy was found to be very inconsistent due to a high degree of fluorescence. A Raman luminescence technique was developed, but this was also inconsistent due to inconsistencies in fabric dye. Digital image analysis and colorimetry provided a means of measuring the colour fade, providing an enhanced visual examination technique. These results could be used to create a test for degradation by measuring the colour of in-use turnout coats, and using a correlation with the breaking force measurements.

6.3 Future Work

There are many ways to extend the results of this research. One suggestion is to delve further into the world of digital image analysis. Research into digital image assessment developed for other applications that use more complex algorithms to assess the texture of fabrics could be incorporated to improve this method (see e.g. [24], [58], [59]). The time constraints of this research limited the possibilities of examining texture as an indicator of degradation in any detail, but the possibility exists for more work into the area.

It is difficult to accurately assess the implications in the field of reduced tensile strength of a fire fighter's turnout coat. One can easily envision a situation in which degradation has occurred to the point of severely reducing the tensile strength of a pair of turnout pants for example. This pair of pants could then become ripped by being caught on a sharp piece of material on the fire ground, or by making a sudden intense movement. This rip in the fabric would place the fire fighter in danger since the flame and heat resistances of the gear would now be compromised. When the outer shell has been exposed to enough heat it becomes extremely brittle, enough so that bending of the fabric in the fingers is enough to cause catastrophic failure in the garment. If there is any way to assess the condition of the garment before it reaches that critical point, it would be beneficial to the safety of the fire fighters who wear the gear.

It has been speculated that the colour of the outer shell selected by the Saskatoon Fire and Protective Services is a limitation for the use of colour analysis. The particular

chromatic properties of browns create problems of colour identification and analysis. Different colours of outer shell may have a positive effect on the suitability of the non-destructive test methods developed during this research. Preliminary work has been conducted to assess the suitability of alternative colours, such as green and blue, for the outer shell. The colour differences created by the thermal degradation of these alternate colours are more noticeable and more appropriate for assessment.

More work should be conducted to examine the repeatability of these results. Due to the constraints of laboratory access and limited fabric specimens, exposures were limited to a single exposure for a given heat flux and duration. Multiple exposures to the same heat flux should be conducted. A larger number of samples will provide a clearer picture of the scatter in the data that was presented. When statistical analysis can be performed on the data, a better understanding of the uncertainty in the methods will be obtained. In the field, turnout gear will face repeated exposures of low heat flux, for this reason testing should also be conducted to examine the influence of cyclic thermal loading on the degradation of turnout gear.

The fact that this research examined a highly constrained case of degradation should be reiterated. More work should be conducted to examine causes of degradation other than strictly radiant thermal exposure. Other causes of degradation that should be studied include the effects of laundering the turnout gear, the effects of ultra-violet light exposures, abrasion, soil and age. All of these factors may adversely affect the performance of the turnout gear, and should not be neglected in a study of degradation.

Spectroscopic techniques should be examined in more detail for this application. More use of the Raman technique should be made to assess the possibility of using other colours than brown. Preliminary tests of green and blue unexposed Nomex® showed that results were more consistent than for the brown outer shell tested in this study. Other light sources should be examined for use with the Raman microscope. It has been suggested that an ultra-violet excitation source may reduce the fluorescence of the outer shell. This technique should be re-examined in the context of ultra-violet light.

7. REFERENCES

1. Council of Canadian Fire Marshals and Fire Commissioners, "Fire Losses in Canada: Annual Report 2000," Human Resources Development Canada, Ottawa, ON, 2002.

2. LeBlanc, P.R. and Fahy, R.F., "Full Report: Firefighter Fatalities in the United States – 2002," National Fire Protection Association, Quincy, MA, 2003.

3. National Fire Protection Association, NFPA 1971 Standard on Protective Ensemble of Structural Fire Fighting 2000 Edition, Quincy, MA, 2000.

4. National Fire Protection Association, NFPA 1851 Standard on Selection, Care, and Maintenance of Structural Fire Fighting Protective Ensembles 2001 Edition, Quincy, MA, 2001.

5. Torvi, D.A. and Hadjisophocleous, G.V., "Evaluating the Useful Lifetime of Firefighters' Protective Clothing," Performance of Protective Clothing: Issues and Priorities for the 21st Century, ASTM STP 1386, American Society for Testing and Materials, C.N. Nelson and N.W. Henry, Eds., West Conshocken, PA, 2000.

6. Institute for Research in Construction, "IRC Helping to Develop Guidelines for the Retirement of Firefighters Protective Clothing," Construction Innovation, Vol. 3, No. 2, 1998.

7. Fire and Emergency Manufacturers and Services Association, Inc., FEMSA Official User Information Guide: Protective Garments for Structural Firefighting, Washington, D.C, 1996.

8. Shorter, G.W. and McGuire, J.H., Hutcheon, N.B., Legget, R.F. "The St. Lawrence Burns ", Quarterly of the National Fire Protection Association, Vol. 53, (4), pp. 300-316, June 1, 1960.

9. Lawson, J.R., Fire Fighter's Protective Clothing and Thermal Environments of Structural Fire Fighting, National Institute of Standards and Technology, NISTIR 5804, Gaithersburg, MD, 1996.

10. Drysdale, D., An Introduction to Fire Dynamics, Second Edition, John Wiley & Sons: New York, 2000.

11. Heath, D. "A liquid cooled heat flux transducer for use in evaluating the thermal protective performance of fire fighter clothing", M. Sc. Thesis, Worcester Polytechnic Institute, 2001.

12. Veghte, J.H., "Fire Fighter's Protective Clothing: Design Criteria," Second Edition, Lion Apparel, Dayton OH, 1988.

13. Lawson, J.R., "Thermal Performance and Limitations of Bunker Gear", Fire Engineering, Vol. 151, No. 8, August 1998.

14. Fire and Emergency Manufacturers and Services Association, "FEMSA Official User Information Guide: Protective Garments for Structural Fire Fighting," Fire and Emergency Manufacturers and Services Association, Washington DC, 1996.

15. DuPont, "Technical Guide for NOMEX® Brand Fiber," Wilmington, DE, 1999.

16. W.L. Gore and Associates, "Gore RT7100 Moisture Barrier," Product website: http://www.crosstech.com/fire.fighting.other.html, accessed February 10, 2004.

17. Scott, R.A., "Textiles in Defence" in Horrocks A.R. and Anand, S.C., eds., Handbook of Technical Textiles, Woodhead Publishing Limited, Cambridge, UK, 2000.

18. Tutterow, R, Varner, B., Sorci, A., Soros, C., Brehm, D., Harms, T., Jilg, T., "PPE Care and Use Guidelines", Fire Industry Equipment Research Organization, 1994.

19. Slater, K. "Textile Degradation", The Textile Institute, Textile Progress Vol. 21, No. 1, 1991.

20. Slater, K. "The Progressive Deterioration of Textile Materials, I: Characteristics of Degradation," Working Paper No. 85-202, University of Guelph, Guelph ON, 1985.

21. Vogelpohl, T.L., "Post-use Evaluation of Fire Fighter's Turnout Coats," M.Sc. Thesis, University of Kentucky, 1996.

22. American Society for Testing and Materials, ASTM D 4108 Thermal Protective Performance of Materials for Clothing by Open-Flame Method, West Conshocken, PA, 1987.

23. Berardinelli, S.P. and Roder, M., "Chemical Protective Clothing Field Evaluation Methods," Performance of Protective Clothing, ASTM STP 900, R.L. Barker and G.C. Coletta, eds., American Society for Testing and Materials, Philadelphia, 1986, pp. 250-260.

24. Cardamone, J.M., Damert, W.C., Phillips, J.G. and Marmer, W.N., "Digital Image Analysis for Fabric Assessment", Textile Research Journal, Vol. 72, No. 10, pp. 906-916, 2002.

25. Fortner B. and Meyer T., Number by Colors: A Guide to Using Color to Understand Technical Data, Telos: New York, 1997.

26. General Electric, “Getting Started Understanding Color,” company website: http://www.gecolorxpress.com/jsp/extranet/user/start/quantifying4.jsp, accessed March 9, 2004.

27. Uroz, J., Luo, R. and Morovic, J., “Perception of Colour Differences in Large Printed Images,” in MacDonald, L. and Luo, M.R, eds., Colour Image Science: Exploiting Digital Media, John Wiley and Sons, West Sussex, GB, 2002.

28. American Society for Testing and Materials, ASTM F 1939-99a Standard Test Method for Radiant Protective Performance of Flame Resistant Clothing Materials, West Conshocken, PA, 1999.

29. Utech, H.P., “High Temperatures versus Fire Equipment,” International Fire Chief, Vol. 39, pp. 26-27, 1973.

30. Thorpe, P.A., Torvi, D.A., "Towards Non-Destructive Test Methods for Fire-Fighter's Turnout Gear," *19th Canadian Congress of Applied Mechanics,* M. Epstein and L. Sudak, Eds., 2003.

31. Threlfall, T.G, Torvi, D.A., Thorpe, P.A., “Full-Scale Fire Tests, Edmonton Alberta, July 2003,” Technical Report, Department of Mechanical Engineering, University of Saskatchewan, Saskatoon, SK (in progress).

32. Threlfall, T.G., Torvi, D.A., Thorpe, P.A., “Exterior Heat Flux Measurements During House Burn and Implications for Building Codes,” Combustion Institute / Canadian Section, Spring Technical Meeting, Kingston, ON, 2004.

33. Dale, D., Ackerman, M., Torvi, D., Threlfall, T., and Thorpe, P., “Interior Temperature and Heat Flux Measurements During House Burn,” Combustion Institute / Canadian Section, Spring Technical Meeting, Kingston, ON, 2004.

34. Thorpe, P.A. & Torvi, D.A., “Development of Non-Destructive Test Methods for Assessing Effects of Thermal Exposures on Fire Fighter’s Turnout Gear,” Journal of the ASTM International (in press).

35. American Society for Testing and Materials, ASTM F 903 Standard Test Method for Resistance of Materials Used in Protective Clothing to Penetration by Liquids, West Conshocken, PA, 1990.

36. American Society for Testing and Materials, ASTM F 1060 Standard Test Method for Thermal Protective Performance of Materials for Protective Clothing for Hot Surface Contact, West Conshocken, PA, 1987.

37. American Society for Testing and Materials, ASTM D 5733 Standard Test Method for Tearing Strength of Nonwoven Fabrics by the Trapezoid Procedure, West Conshocken, PA, 1995.

38. American Society for Testing and Materials, ASTM D 5034 Standard Test Method for Breaking Force and Elongation of Textile Fabrics (Grab Test), West Conshocken, PA, 1995.

39. American Society for Testing and Materials, ASTM D 4108 Standard Test Method for Thermal Protective Performance of Materials for Clothing by Open-Flame Method, West Conshocken, PA, 1996.

40. Reinhart, T.J., Engineered Materials Handbook, Vol. 2, Metals Park, OH: ASM International, 1987, pp. 367, 511.

41. Foreman, J., Riesen, R., Schubell, M. "Heat flow measurements during weight changes using TGA/SDTA," in American Laboratory, January 2001.

42. Bajaj, P., "Heat and Flame Protection," in Horrocks, A.R. and Anand, S.C. eds., Handbook of Technical Textiles, Woodhead Publishing Limited: Cambridge, EN, 2000.

43. General Services Administration, Federal Test Method Standard 191A, Method 5512, Water Resistance of Coated Cloth; High Range, Hydrostatic Pressure Method, 1978.

44. American Society for Testing and Materials, ASTM F 1670 Standard Test Method for Resistance of Materials Used in Protective Clothing to Penetration by Synthetic Blood, West Conshocken, PA, 1998.

45. Hoschke, B.N., "Standards and Specifications for Firefighter Clothing," Fire Safety Journal, 1981, pp. 125-137.

46. Laserna, J. "An Introduction to Raman Spectroscopy: Introduction and Basic Principles", Spectroscopy Now, John Wiley & Sons Ltd, 2004.

47. Jayasooriya, U.A. and Jenkins, R.D., "Introduction to Raman Spectroscopy" in Andrews, D., Demidov, A., eds., An Introduction to Laser Spectroscopy 2nd Edition, Klewer Academic/Plenum Publishers: New York, 2003.

48. Holme, I., "Colorization of Technical Textiles" in Horrock, A.R. & Anand, S.C. eds., Handbook of Technical Textiles, Woodhead Publishing Limited: Cambridge, EN, 2000.

49. Spectso, "Spectroscopy – Raman," informational website, http://www.spectso.com, accessed March 25, 2004.

50. Roberts, M., "The RGB Colour Model," informational website, http://www.cs.bham.ac.uk/~mer/colour/rgb.html, accessed March 25, 2004.

51. Marshall, D.A., "CIE Chromaticity Diagram," Multimedia Module No. CM0340, Cardiff University, Wales, 1999.

52. Uroz, J., Luo, R. and Morovic, J., "Perception of Colour Differences in Large Printed Images," in MacDonald, L. and Luo, M.R, eds., Colour Image Science: Exploiting Digital Media, John Wiley and Sons: West Sussex, GB, 2002.

53. Lindbloom, B., "CIE Color Calculator," Java applet, www.brucelindbloom.com, accessed March 25, 2004.

54. Rhyzkov, I., "Lab Equipment in the Focus of View," informational website, http://www.lab.ru, accessed March 25, 2004.

55. Thomson, M and Westland, S. "Spectral colour statistics of surfaces" in MacDonald, L.W. and Luo, M.R. *eds*. Colour Image Science: Exploiting Digital Media, John Wiley and Sons: London, England, 2002.

56. Bright, D.S., "Digital Image Processing with NIH Image (Mac) & Scion Image (PC)", National Institute of Standards and Technology, Gaithersburg, MD, 20899-8371.

57. Torvi, D.A., "Heat Transfer in Thin Fibrous Materials Under High Heat Flux Conditions", PhD Thesis, University of Alberta, Edmonton, AB, 1997.

58. Kody, R.S. & Martin, D.C., "Quantitative Characterization of Surface Deformation in Polymer Composites Using Digital Image Analysis," Polymer Engineering and Science, Vol. 36, pp. 298-304, 1996.

59. Rae,P., Goldrein,H., Palmer, S. and Field, J., "The Use of Digital Image Cross-Correlation (DICC) to Study the Mechanical Properties of a Polymer Bonded Explosive (PBX)," Cavendish Laboratory, Cambridge: UK, 2002.

Appendix A: Scanned Images of Fabric Specimens

Turnout ensemble specimens were subjected to a specified heat flux for a given duration using an ASTM F 1939 radiant panel performance testing apparatus (refer to Section 2.3 for details). Following these exposures the outer shells were scanned using a Hewlett-Packard Scanjet 4400c digital scanner. Resolution was set to 150 dpi, so there are 150 pixels per inch of specimen. These images were then used in the digital image analysis portion of the research (See Section 4.3). Figures A.1 to A.29 give the scanned images for the exposures used in this research.

Figure A.1: 600 s at 5 kW/m^2

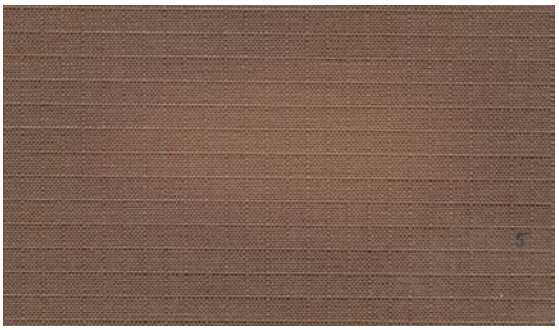

Figure A.2: 1200 s at 5 kW/m^2

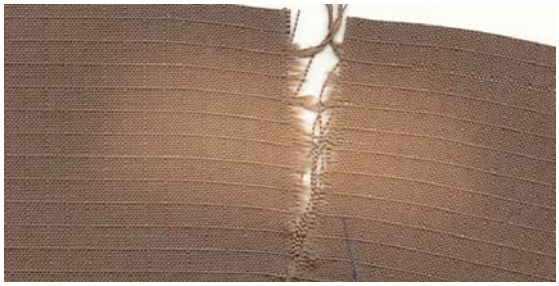

Figure A.3: 1800 s at 5 kW/m^2

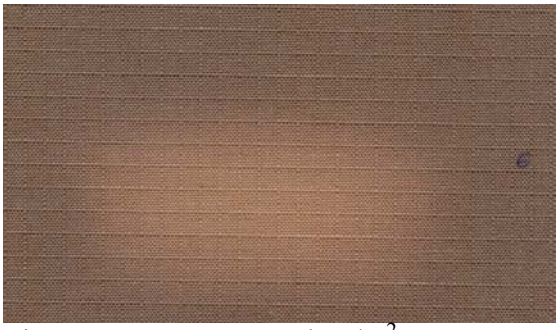

Figure A.4: 2400 s at 5 kW/m^2

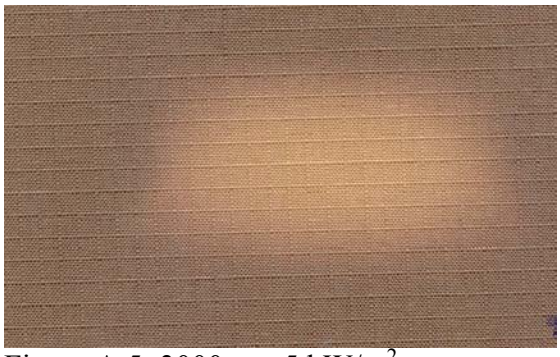

Figure A.5: 3000 s at 5 kW/m^2

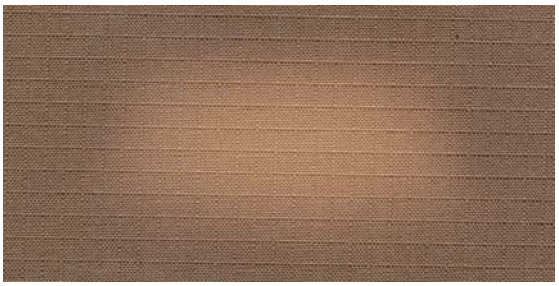

Figure A.6: 3600 s at 5 kW/m^2

Figure A.7: 120 s at 10 kW/m^2

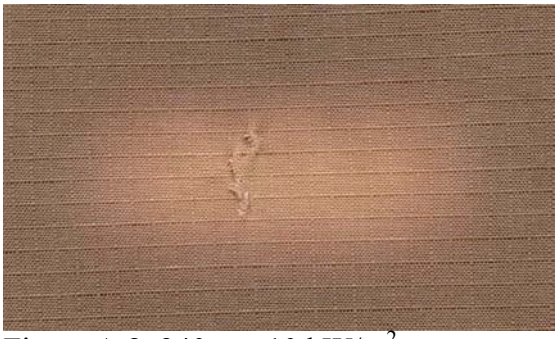

Figure A.8: 240 s at 10 kW/m^2

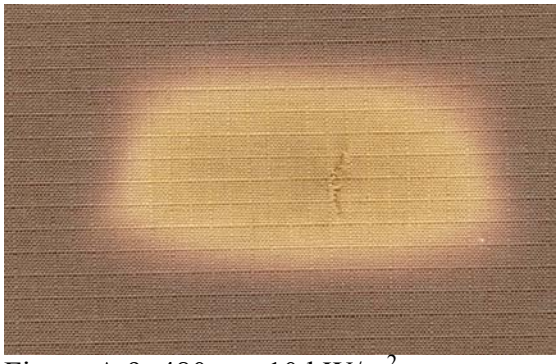

Figure A.9: 480 s at 10 kW/m^2

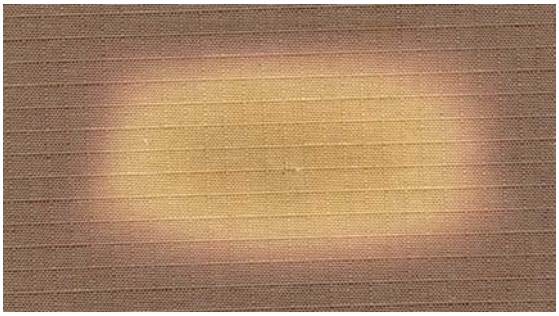

Figure A.10: 600 s at 10 kW/m^2

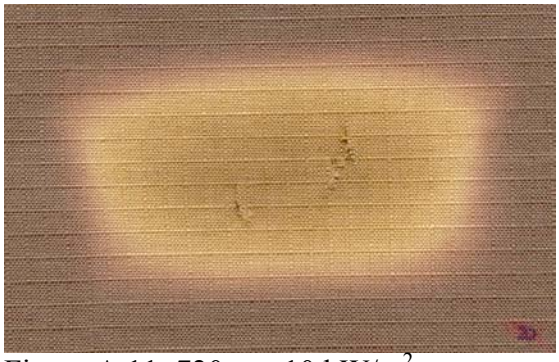

Figure A.11: 720 s at 10 kW/m^2

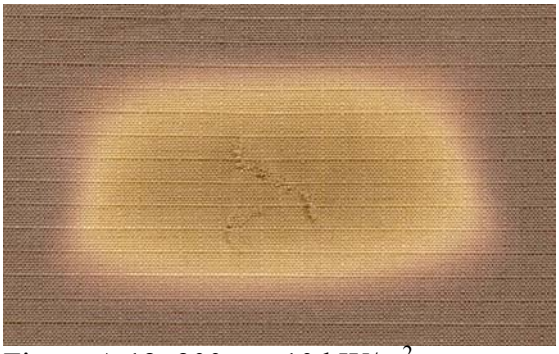

Figure A.12: 900 s at 10 kW/m^2

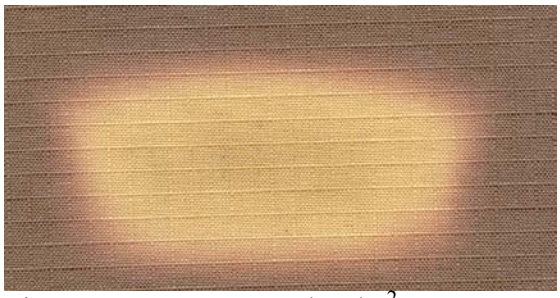

Figure A.13: 60 s at 15 kW/m^2

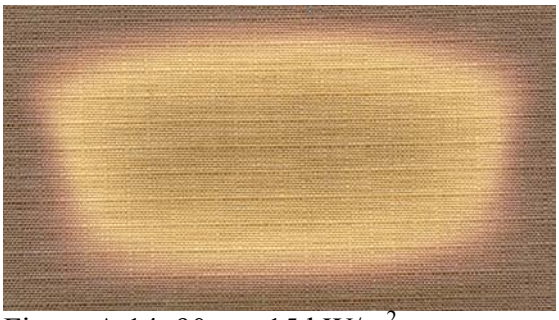

Figure A.14: 90 s at 15 kW/m^2

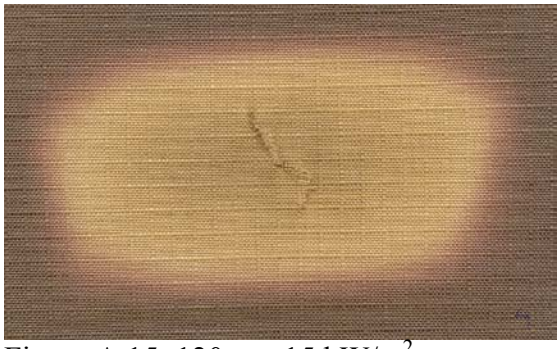

Figure A.15: 120 s at 15 kW/m^2

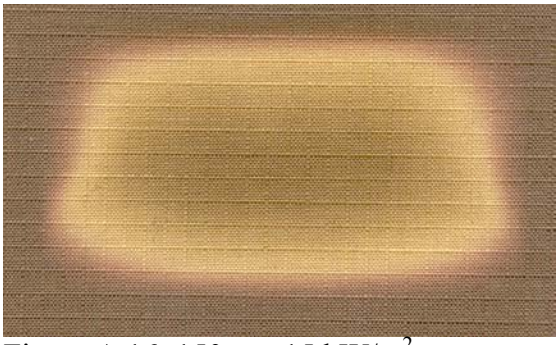

Figure A.16: 150 s at 15 kW/m^2

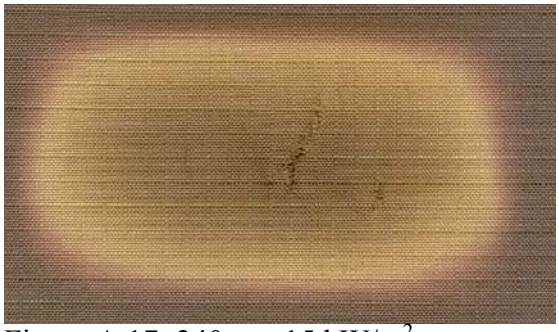

Figure A.17: 240 s at 15 kW/m^2

Figure A.18: 360 s at 15 kW/m^2

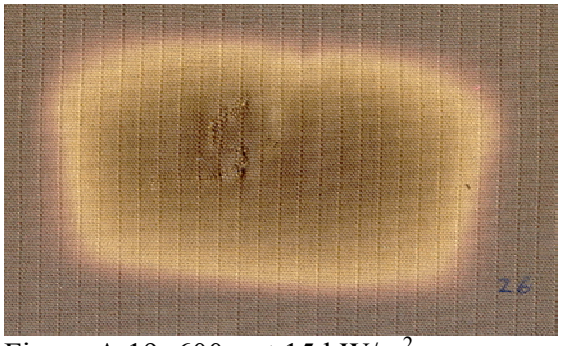

Figure A.19: 600 s at 15 kW/m^2

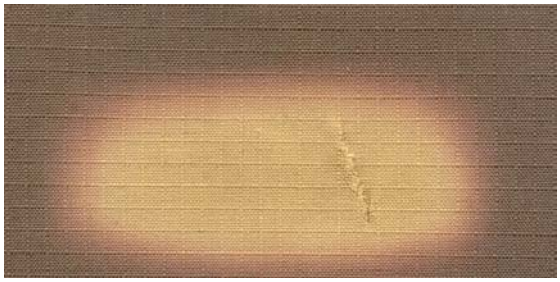

Figure A.20: 30 s at 20 kW/m^2

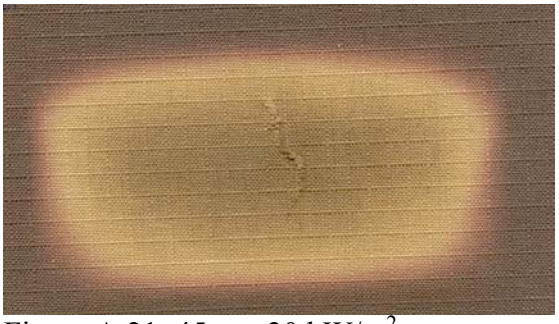

Figure A.21: 45 s at 20 kW/m^2

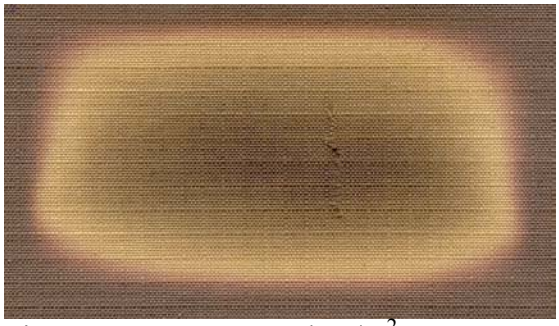

Figure A.22: 60 s at 20 kW/m^2

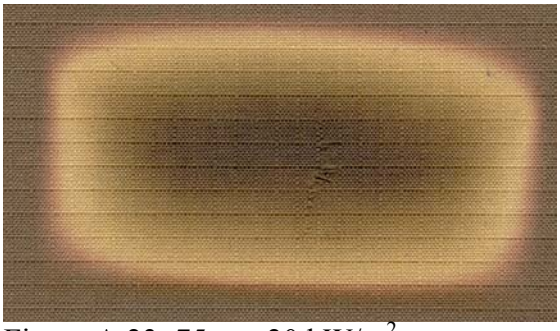

Figure A.23: 75 s at 20 kW/m^2

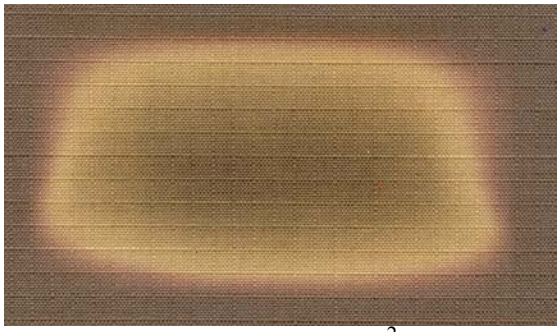

Figure A.24: 90 s at 20 kW/m^2

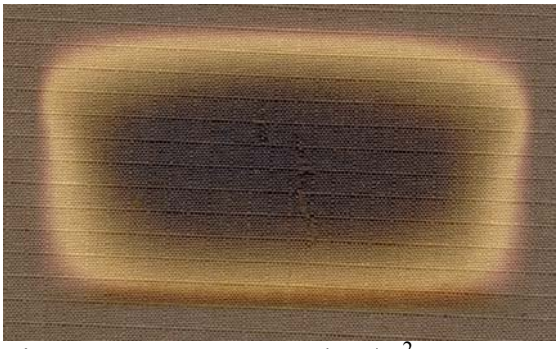

Figure A.25: 120 s at 20 kW/m^2

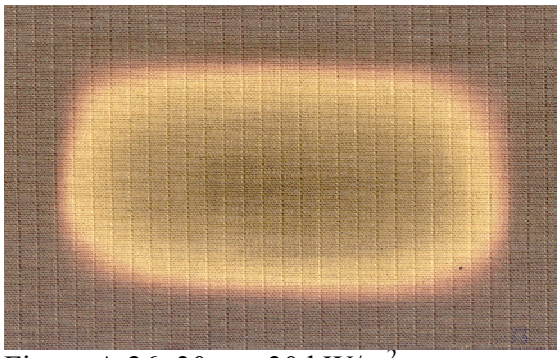

Figure A.26: 30 s at 30 kW/m^2

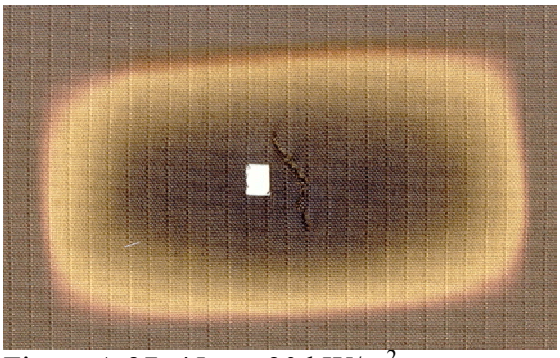

Figure A.27: 45 s at 30 kW/m^2

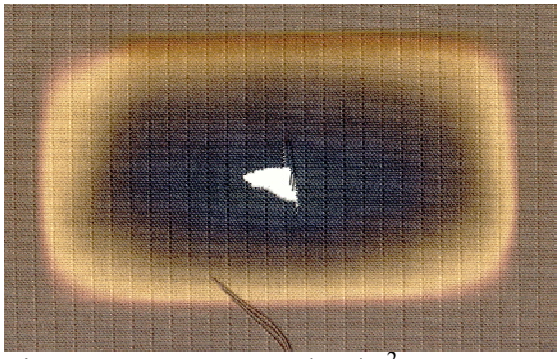

Figure A.28: 60 s at 30 kW/m^2

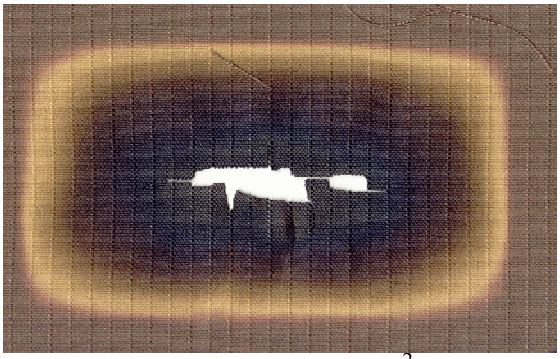

Figure A.29: 120 s at 30 kW/m^2